Author:
Furniss, Jonny A

Title:
Investigating In Vitro Platelet Production Through a Microscopy Lens

Author:
Furniss, Jonny A

Title:
Investigating In Vitro Platelet Production Through a Microscopy Lens

Investigating *In Vitro* Platelet Production Through a Microscopy Lens

Jonathan Alan Furniss

A dissertation submitted to the University of Bristol in accordance with the requirements for award of the degree of Masters by Research in Physiology, Pharmacology and Neuroscience in the Faculty of Life Sciences. Submitted to the school of Physiology, Pharmacology and Neuroscience, September 2023.

Word count: 25639 (excluding references, and content pages)

Abstract

Platelets were once viewed merely as blood clotting cells. Their functions have been shown to be far more diverse, including immune and cancer modulation. How platelets are produced from their precursor cell, megakaryocytes, is a highly debated topic. There are two main theories of where platelets are produced: bone marrow sinusoids and the lung vasculature. These concepts has been mimicked *in vitro* to produce platelets for therapeutic purposes. Efficient *in vitro* platelet production has however been challenging. To produce platelets, the Poole group (UK) used an *in vitro*, microfluidics device with a branched structure, modelled from the architecture of the lung vasculature. Here, two alternative microfluidics systems were designed. The 'smooth branched' design maintained the branching structure of its predecessor but had rounded edges instead of sharp. The sinusoidal' design consisted of straight channels where the width increased and decreased in a pulsatile manner. The efficiency and platelet producing mechanisms of these three systems were characterised using brightfield, laser scanning confocal and scanning electron microscopy as well as flow cytometry. The branched system was the most efficient at producing platelets. Removal of sharp corners from this system seemed to have little to no effect on production efficiency or damage to cells. All three systems exhibited proplatelet formation. Blockages and debris were commonly observed, indicating flawed chip design and high stress levels. The data from this work should be used to influence future microfluidic device designs. Branching points appear useful for inducing catch and release, however branching points should be redesigned to reduce blockages.

Author's Declaration

I declare that the work in this dissertation was carried out in accordance with the requirements of the University's Regulations and Code of Practice for Research Degree Programmes and that it has not been submitted for any other academic award. Except where indicated by specific reference in the text, the work is the candidate's own work. Work done in collaboration with, or with the assistance of, others, is indicated as such. Any views expressed in the dissertation are those of the author.

SIGNED: Jonathan Alan Furniss  DATE: 31/08/23

Acknowledgements

First and foremost, I would like to thank my principal supervisor, Professor Alastair Poole for his huge amount of support and guidance throughout the project. I thoroughly look forward to returning to complete my PhD under such a caring supervisor. I must also thank all the members of the Bristol Platelet group for all their support, both with laboratory work and with keeping my spirits high when experiments were not. Thank you to Semra Zuhal Birol for her expertise on microfluidic systems. Without her guidance, this project would have been far more difficult. Special thanks are due to Jordan Vautrinot for all his mentorship and Dr Luis A Moran Lara for his practical support. This work would not have been able without the members and facilities of the Wolfson Bioimaging facility. Thank you to Dr Stephen Cross for coding macros for quantifying images. Special thanks must be offered to Dr Lorna Hodgson and Dr Chris Neal for their guidance and support on scanning electron microscopy. I would like to thank all my close family for their support. Thank you to my mother and sister for their unrelenting support, even if what I was explaining meant nothing to you. I would also like to thank my grandfather, Alan, who has always supported my work and has wanted nothing but the best for me. Although none of them will ever interact with this piece of work, I would like to thank all my training partners and coaches at Pedro Bessa Brazilian Jiu Jitsu for humbling me on the good days and uplifting me on the bad. Thank you to Rest Bay for having mediocre waves that bring such joy and Bannau Brycheiniog for providing such a beautiful scenery to escape to on weekends. Finally, I must acknowledge my extreme gratitude for Alice. The support you have provided cannot be articulated but is never overlooked. I am excited for what the future of our respective works holds.

List of Tables and Figure

Figure 1 – Schematic of Platelet Production Locations **14**

Table 1 - In vitro platelet production systems **16**

Figure 2 – Uses of Artificially Produced Platelets **18**

Table 2 – Primary Antibodies Used **19**

Table 3 – Secondary Antibodies Used **20**

Table 4 – Dyes Used **20**

Figure 3 – Non-specific labelling of mouse bone marrow cells **28**
Figure 4– Bleed through and non-specific binding images of mouse bone marrow cells **29**
Figure 5 – Mouse megakaryocytes captured using a partially optimised protocol **30**
Figure 6 – Permeabilization of Mouse Megakaryocytes Using 0.2% Triton X-100 for 1 hour is Optimal for Imaging Microtubules and α-granules **32**
Figure 7 – The Structure of the 3 Microfluidics Systems **34**

Figure 8 – 'Branched' system is the most efficient platelet producing system **36**
Figure 9 – Mouse Megakaryocytes Following 0, 1, 3 or 6 Passages Through the 'Branched' System **38**
Figure 10 - Mouse Megakaryocytes Following 0, 1, 3 or 6 Passages Through the 'Smooth Branched' System **39**
Figure 11- Mouse Megakaryocytes Following 0, 1, 3 or 6 Passages Through the 'Sinusoidal' System **40**
Figure 12 – Quantification of Laser Scanning Confocal Images of Megakaryocytes Passages Through the 3 Systems 0, 1, 3 or 6 Times **43**

Figure 13 – Platelets Produced Using 3 Different Microfluidics Systems **45**
Figure 14 – Megakaryocytes Enucleate in All 3 Microfluidics Systems **46**
Figure 15 – All 3 Microfluidics Systems Exhibit Signs of Causing Cell Stress **48**
Figure. 16 – Scanning Electron Micrographs of Debris Produced From All 3 Microfluidics Systems **50**

Figure 17 – Scanning Electron Micrographs of, Suspected, Apoptotic Cells Produced From the 3 Microfluidics Systems **51**

Figure 18 – Scanning Electron Micrographs of Resting Platelets **52**

Figure 19 – Scanning Electron Micrograph of Preactivated Platelets Produced From the 3 Microfluidics Systems **53**

Figure 20 – Scanning Electron Micrographs of Platelet Barbells Produced From the 3 Microfluidics Systems
54

Figure 21 – Scanning Electron Micrograph of a 'Tri-bell' Produced From the 'Sinusoidal' Microfluidics System **55**

Figure 22 – Scanning Electron Micrographs of Deformed Cell-like Objects Produced From the 3 Microfluidics Systems **56**

Figure 23 – Catch and Release is Hypothesised as the Mechanism of Platelet Production in all 3 Microfluidics Systems **58**

Figure 24 – Schematic of Locations Imaged for Quantification of Cellular Blockages within the 'Branched' and 'Smooth Branched' Microfluidics Systems **59**

Figure 25 – The Outlet of the 'Branched' Microfluidics System Becomes the Most Blocked Due to Chip Architecture and Shear Stress **61**

Figure 26 - The Outlet of the 'Smooth Branched' Microfluidics System Becomes the Most Blocked Due to Chip Architecture and Shear Stress **63**

Figure 27 – Brightfield Images of Blockages Within the 'Sinusoidal' Microfluidics System **64**

Figure 28 – Simplified Schematic of Hypothesised Mechanisms Within the 'Branched' and 'Smooth Branched' Microfluidics Systems **78**

Abbreviations

AWERB	Animal Welfare and Ethical Review Body -
BSA	Bovine serum albumin
CGS	Citrate glucose salt
CTC	Circulating tumour cells
EDTA	ethylenediaminetetraacetic acid
EMT	Epithelial-to-mesenchymal transition
FBS	Fetal bovine serum
FITC	Fluorescein isothiocyanate
HLA	human leukocyte antigen
HSC	Haemopoietic stem cell
IgG	Immunoglobulin G
IMDM	Iscove's Modified Dulbecco's Medium
IMS	Invaginated membrane system
ITAM	Immunoreceptor tyrosine-based activation motif
MK	Megakaryocyte
PBS	Phosphate buffered saline
PDGF	Platelet derived growth factor
PDL1	Programmed death ligand 1
PDMS	Polydimethylsiloxane
PE	Phycoerythrin
Pen/Strep	Penicillin/ Streptomycin
PFA	Paraformaldehyde
PGE1	Prostaglandin E1
SCF	Stem cell factor
SEM	Scanning electron microscopy
S.E.M	Standard Error of the Mean

TGF- β1	Transforming growth factor- beta 1
TPO	Thrombopoietin
VEGF	Vascular endothelial growth factor
vWf	Von Willebrand Factor

Table of Contents

Abstract **2**

Author's Declaration **2**

2

Acknowledgements **3**

List of Tables and Figure **4**

Abbreviations **6**

1. Introduction **11**

1.1 Platelets and Megakaryocytes *11*

1.2 Platelet Production Theories *11*

1.3 In vitro Platelet Production *14*

1.4 Different Sources of Megakaryocytes *16*

1.5 Uses of Produced Platelets *17*

1.5 Aims *18*

2. Material and Methods **19**

2.1 Materials *19*
2.11 Antibodies and Dyes 19
2.12 Buffers 21
2.13 Cell Culture 21
2.14 Fixatives and Microscopy Reagents 21
2.15 Microfluidics System Fabrication and Operation 21
2.16 Microscopes 21

2.2 Methods *22*
2.21 Mice 22
2.22 Culturing and Differentiation of Murine Megakaryocytes 22
2.23 Flow Cytometry sorting and Gating Strategy 22
2.24 Microfluidics System Fabrication 23
2.25 Microfluidics System Operation 23
2.26 Brightfield Imaging of Microfluidics Systems 24
2.27 Confocal Microscopy Preparation and Image Acquisition 24
2.28 Scanning Electron Microscopy Acquisition and Image acquisition 25
2.29 Statistics and Analysis 25

3. Results **26**

3.1 Laser Scanning Confocal Microscopy Optimisation *26*
3.11 Introduction 26

3.12 Proteins and organelles of interest 26
3.13 Pre-optimisation protocol 27
3.14 Partially optimised protocol 27
3.15 Altering permeabilization 30

3.2 Assessing Productivity of Microfluidics Systems *33*
3.21 Microfluidics system designs 33
3.22 Platelet producing efficiency 35

3.3 Using Microscopy to Investigate In Vitro Platelet Production *37*
3.31 Changes to megakaryocytes, following passage through microfluidics 37
3.32 Characterisation of produced platelets, enucleated megakaryocytes and debris 44
3.33 Characterising generated platelets using scanning electron microscopy 51
3.34 Platelet producing mechanisms and blockages within the microfluidics systems 56

4. Discussions **65**

4.1 Platelet Counting – Limitations and Justifications *65*
4.11 Summary 65
4.12 Gating 65
4.13 Platelet Functionality 66
4.14 Megakaryocyte Counting 67
4.15 Cell death 67
4.16 Data Presentation 67
4.17 Conclusion 68

4.2 Fluorescent Intensity Analysis – Limitations and Alterations *68*
4.21 Summary 68
4.22 Experimental Design 68
4.23 Image Presentation 69
4.24 Quantifying Macro 69
4.25 Conclusions 69

4.3 Cellular Debris Produced – Theories *70*
4.31 Summary 70
4.32 Suggestions of the identity of debris 70
4.33 Suggestions of the identify of deformed cell-like objects 70
4.34 Conclusions 71

4.4 Observed In Vitro Platelet Production Mechanisms *71*
4.41 Preplatelets, proplatelets and barbells 71
4.42 Proplatelets in the chips 72
4.43 Durations of cell passaging 72
4.44 Cellular compression 73
4.45 Conclusions 73

4.5 Microfluidic Channel Blockages – Theories and Future Designs *74*
4.51 Blockage composition and fixes 74
4.52 Chip structure causes blockages 74
4.53 Increasing throughput 75
4.54 Conclusions 75

4.6 Conclusions about the physical parameters within the different systems *76*

4.61 Introduction 76
4.62 Compression 76
4.63 Shear stress 76
4.64 Branch points 76
4.65 Laminar flow vs turbulent flow 77
4.66 Future experiments 77
4.67 Comparison to *ex vivo* model 77

4.7 Summary of the 3 Microfluidics Systems *78*

4.8 Final words and future directions *79*

5. Bibliography **80**

1. Introduction

1.1 Platelets and Megakaryocytes

Although they are the smallest blood cells, platelets are crucial for mammalian survival(1). They were traditionally viewed as mediators of haemostasis, filling injured vessel walls to prevent excessive blood loss(2). Although true, their roles are far more diverse than once believed. Release of various cytokines and growth factors from activated platelets facilitate tumour development, growth and progression. Examples of these chemical mediators include the following. Transforming growth factor-beta 1 (TGF-β1) released from activated platelets promotes growth of ovarian tumours in mouse models(3, 4). Vascular endothelial growth factor (VEGF) and platelet derived growth factor (PDGF) both drive novel blood vessel growth (angiogenesis). These new blood vessels supply tumours with the nutrients required to proliferate and cause further harm to the host organism(3, 5-7). Platelets also facilitate the migration of tumour cells around the body (metastasis). Metastasis is associated with a poorer patient prognosis(8-10). Platelets can induce epithelial-to-mesenchymal transition (EMT) signalling within tumour cells(11). EMT will provide circulating tumour cells (CTCs) with the machinery required to invade new tissues(12). Furthermore, platelets are known to bind CTCs and thus hide CTCs from natural-killer cell driven destruction of tumours(13, 14). These mechanisms of platelets facilitates cancer progression, leading to increased patient deaths(15). These platelets also interact with other parts of the immune system. Platelets store and release a multitude of inflammatory molecules in response to foreign stimuli and vascular injury. Platelets can detect pathogens via Toll-like receptors, a pathogen recognizing protein(16). These examples highlight the double-edged nature of platelet functionality, preventing blood loss whilst facilitating disease states.

Platelets are produced from the, enormous, precursor cells, megakaryocytes (MKs). MKs are derived from haemopoietic stem cells (HSCs)(17). Chemical signalling and the bone marrow microenvironment induces HSC differentiation into MK-progenitors which then develop into early iterations of MKs, called megakaryoblasts(17). Megakaryoblasts undergo several developmental processes to become the final mature MK, capable of producing platelets. MK development is heavily driven by the cytokine, thrombopoietin (TPO)(17-19). A key part of their development is cells undergoing several mitotic divisions which are prematurely interrupted, causing the replication of DNA without the division into daughter cells (endomitosis). Multiple cycles of endomitosis ensue, leaving MKs with an average ploidy of 16n with some cells reaching 128n(17, 20, 21). It is hypothesized that this increased ploidy facilitates production of large amounts of protein needed to produce thousands of platelets per MK. The cytoplasm of the MK increases and copies of organelles needed for platelet function are synthesized(22). Further to this, MKs develop an extended membrane system called the invaginated membrane system (IMS). The IMS is believed to provide the large quantities of plasma membrane needed to produce nigh on 3000 platelets per MK(23). When fully developed, MKs are very large, with diameters reaching 100μm in humans(19). The mean MK diameter is nearer 50μm(24). MKs and platelets alike are well characterized cells, however the mechanism by which MKs form platelets is heavily debated and poorly understood.

1.2 Platelet Production Theories

Although platelets were discovered almost 150 years ago, the mechanism of their production is still unclear(25). Their production is believed to occur in bone marrow sinusoids and/or the pulmonary vasculature. The existing evidence in the literature indicates that both locations are viable platelet production sites(26). Platelets may be produced in both location, as well as in other organs. This section will present data supportive and challenging of both theories. Fig. 1 illustrates these two theories in a simplified schematic.

Firstly, supporting the bone marrow sinusoid theory. Exceptional scanning electron microscopy (SEM) techniques visualized megakaryocytes exiting the bone marrow into the local circulation and platelets localized to this region also(27). Megakaryocytes growing in culture are shown to extend their cytoplasm to form protrusions. These protrusions are referred to as proplatelets. The same experiments showed small, platelet sized cytoplasmic fragments localized near these protrusions(28, 29). It is theorised that once these proplatelet extensions penetrate into the vasculature, the shear stress from flowing blood will break the proplatelet away from the cell body of the MK (20, 30). Proplatelets in the blood are then believed to form a large platelet precursor; the preplatelet. Each preplatelet sheds into two discoid platelets, via a barbell-shaped intermediate. This phenomenon has been observed *in* vitro and ex *vivo*(31). The bone marrow and pulmonary vasculature theories of platelet production do exhibit overlap. Some believe that preplatelets circulating in the blood and reach the capillary bed of the lungs. Due to their large size, they become trapped. The shear stress on these static cells, pulls platelets from the preplatelet(20). The major point of difference between the two theories is that the pulmonary vasculature model believes that full MKs become trapped in the lungs, to then produce platelets. The proplatelet theory has limitations. There is limited data visualizing live platelet production from bone marrow proplatelets(26). It has been suggested that proplatelets are a 'in the dish' phenomenon and not physiological. Alternatively, the elongation of a MK membrane may facilitate the pulmonary vasculature theory of platelet production. Brown et al (2018) used correlative light electron microscopy to visualise MKs *in vivo*(32). They showed MKs extruding large membrane protrusions into bone marrow sinusoids. More than 90% of protrusions observed were too large to be characterised as proplatelets. These large protrusions were able to anchor to endothelial cells and aid intravasation into the vasculature. This provided strong evidence that MKs migrate out of the bone marrow, to then produce platelets elsewhere. Proplatelet extensions were seen in this study, indicating extension of proplatelets out of the bone marrow niche may be a contributing mechanism to platelet production. However, proplatelets were in the minority, suggesting other mechanisms of platelet production may be involved.

Once MKs have entered the venous circulation using this large protrusion mechanism, they will be delivered to the right side of the heart. Contraction of the heart will force the blood, and thus the MKs contained, up into the vasculature of the lungs via the pulmonary artery. This is the first capillary bed that MKs reach following their exit from bone marrow(26). Using histological data and computational simulations, it was shown that human blood contains sufficient MKs to produce enough platelets to maintain physiological platelet counts(33),(34). This is strong evidence supporting the pulmonary vasculature hypothesis of platelet production. It is worth noting that the literature states different estimates of the percentage of platelet production that can be accounted for by the lungs. This is due to a lack of a conserved method of estimating platelet production rate(35). Further supporting evidence is that the platelet count in post-pulmonary capillary blood is greater than pre-pulmonary capillary blood(36). Note that the sample size of this study was relatively low and should potentially be treated

with caution. Arguably the most direct evidence of lung platelet production is the intravital imaging of mouse lungs conducted by Lefrançais et al(37). They visualised MKs, wedging in the pulmonary vasculature and forming proplatelets, resulting in platelet production. The proplatelet shape of the MKs in the lungs and visualised platelet release shows that proplatelets are not exclusively a 'in the dish' phenomenon and have physiological applications.

Some less direct evidence also supports the lung vasculature theory. Suggestions of other capillary beds producing platelets indicates that this mechanism of platelet production may be conserved throughout the body. Placental capillary beds contained MKs, suggesting a site of platelet production for foetuses. This hypothesis is originated by the fact that insufficient volumes of blood pass through foetal lung capillaries to produce the platelet counts found in foetal blood(38). However, some published studies state that MKs are rarely found within lung capillary beds and find only low MK counts in the blood, refuting the role of the lungs in platelet biogenesis(39, 40). If the lungs are vital for platelet production, one would expect patients with sub-optimal lung function to have low platelet counts. The literature produces conflicting data on this topic. In some lung pathologies, e.g. severe acute respiratory syndrome, approximately 50% of patients have low platelet counts (thrombocytopenia)(41). The fact that not all patients have low platelet counts does contradict the idea of the lung vasculature theory being the sole mechanism of platelet production. Patients with normal platelet counts could be explained by redundancy in platelet producing mechanisms, supporting the idea of multiple sites of production.

Other platelet release theories exist. This includes the protoplatelet and explosive fragmentation theory(42). These theories do not exhibit proplatelets as a platelet releasing component.

In summary, the two main hypothesised locations of platelet production are the bone marrow and in the vasculature of the lungs. Both theories have substantial supporting evidence, as well as limitations. Both theories should be considered when questioning platelet production. As mentioned, there is the possibility of both theories existing *in* vivo. The author believes this likely. Redundancy is often seen *in vivo.* The evidence presented is by no means exhaustive on this topic.

Figure 1

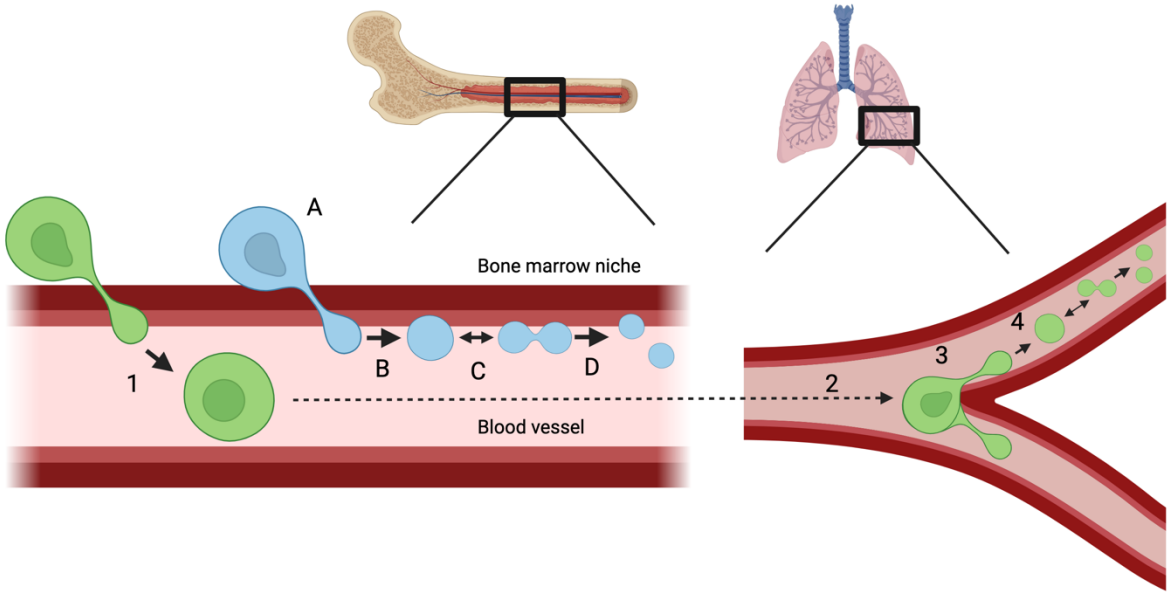

Figure 1 – Schematic of Platelet Production Locations

Blue cells indicate bone marrow theory of platelet production. (A) Megakaryocytes (the large, nucleated cell) in the bone marrow niche, extend proplatelets through the bone marrow and into the local vasculature. (B) Shear stress from blood flow pulls proplatelets into long strands and eventually breaks the proplatelet off. Proplatelets can then convert into large, spherical, preplatelets. (C) Preplatelets reversibly form barbell platelets. (D) Barbell platelets sever to form platelets. Green cells indicate the lung vasculature theory of platelet production. (1) Megakaryocytes extravasate out of the bone marrow niche and into the local blood circulation. (2) The megakaryocytes are carried to the pulmonary vasculature. (3) Megakaryocytes become lodged on branching points in the vasculature and extend proplatelet extensions. (4) Proplatelets break off to form preplatelet and barbell platelets and subsequently forming platelets as described in B-D. Inspiration for these schematics was derived from (20, 35). Created using Biorender.com

1.3 In vitro Platelet Production

Facilitated by the knowledge on platelet production mentioned in the previous section, various groups have attempted to replicate this *in vitro(43)*. *In vitro* platelet production began in 2003. Lansky and Yang created multiple iterations of systems utilising MK capture(44, 45). Other groups have since designed many systems, with differing rationales and designs. Blin et al used a microfluidics system, utilising shear stress and laminar flow. This system was a mimetic of the bone marrow sinusoids(46). High platelet numbers were produced, but the efficiency of platelet production relative to the number of MKs loaded was poor. Thon et al used a different bone marrow mimicking system(47). This system visualised MKs extending proplatelets through gaps in a membrane in a manner similar to the bone marrow production

schematic in Fig. 1. Both these discussed systems were synthesised in a polymethyldisiloxane (PDMS), like the designs in this dissertation (more detail on this can be found in the materials and methods section). An alternative approach was taken by the Balduini group working under the company SilkFusion. They created a bone marrow mimetic system using silk from silkworm cocoons(48). Many of the bone marrow mimetics exhibit a similar problem. Each proplatelet produced many platelets, however not many MKs captured/ became immobilised so the overall efficiency was very low (43, 46, 48). The Eto group have taken an alternative approach to platelet production. Instead of using microfluidics, they used a large scale, fluid bioreactor and turbulent flow to produce high number of functional platelets(49). The Strassel group published a novel system, implementing turbulent and laminar flow(50). Their system is synthesised of polypropylene, a far more rigid polymer compared to PDMS. The system mimics the fluid dynamics of repeated pipetting and yields good platelet productivity. These systems mentioned are not exhaustive of the field and some of these are discussed in further detail in the discussions section. Although many of these systems are efficient and can produce platelets, high throughput functional platelet production is still limited. Brief summaries of *in vitro* platelet producing systems reported in the literature is found in Table 1. Note that other systems may exist, but the author was unable to find these in the literature.

Zhao et al presented an *ex vivo* platelet production system capable of producing physiological levels of platelet per MK(51, 52). This system utilised a mouse's heart and lung circulation as an isolated system capable of MK infusion. This system is an excellent research tool, providing much evidence supporting the theory of platelet production in the lung, however it is not a feasible high throughput system. This system cannot be scaled to an industrial size required for the clinic. This owes to the high surgical skill required, long operation time and ethical conflicts of large-scale animal use. Thus, *in vitro* systems which are less technically difficult and can be scaled up were proposed. Zhao et al proposed that a microfluidics system, based upon a lung capillary bed design, would be suitable. A series of chambers could be designed to induce different pathways of flow, varying amounts of shear stress and compression onto cells passing through the system. It has been shown that shear stress is key in producing platelets, both *in vitro* and *in vivo(53).*

This dissertation studies and compares the microfluidics design used by Zhao et al and then two additional designs. Schematics of the designs and the rationale for the designs is found in the results section.

Table 1

Laboratory Group	Brief Description	Platelet Producing Productivity (platelets per megakaryocyte)
PlatOD (46)	Microfluidics system synthesised in PDMS. Many, von Willebrand factor coated pillars intended to immobilise megakaryocytes.	3.7
Megakaryocytes to Platelets Research Group (J.E Italiano) (47)	Microfluidic bone-marrow niche replicate synthesised in PDMS. Mimicry of megakaryocytes extending out of bone marrow niches into local circulation.	20 ± 12
SilkFusion (A. Balduini)(48)	Bone-marrow niche replicate synthesised in silk fibroin	Not clearly stated
The Koji Eto Lab (49)	Large tank bioreactor inducing turbulent flow	70-80
The Strassel Lab(50)	Polypropylene spheres resulting in turbulent and laminar flow. Mimicking of repeated pipetting	100

Table 1- *In vitro* platelet production systems

The laboratory group, principal investigator and/or the company associated with this system are listed. This is followed by a brief description of the system and, where applicable, how many platelets per megakaryocyte the system is reported to produce.

1.4 Different Sources of Megakaryocytes

When working to produce platelets *in vitro* a decision about which MKs to use. Traditionally, mouse MKs have been used to study both megakaryocyte development and platelet production(48, 54, 55). These are commonly isolated from fetal livers and/or bone marrow.(56) Extraction from the spleen is also present in the literature (57). Although using mouse cells works, ultimately this work but translate into humans. Human MKs can be attained for research. CD34+ haemopoietic progenitor cells can be isolated from umbilical cord blood and other sources(58). These cells can then be encouraged into differentiating into MKs, in culture. The Eto lab have developed an immortalised MK cell line (imMKCLs)(59). The Ghevaert lab use a forward programming approach to produce human MKs(60). Although the development of these cell lines is a success for the platelet production field, the Poole lab has experienced difficulties producing platelets with all these human MK approaches. Thus, for this study,

mouse MKs were used. Previous data from the Poole lab has showed platelet production using mouse MKs meaning that large numbers of platelets could be produced for analysis(52). Bone-marrow derived MKs were the preferred method chosen. The rationale for this was that mouse bone marrow is more readily accessible than fetal livers. Furthermore, complex breeding schedules do not need to be maintained. Although using a human MKs would be more translatable, at this stage, their use would have been more deleterious to the work than beneficial.

1.5 Uses of Produced Platelets

The ability to artificially produce platelets has many clinical applications (Fig. 2). As discussed in section 'I. Platelets and Megakaryocytes', platelets interact heavily with many different cell types via many different proteins. Many of these interactions are cytokine controlled. Some cytokines work beneficially whilst some cytokines induce pathological effects. In theory, if an efficient *in vitro* platelet producing system was created, MKs could be genetically modified to then produce platelets with modified granule content. Thus, certain disease states could be modulated by infusing modified platelets into a patient. For example, platelets lacking angiogenic factors VEGF and PDGF could be infused into cancer patients to reduce tumour growth and stability by reducing angiogenesis (3, 5-7). Another example includes deleting expression of tumour interacting surface proteins, such as the immunoreceptor tyrosine-based activation motif (ITAM) receptor family, from platelets to prevent tumour cloaking and thus reducing metastasis(61).

The diverse interactions of platelets can be manipulated for therapeutic benefit, via a different mechanism. Lu et al (2022) hijacked platelets' tendencies to uptake and package substances from their local environment. Platelets were incubated with a cell cycle inhibiting chemotherapy drug, doxorubicin, and, had nanogels consisting of many anti programmed death ligand 1 (PDL1) antibodies attached to their plasma membrane. P-selectin on the surface of activated platelets interacts with CD44 on tumour cells. This physically held the two cell types close to each other, allowing both doxorubicin and anti PDL1 to induce anti-tumour effects(62). This work presented the potential application of using platelets as a drug delivery vector. If platelets without recognition antigens, i.e. human leukocyte antigens (HLAs), can be generated, they could be loaded with drugs for specific drug delivery(63). The major benefit of this is improved drug selectivity, thus reduced adverse effects of a drug(62). Although this is something that could be achieved by using platelets from donors whose platelets are unreactive upon transfusion (universal donors), difficulties with obtaining sufficient donations for transfusion medicine already exists. Between 2007 and 2015, the demand for platelets has increased by 55,000 individual doses: a 25% increase. Unfortunately, the number of consistent donations has decreased. A 35% decrease in active donors was observed from 2000 to 2015(64). Additionally, donated platelets are not easily stored. Approximately 8% of blood donations worldwide are discarded. Of these lost donations, 33% are lost due to expiry(65). Donated platelets can only be stored for 5-7 days. After this period of time, storage lesions (changes in platelet function due to storage) occur due to changes in pH and platelets are likely to become contaminated with bacterial infections(55, 66). Not only is this wasteful, but it is also an expensive loss. Platelets are the most expensive isolated blood component, with one unit costing

£193.15(55). An efficient *in vitro* system to produce platelets could allow rapid, continual and personalised production of platelets which could prevent platelet shortages and save money. This would facilitate transfusion medicine. The majority (67%) of platelet transfusions are to thrombocytopenic (low platelet count) cancer patients(64). These patients would greatly benefit from consistent and planned production of platelets for transfusion.

In summary, an efficient platelet production system could not only fulfil the role of platelet donors but has many more applications in a variety of clinical circumstances, including cancers.

Figure 2

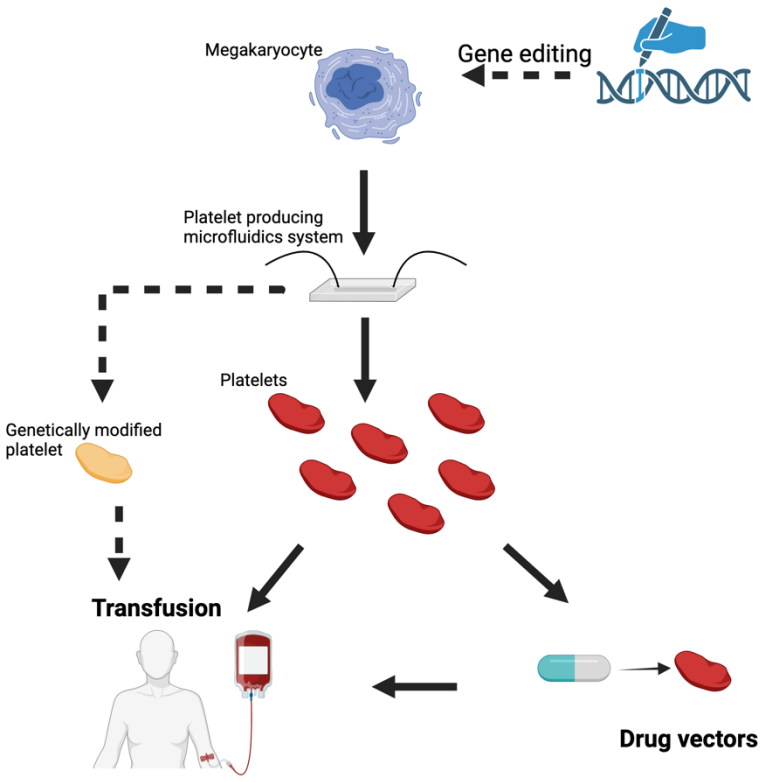

Figure 2 – Uses of Artificially Produced Platelets

Megakaryocytes are loaded into the platelet producing system to produce high numbers of platelets. These can then be infused into patients requiring platelet donations or loaded with or coated with drug compounds prior to transfusion. The megakaryocytes could be genetically modified prior to loading into the platelet producing system. They would then produce genetically modified platelet that could be transfused into patients. Created using Biorender.com

1.5 Aims

The overall aim of this dissertation was to study and optimise an *in vitro* system for platelet production. Using three different designs of microfluidics device, the aim was to address a series of hypotheses. These were as follows.

1. Address the hypothesis that branching structures aid platelet production
2. Address the hypothesis that compression of megakaryocytes is beneficial for platelet production
3. Address the hypothesis that sharp edges within a microfluidics system are deleterious
4. Address the hypothesis that megakaryocytes passing through the microfluidics systems exhibit biophysical changes

2. Material and Methods

2.1 Materials

2.11 Antibodies and Dyes

Table 1 shows the antibodies, immunoglobulin Gs (IgGs) and dyes used. All products were used at (approximately) the manufacturer recommended working concentrations.

Table 2

Antibody or dye name	Conjugated?	Catalogue Number	Supplier	Use
Fluorescein isothiocyanate (FITC)-conjugated rat anti-mouse CD41	Yes	133904	Biolegends (San Diego, USA)	Primary hybridisation - Pre optimisation, laser scanning confocal microscopy
CD41 rat anti-mouse monoclonal antibody	No	14-0411-82	Invitrogen (California, USA)	Primary hybridisation - Optimised laser scanning confocal microscopy
Goat anti-mouse/anti-rat CD62P	No	AF737	R&D Systems (Abingdon, UK)	Primary hybridisation -Optimised laser scanning confocal microscopy
Rabbit α-tubulin (11H10)	No	2125S	Cell Signalling Technologies (Leiden, Netherlands)	Primary hybridisation -Optimised laser scanning confocal microscopy
FITC conjugated rat IgG1, k isotype control antibody	Yes	400406	Biolegends (San Diego, USA).	(Pre-optimisation) IgG control for specific binding - laser scanning confocal microscopy
Rat IgG1 k isotype control	No	14-4301-82	Invitrogen (California, USA)	IgG control for specific binding – laser scanning confocal microscopy
Normal goat IgG control	No	AB-108-C	(R&D Systems) (Abingdon, UK)	IgG control for specific binding - laser scanning confocal microscopy
Normal rabbit IgG control	No	2729S	Cell Signalling Technologies (Leiden,	IgG control for specific binding - laser

			Netherlands)	scanning confocal microscopy
Phycoerythrin (PE) rat anti-mouse CD41	Yes	133906	Biolegends (San Diego, USA)	Primary hybridisation - Flow cytometry
PE rat IgG1 k isotype control	Yes	400408	Biolegends (San Diego, USA)	IgG control – flow cytometry

Table 2 – Primary Antibodies Used

The following is described. Name of antibody. Whether an antibody had a fluorophore conjugated. The catalogue of the product. Supplier and country of origin. Brief description of its use in this piece of work.

Table 3

Antibody or dye name	Conjugated?	Catalogue Number	Supplier	Use
Alexa Fluor 488 donkey anti-rat	Yes	A-21208	Invitrogen (California, USA)	Secondary hybridisation – Optimised laser scanning confocal microscopy
Alexa Fluor 568 donkey anti-rabbit	Yes	A10042	Invitrogen (California, USA)	Secondary hybridisation – Optimised laser scanning confocal microscopy
Alexa Fluor 647 chicken anti-goat	Yes	A-21469	Invitrogen (California, USA)	Secondary hybridisation – Pre-optimisation laser scanning confocal microscopy
Alexa Fluor 647 donkey anti-goat	Yes	1-21447	Invitrogen (California, USA)	Secondary hybridisation – Optimised laser scanning confocal microscopy

Table 3 – Secondary Antibodies Used

The following is described. Name of antibody. Whether an antibody had a fluorophore conjugated. The catalogue of the product. Supplier and country of origin. Brief description of its use in this piece of work.

Table 4

Antibody or dye name	Catalogue Number	Supplier	Use
Vectashield Hardset antifade mounting medium with DAPI	H-1500-10	2Bscientific (Kirtlington, UK)	Mounting coverslips onto cell layer on glass cover slips. Stain nucleus simultaneously
Calcein AM	5119	Tocris (Abingdon, UK)	Viability stain – flow cytometry

Draq5	65-0880-92	Invitrogen (California, USA).	Nuclear stain – flow cytometry
Trypan Blue	15250061	Thermo Fischer Scientific (Grand Island, New York).	Counting megakaryocytes on haemocytometer

Table 4 – Dyes Used

The following is described. Name of stain. The catalogue of the product. Supplier and country of origin. Brief description of its use in this piece of work.

2.12 Buffers

Sigma-Aldrich phosphate buffered saline (PBS) tablet diluted in deionised water (Dorset, UK). Citrate glucose salt (CGS) buffer (pH 6.5) was mixed using 3.8% Trisodium Citrate Dihydrate (13mM), sodium chloride (120mM) and 20% glucose (22mM). Fatty acid free bovine serum albumin (BSA) from Sigma-Aldrich was dissolved in PBS (Dorset, UK).

2.13 Cell Culture

1X Iscove's Modified Dulbecco's Medium with Glutamax (IMDM-Glutamax) from Gibco was used as cell culture media (Paisley, UK). Media with supplemented with penicillin/ streptomycin (Pen/Strep) from Corning (Manassas, USA), Fetal bovine serum (FBS) or Knockout Serum Replacement, supplied from Gibco (USA). During culturing step, Peprotech recombinant murine thrombopoietin (TPO) and recombinant murine stem cell factor (SCF) were also added (New Jersey, USA).

2.14 Fixatives and Microscopy Reagents

Cells were fixed using paraformaldehyde (PFA) (96% pure) dissolved in based deionised water [Cat No.: 10443361] (Thermo Scientific Chemicals) (Loughborough, UK). In some preparations, the PFA solution had glutaraldehyde [Cat No.: 340855] (Sigma Aldrich) (Dorset, UK). Triton X-100 was used for cell permeabilisation [Cat No.: X-100] (Sigma Aldrich) (Dorset, UK). Donkey Serum and BSA dissolved in PBS used as a blocking buffer [Cat No.: D9663] (Sigma Aldrich) (Dorset, UK). Sodium Cacodylate and Osmium tetroxide was provided by the Wolfson Bioimaging facility (Bristol, UK).

2.15 Microfluidics System Fabrication and Operation

Polydimethylsiloxane (PDMS) microfluidics system fabricated by Klearia (Nice, France). SU-8 silicone wafer used as template for fabricating microfluidics chamber. Prostaglandin E1 (PGE1), apyrase and ethylenediaminetetraacetic acid (EDTA) all from Sigma-Aldrich (Dorset, UK). Blunt-end Luer lock syringe needles (20G), stainless steel straight PDMS couplers and Tygon ND 100-80 tubing (0.76mm x 2.29mm) from Darwin microfluidics (Paris, France). AL-1000 syringe pumps bought from World Precision Instruments (Hertfordshire, UK).

2.16 Microscopes

The laser scanning confocal microscope used had the following specifications: Leica SP8 AOBS confocal laser scanning microscope attached to a Leica DM I8 inverted epifluorescence microscope was used to capture images. A FITC, RHOD and DAPI filter was used. The 405, 488, 561 and 647nm lasers were used. The 63x HC PL APO CS2 oil lens was used. Z stacks were captured using the optimal z distance produced by the software. The laser scanning confocal microscope is labelled 'confocal 12'. The scanning electron microscope used was a Quanta 200 – FEIFEG-SEM. The widefield microscope used to acquire brightfield images of the microfluidics systems was a Leica DMI6000 inverted epifluorescence microscope. 10X HC PL Gluotar and 20X N PLAN lenses were used. Both lenses were dry. The widefield microscope used had the following specifications: Leica LASX live cell imaging workstation with Photometrics Prime 95B sCMOS camera (1200x1200 11µm pixels, 8 ,12 bit or 16 bit, 70 fps full frame). The name of the microscope is 'Widefield 5'. All microscopes used were located in the Wolfson Bioimaging facility (Bristol, UK). Further details and specifications of specific microscopes can be found on the Bristol University website, under the Wolfson Bioimaging Facility section. The numerical names of the microscopes used is given above. All macros used for quantification of acquired images were produced by Dr Stephen Cross (Bristol, UK).

2.2 Methods

2.21 Mice

Wild-type male or female C57BL/6 mice purchased from Envigo. Use of animals was approved by Animal Welfare and Ethical Review Body (AWERB) and licensed under the UK Home Office project license 5643338. Following training by the local Animal Service Unit, all techniques were carried out with utmost care to minimise animal suffering.

2.22 Culturing and Differentiation of Murine Megakaryocytes

6–12-week-old C57BL/6 mice were sacrificed in a rising CO_2 chamber before confirmation of death via neck dislocation or exsanguination (Schedule 1 approved). Femurs and tibias were isolated and stored in PBS. Under sterile conditions, the bone marrow was PBS flushed before centrifuging at 300g for 5 minutes. Bone marrow pellet was resuspended in growth media. Media used was IMDM + Glutamax containing ~2% pen/strep and ~15% FBS with recombinant murine TPO and, occasionally, recombinant murine SCF at approximately 50ng/ml. SCF use was not essential, thus was ceased part way through the project. Cultures were grown in 12 well plates from days 1-3. Culture was transferred into 6 well plates on day 3 and subsequently had media changes every 2-3 days. Mature megakaryocytes were harvested for experimentation from days 4-15. Cultures were incubated at 37°C and 5% CO_2.

2.23 Flow Cytometry sorting and Gating Strategy

A BD Accuri™ C6 Plus flow cytometer was used. Firstly, doublets were removed by using a forward scatter height vs forward scatter width plot. Generated platelets were gated off the size and granularity of washed mouse platelets. Viability was gated from a washed mouse platelet preparation where half of the sample was boiled at 95°C for 5 minutes before plunging into ice for 5 minutes. Two populations

were created indicating the divide between live and dead cells. Draq5 was gated by mixing a sample of mouse haemopoietic stem cells and washed mouse platelets. This then created a dual population of nucleated cells and anucleate cells. The split of these populations allowed gating for DNA content in produced platelets. Background PE fluorescence was set by mixing PE anti-CD41 stained washed mouse platelets and unstained washed mouse platelets. Two populations occurred, indicating where background fluorescence was distinguished from CD41 labelling. Using this gating strategy, platelet sized particles which were free of DNA, viable cells and express PE was counted. A template from this was created. Following resuspension of generated platelets, as above, produced platelets were stained in a 96 well plate. Each stain was used in isolation and a final well with all stains was also present. 5ul of PE-CD41 was added to wells (final well total was 50µl (prior to addition of 8% PFA)). Calcein AM was added at 2µm. Draq5 was added at 1:500 from original stock vial. 42µl of platelet suspension was used in all wells. Tyrode's solution was used to make the volume of all wells up to 50µl. Cells were left to stain for 30 minutes, covered from light. 8% PFA was added 1:1 into each well, mixed and then analysed with the flow cytometer as quickly as possible. Each well was run for 10,000 events. The number of 'platelet' events per µl was multiplied by 2.38 (scaling factor because each well had 100µl final volume and 42µl of that was platelet suspension) and divided by 8 (as solution passage through systems originally had 8 MK/µl). This gave a platelet per MK estimate. Mouse platelets, for gating, were obtained via venepuncture of the inferior vena cava, following schedule 1. This was conducted with a 25G needle (orange) and 1ml syringe preloaded with acid citrate dextrose and 4% citrate.

2.24 Microfluidics System Fabrication

Three different microfluidics systems were used. The 'Smooth Branched' and 'Serpentine' microfluidics systems were later iterations of the original 'Branched' system. The structure of these is visualised in Fig. 7. The Branched and smooth branched microfluidics systems used were designed to mimic human lung vasculature. The branched and smooth branched designs were composed of branching rectangular channels of 15µm depth. The inlet channel was 100µm wide. Each channel branches into 16 channels with a halved width resulting in the narrowest channels with a width of 12.5µm. The sinusoidal system consisted of 200µm channels with multiple 50µm regions. The depth of these channels was 50µm**.** The chambers had one inlet port and one outlet port. The chamber was fabricated in PDMS using soft lithography. A SU-8 silicone wafer template was created using a direct laser writer device. PDMS and curing agent (10:1 mixture) was poured over the SU-8 wafer. The wafer was degassed in a vacuum desiccator prior to this. PDMS was cured at 80°C for 2 hours. Inlet and outlet holes were punched into the PDMS using a 0.5mm OD biopsy puncher (Elveflow) (Paris, France). The PDMS was finally plasma bonded to a glass slide for 3 minutes (Diener Plasma Systems) (Ebhausen, Germany).

2.25 Microfluidics System Operation

MK cultures were spun at 1000RPM for 10 minutes. The cell pellet was resuspended in ~2ml of IMDM + Glutamax media without FCS or Pen/Strep (raw IMDM). This was gently layered on a 4% and 2% BSA gradient in a 50ml Falcon tube (4ml of each BSA concentration. This gradient was left at 37°C and 5% CO_2 for 20-45 minutes. If a pellet could be seen by eye the gradient was stopped. This was in an attempt to minimise HSCs within the pellet. Isolated MKs were resuspended in raw IMDM. If MKs were being used for flow cytometry, the cells were stained with PE-CD41 antibody for 3 hours at 37°C, with a mixing step at hours 1 and 2 to provide more even staining. If MKs were used for microscopy, no pre staining of

antibody was required. MKs were counted on a haemocytometer, using trypan blue. For flow cytometry, cell concentration was adjusted to ~8 MKs/ml CGS. For microscopy, cell concentration was not adjusted. To minimise bias, due to the subjective nature of cell counting, at least two samples were counted, and an average taken. Use of a second lab member was also used to reduce counting bias. Immedietly prior to passaging, platelet inhibitors were added to the MK solution to reduce platelet clotting inside channels. The following inhibitors and their working concentrations were used: PGE1, 2.8mm; Apyrase, 1 unit/ml; EDTA, 5mM. The MK solution was then loaded into a syringe, mounted onto a syringe pump, and connected to the microfluidics system of choice. This consisted of a microfluidics chip with a 20G coupler at the inlet and outlet connected to tygon tubing. The inlet tubing had a blunt end Leur lock 20G syringe needle to attach the tubing to the syringe. The radius was adjusted as per manufacturer instructions and flow rate set to 0.3ml/minute. 2.5ml Thermo-Fischer syringes were often used and a radius of 8.7mm was picked. After passaging the solution through the microfluidics system, the perfusate was gently mixed and drawn back into the syringe and mounted again. The MK solution was passaged multiple times. A 2ml CGS flush was completed after the final passage to remove any solution or cells remaining within the microfluidics chamber. For flow cytometry, the perfusate was spun at 700G for 10 minutes and the pellet resuspended in 500ul of Tyrode's buffer so platelets per MK could be more accurately calculated.

2.26 Brightfield Imaging of Microfluidics Systems

All 3 microfluidics devices were imaged after the third and sixth passage. For the branched and smooth branched chip, some common locations were imaged for comparison and to observe in cells within the system. These regions are shown in Fig. 24. *These* areas were decided to be representative of the entire system. Any other areas of interest were also imaged to collect as much information about potential platelet producing mechanisms within the systems. These other images were not included in the quantification of blockages. In the sinusoidal system, multiple regions of all 10 channels were imaged. Note that the branched chip was mounted on a custom built, coverslip glass whilst the smooth branched and sinusoidal chip were mounted on thicker sections of glass, altering the diffraction of light, and thus differing the magnification seen at different lenses.

2.27 Confocal Microscopy Preparation and Image Acquisition

Cells were fixed with an 8% PFA solution, using a 1:1 dilution. In some preparations, this solution contained 4% glutaraldehyde. Cells were fixed for 20-30 minutes. The author found that 20-minute fixation yielded the highest quality images. Fixative was washed out by spinning at 100G for 5 minutes if imaging megakaryocytes or at 1000G for 10 minutes if imaging platelets. All subsequent washes followed this protocol. Triton X-100 in PBS was used to permeabilise the cells, before washing again. Next, cells were blocked in a 2% BSA/ 2% donkey serum, PBS solution for a minimum of 30 minutes. Antibodies (or IgG equivalent) were added to solution and left to stain overnight, under agitation at 4 °C. The next day, primary antibodies were washed out and then washed three times. Cells were resuspended in the BSA/donkey serum solution and secondary AlexaFluor conjugated antibodies were added. Cells were incubated with secondary antibodies under agitations for 3-4 hours at room temperature. Secondary antibodies were washed off, followed by three further washes. Final cell samples were resuspended in 300-500ml PBS. Cell solutions were spun onto acid washed, microscopy slides using a Epredia Cytospin4. Megakaryocyte preparations were spun at 500 RPM for 5 minutes with

low acceleration or at 1200 RPM for 7 minutes with high acceleration if imaging platelets. A 13mm coverslip was mounted onto the microscopy slide using DAPI-containing mounting media. After the mounting media has cured, slides were stored at 4°C prior to imaging. All images were captured using oil lenses. Samples were scanned sequentially using four different lasers: 405nm, 488nm, 561nm and 647nm and standard FITC, RHOD and DAPI filters. Z-stacks were taken with the automatically optimised step size. When imaging the perfusate from the microfluidic devices, fields of views for imaging were chosen using the following technique. Once focused, the navigate function was used and an area randomly selected using the CD41 and brightfield channels. If a CD41 positive cell was seen in this field of view, the surrounding area was searched to maximise number of cells in the field of view. The original cell seen when searching is always ensured to remain in the field of view. 5-10 images per preparation were captured. Ideally more fields of view would be imaged, however due to large sample number this was not feasible.

2.28 Scanning Electron Microscopy Acquisition and Image acquisition

The perfusate from microfluidics systems was collected after 6 passages and a CGS flush. The samples were quickly fixed 1:1 with an 8% PFA solution in PBS for 20-30 minutes at room temperature. Following this, samples were spun at 100g for 5 minutes to pellet megakaryocytes. This pellet was discarded. The supernatant was gently transferred to a fresh falcon tube and spun at 1000g for 10 minutes to pellet platelets in the solution. Pellet was resuspended in 100ul of PBS. 50-100ul of platelet suspension was dropped onto pre-warmed poly-L-lysine coated cover slips and left at 37°C for at least 2 hours. Platelet suspension was gently aspirate off and gently covered with PBS to prevent drying out before next washing steps. Cover slip was washed 3 times using 0.1M sodium cacodylate buffer (3 minutes per wash), avoiding agitation to prevent cells detaching from cover slip. Next, cells were exposed to a 30-minute post fixation using 1% Osmium tetroxide in a 0.1M sodium cacodylate buffer and deionised water. Another 3 washing steps were then conducted. Cells were then dehydrated using an ethanol dehydration series consisting of 30%, 50%, 70%, 90% and 100% for 3 minutes each. Following this, coverslips were submerged in hexamethyldisilazane for 30 minutes. After this, cover slips are left to air dry in the fume hood overnight. Next day, cover slips were mounted onto stubs using double sided, carbon sticky pads. Cover slips were then sputter coated in a gold/platinum mixture using a sputter coater for 45 seconds at 40mA. Stubs were stored at room temperature in a box, away from dust until imaging. Image acquisition was completed on a Quanta 200 scanning electron microscope.

2.29 Statistics and Analysis

All numerical data was visualised and analysed using GraphPad Prism 9. Statistical analyses for each data set are as follows. Figure 8, a Friedman's test with Dunn's post hoc was used. A non-parametric test was chosen due to failed normality. In figure 12, mixed-effects analyses with Dunnett's multiple comparison post hoc tests were used as data was paired. In figures 25 and 26, two-way ANOVA with Tukey's post-hoc test were used. Microscopy images were analysed using FIJI (FIJI Is Just Image-J) and Leica LASX software. Immunofluorescent images were analysed using a trained macro, uploaded into FIJI that segmented and outlined MKs using CD41. Each cell was then randomly assigned a number and then intensity of each fluorescent channel for each cell was then measured for the entirety of the Z-stack. Cell diameter and cell sphericity was also measured using this software. Blockages within the chip was quantified using a different macro that outlined and measured the area of the channels and then

detected and measured the percentage of the channel covered by cells. This macro was trained using images of the branched system. It was thus optimised for quantifying the branched chip. The macro was also used on the smooth branched chip due to the similarity in chip designs.

3. Results

Discussion of results was kept to a minimum. Where brief justifications were required for ease of understanding or if interpretations should be treated with caution, this was stated.

3.1 Laser Scanning Confocal Microscopy Optimisation

3.11 Introduction

Flow cytometry is a widely used technique in biomedical science, and the platelet production field is no exception to this. It is an excellent tool for studying *in vitro* platelets production, however other techniques are required to understand the platelet producing mechanisms within the microfluidics chips. Note, for ease of communication, the *in vitro* microfluidics systems will be referred to as 'chips' from this point onwards. Microscopy enabled the viewing of samples entering the chips, passaging through and the product exiting the chips. This revealed a new, and more in-depth insight into the functionality of the chips. Laser scanning confocal microscopy was one of the techniques used. This was chosen as it provided the magnification and resolution required to image fluorescently labelled platelets and MKs. These fluorescent tags allowed identification of true platelets, disregarding artefacts and irrelevant cells. It also enabled analysis of any changes that occurred to MKs after passaging through the system. To confidently study cells using laser scanning confocal microscopy, a trusted and optimised protocol was required. Multiple experiments and consultation with other researchers were required to design the finalised protocol.

3.12 Proteins and organelles of interest

For all fluorescent images, the same four markers were stained for. Firstly, nuclear content (DNA) was stained using a dye (DAPI). This allowed observation of the large, lobular, polyploid nucleus of megakaryocytes and could be used to exclude platelet sized cells, as platelets are anuclear. Secondly, CD41, also known as the αIIb integrin, one-half of the αIIbβ3 integrin complex vital for cross linking platelets. This was used as a membrane marker in both platelets and megakaryocytes. It allowed the perimeter of these cell to be marked, so cell size could accurately be measured. Furthermore, CD41 is

the first marker of commitment to megakaryocytes, thus is exclusively expressed in megakaryocytes and platelets(67). This marker allowed megakaryocytes and platelets to be distinguished from HSCs. CD41 also marked the invaginated membrane system (IMS) of MKs. The IMS was potentially an important structure to observe in platelet production due to the hypothesis that the large amount of internal membrane of MKs is present for forming the plasma membrane of platelet offspring(23).Thirdly, tubulin was stained. Tubulin exists as α and β isotypes. For the finalised protocol α-tubulin was stained. During the early stages of this work, β -tubulin was stained. α-tubulin and β-tubulin dimerise. These heterodimers polymerise to form large microtubules(68). Microtubules have been cited as critical for platelet production. The elongation of proplatelet protrusions from MKs is microtubule driven(32, 69). Staining of microtubules allowed identification of all cells in the preparation. Furthermore, true platelets exhibit a microtubule ring (often called a marginal band)(69). Microtubule staining helped in confidently identifying produced platelets. Moreover, microtubules changes in MKs, following passages through the microfluidics chips may have provided information on the platelet producing mechanisms occurring. Finally, P-selectin was stained. Also referred to as CD62P, this adhesion protein is packaged in α granules of MK and platelets(70). Another helpful marker in identifying true platelets as platelets and MKs were the only cells in these experiments that expressed P-selectin. Furthermore, changes in granularity of MKs following passages may have indicated if α-granules from MKs were being trafficked into produced platelets. CD41, α-tubulin and P-selectin were all stained for using protein specific primary antibodies and fluorophore labelled secondary antibodies. Details on antibodies used can be found in *table* 1. These four markers allowed for a detailed investigation and analysis of MKs and platelets using laser scanning confocal microscopy.

3.13 Pre-optimisation protocol

The starting protocol used was heavily flawed and produced poor quality images which could not be interpreted. Figs 3 and 4 were captured using this starting protocol. This protocol was as follows: Cells were stained in wells on 13mm coverslips. Cells were permeabilised for 15 minutes using 0.1% Triton X-100 followed by a blocking step using 3% BSA. This was meant to block non-specific binding of antibodies. Conjugated antibodies and primary antibodies were added to the samples, simultaneously. Cells were washed 2-3 times before addition of secondary antibodies. A final washing step and mounting of coverslips onto glass microscope slides was conducted before imaging. The antibody incubations were at room temperature, for 1 hour. Fig. 3 showed the four stained fluorescent channels with an overlay of all colours. Between the P-selectin, β-tubulin and CD41 channels no difference in staining patterns was seen. This indicated non-specific binding of antibodies to regions other than the proteins of interest. The likely cause of this was poor blocking steps, bad washing technique and a lack of care taken when considering species cross reactivity. Furthermore, cells were not blocked under agitation, causing cell settling. Fig. 4 exhibited further issues. The FITC labelled P-selectin produced a stronger signal under the 405 laser, as opposed to the expected 488 laser. This indicated some form of cross reactivity or bleed through between the nuclear DNA channel (405) and the P-selectin channel. Identifying one specific variable which caused the poor-quality images seen in Figs 3 and 4 was not possible as there was likely many.

3.14 Partially optimised protocol

Using these images, study of the literature and consultation with Dr Steve Thomas (Birmingham, UK) facilitated designing of a better-quality protocol. Figs 3 and 4 indicated that more care was needed when blocking non-specific binding and a new panel of antibody combinations was required. This newly

designed protocol is described in much detail within the material and methods section. The key changes implemented were as follows. All steps were conducted on cells suspended in solution, as opposed to having cells stuck to a cover slip. The rationale for this was to reduce waste caused by broken cover slips and to apply more thorough wash steps by spinning cells and resuspending. Better washing would reduce background fluorescence and more evenly apply reagents in solution under agitation. Donkey serum was added to the blocking solution, along with BSA. This would aid in blocking further non-specific binding sites, not blocked by BSA. This was particularly beneficial as the secondary antibodies used were raised in donkey. No primary antibodies were raised in donkey. The cells were also blocked for, at least, 30 minutes prior to addition of primary antibodies in an attempt to reduce non-specific binding. The antibodies used were also changed. CD41, α-tubulin and P-selectin were all stained with a primary – secondary antibody approach, using validated immunocytochemistry antibodies. Note that Fig. 5 was captured using a FITC-conjugated CD41. This was later changed for a conjugated anti CD41 antibody, which significantly improved CD41 staining. The panel of antibodies was designed to prevent species cross reactivity. The use of primary and secondary antibodies would amplify any weaker signals seen. The duration of antibody incubations was also changed. Cells were stained with primary antibodies over night at 4°C. Next day, the secondary antibodies were incubated for 3-4 hours at room temperature, following thorough washing. It was found that these durations gave thorough binding of proteins with minimal non-specific binding.

Controls were conducted for the new protocol. These controls included replacement of primary antibodies with IgG controls to prove non-specific binding was absent or minimal. These controls showed little to no staining (data not shown). Another control conducted was imaging samples with only one primary antibody marker, but with all the secondary antibodies as usual (data not shown). This confirmed that the labelling seen was the protein of interest. A simple control on every experiment was conducted to check for bleed through between laser channels. This was done by imaging on a channel, turning off the corresponding laser and turning on a neighbouring laser channel. This showed little to no image, indicating that the fluorescence seen in this channel was indeed the protein of interest and not bleed through.

Figure 3

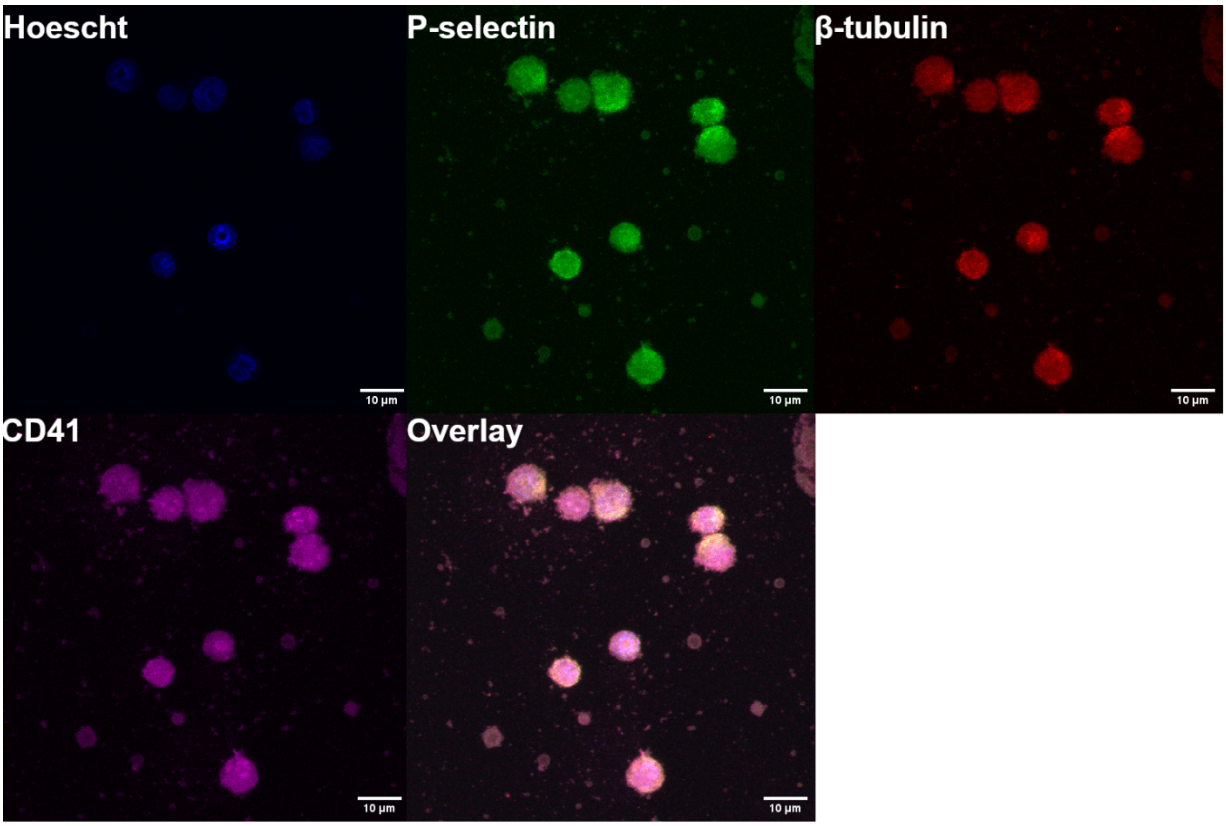

Figure 3 – Non-specific labelling of mouse bone marrow cells

Representative laser scanning confocal microscopy image of megakaryocytes presented as maximum intensity projections of Z-stacks. Four channels shown with an overlay of all channels. The nucleus (stained with Hoescht 33342), a-granules (P-selectin; stained with FITC-CD62P antibody), microtubules (b-tubulin; stained with b-tubulin primary and Alexa Fluor 568 secondary antibodies) and plasma membrane (CD41; stained with APC-CD41 antibody). Note that care was not taken of species specificity and cross-reactivity in this early protocol. Scale bars = 10mm. Images captured using a Leica SP8 multi-laser confocal laser scanning microscope with the 63x HC PL APO oil lens equipped. Further details on microscopy specifications are found in the Materials and Methods section.

Figure 4

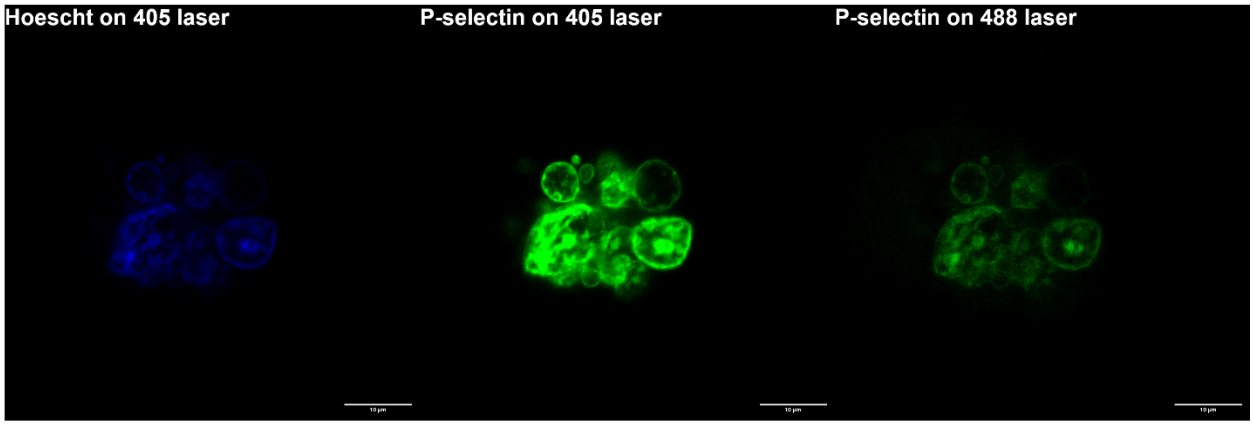

Figure 4 – Bleed through and non-specific binding images of mouse bone marrow cells

Representative laser scanning confocal microscopy images presented as maximum intensity projection of Z-stacks. Nuclear stain (Hoescht 33341) which was excited by the 405 laser shown. The FITC-CD62P antibody used to label P-selectin should have excited on the 488 laser. Here, P-selectin was shown brighter on the 405 laser than the 488 laser. The labelling between the nucleus and P-selectin was very similar, indicating non-specific binding and/or bleed through. Scale bars = 10mm. Images captured using a Leica SP8 multi-laser confocal laser scanning microscope with the 63x HC PL APO oil lens equipped. Further details on microscopy specifications are found in the Materials and Methods section.

Fig. 5 shows a mouse MK imaged using the improved, partially optimised protocol. It was a significant improvement in image quality. Labelling was specific, there was minimal non-specific binding and background. More could be interpreted from these images, however it still had limitations. As mentioned, the quality of the CD41 stain was moderate, with much of the background of the cell being stained. Furthermore, there was some bleed through between the CD41 and α-tubulin channels. The quality of the α-tubulin was also not optimal. The characteristic web-like structure was not seen. P-selectin labelling was low, considering MKs should have many α-granules(71). The hypothesis was that the poor labelling of α-tubulin and P-selectin was caused by under-permeabilization of the megakaryocytes. In Fig. 5 the cells were only permeabilised for 15 minutes using 0.1% triton X-100. Thus, a titration experiment of triton X-100 was conducted on megakaryocytes.

Figure 5

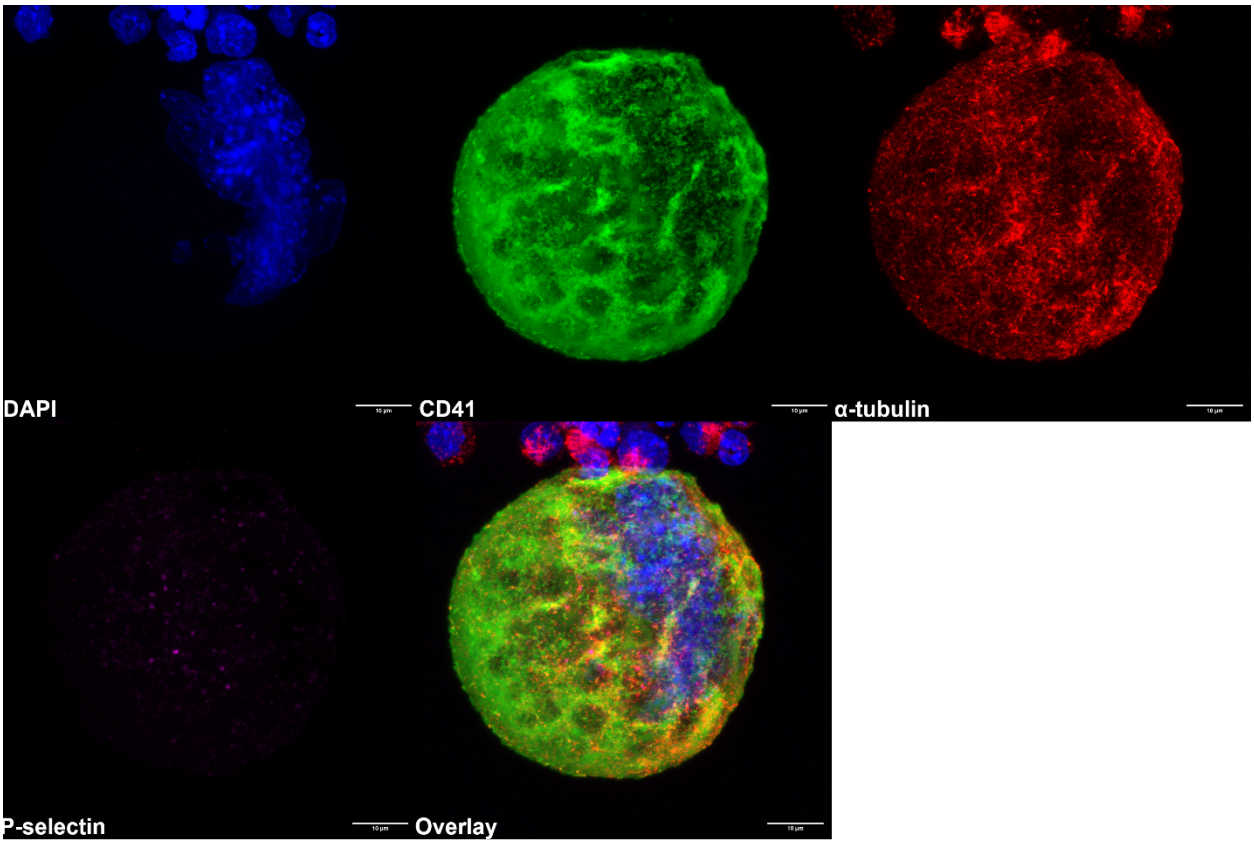

Figure 5 – Mouse megakaryocytes captured using a partially optimised protocol

Representative laser scanning confocal microscopy images presented as maximum intensity projection of Z-stack. First set of images captured using a partially optimised protocol. Cells were permeabilized for 15 minutes using 0.1% Triton X-100. DNA nucleus stained with DAPI. Plasma membrane stained using FITC-conjugated rat-CD41 antibody and donkey anti-rat Alexa Fluor 488 secondary antibody. Microtubules stained using rabbit a-tubulin antibody and donkey anti-rabbit Alexa Fluor 568. a-granules stained with goat CD62P and chicken anti-goat Alexa Fluor 647. Scale bars = 10µm. Images captured using a Leica SP8 multi-laser confocal laser scanning microscope with the 63x HC PL APO oil lens equipped. Further details on microscopy specifications are found in the Materials and Methods section.

3.15 Altering permeabilization

The result of this Triton X-100 titration was shown in Fig. 6. The main finding was that 0.2% triton X-100 applied to megakaryocytes for 1 hour was optimal for visualising the separated microtubules, the invaginated membrane and α-granules. Permeabilising with 0.1% for 1 hour was an improvement from using 0.1% for 15 minutes however it still had limitations. The web-like nature of tubulin was not fully developed, therefore any future experiments where quantitative analysis of tubulin was required, analysis would be flawed. Furthermore, α-granule labelling, using P-selectin as a marker, was weaker compared to 0.2% (when inspected by eye). Note that each granule was marked by a bright, magenta spot as seen in Pluthero and Kahr (2018)(72). The hypothesis was that primary and/or secondary antibodies were unable to penetrate that deep into the extremely large and highly membraned megakaryocyte. Conversely, 0.3% triton X-100 for 1 hour appeared to over-permeabilise the cells. The plasma membrane (CD41 labelled) and microtubules (α-tubulin labelled) seemed to have lost their structural integrity. Granule staining was more thorough however changes to MKs would not be able to

be fairly interpreted when other markers were affected by over-permeabilisation. Although all these interpretations were qualitative, it was decided that permeabilising the MKs for 1 hour using 0.2% triton X-100 would allow for the best interpretation of future analyses. Furthermore, a common issue seen in pre-optimised preparations was that some cells were well stained whilst some were extremely under-stained and other over saturated with antibody. This issue was resolved by conducting all blocking, permeabilisation and staining steps under agitation. This prevented MKs settling in the bottom of the container, thus creating more evenly stained samples (data not shown).

An efficient protocol which produced high quality and representative images of mouse megakaryocytes had now been finalised. This protocol was taken forward to begin analysing *in vitro* platelet producing mechanisms.

Figure 6

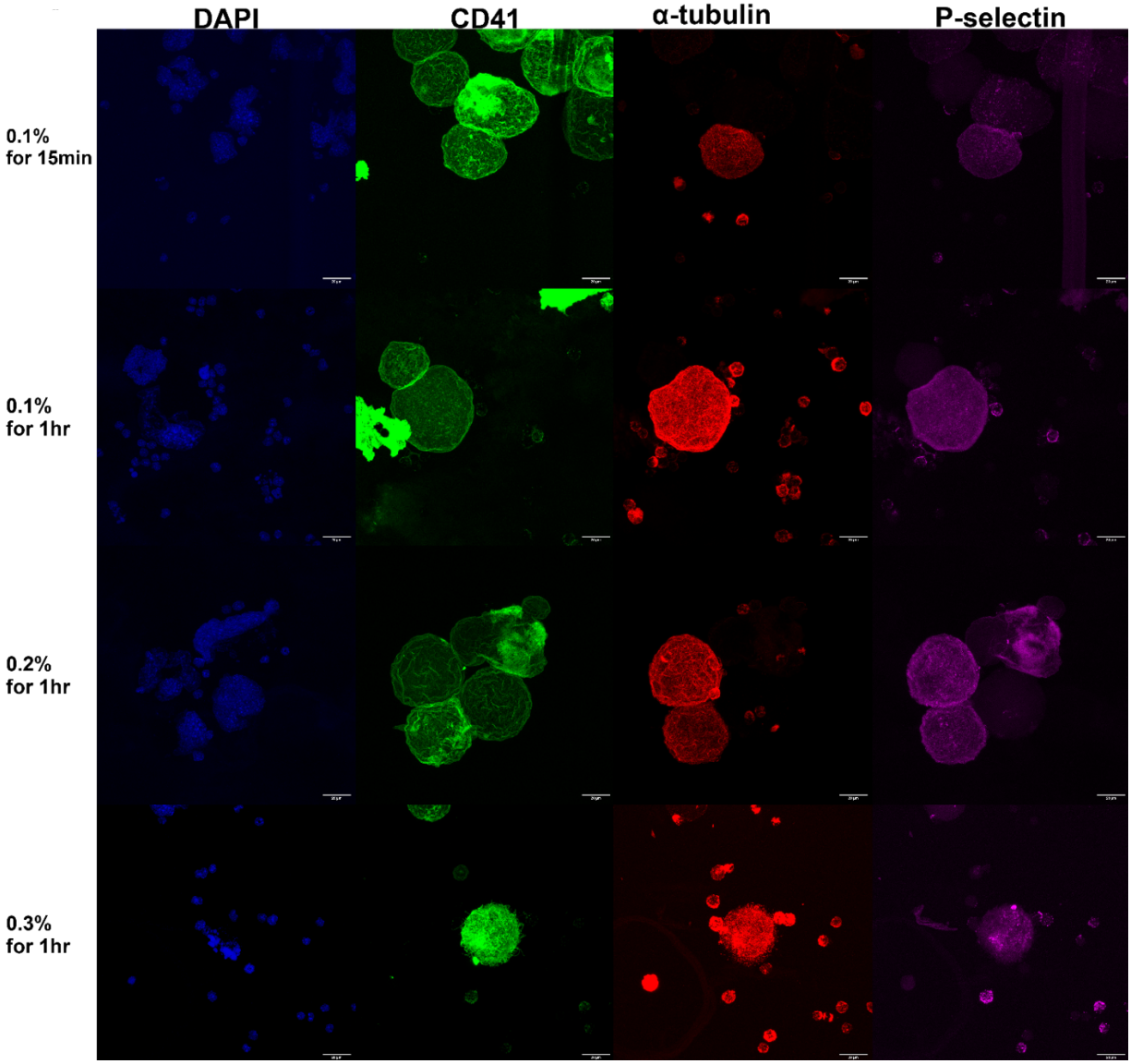

Figure 6 – Permeabilization of Mouse Megakaryocytes Using 0.2% Triton X-100 for 1 hour is Optimal for Imaging Microtubules and a-granules

Representative laser scanning confocal microscopy images presented as maximum intensity projections of Z-stacks. A titration of triton X-100 concentrations with varied incubation times. Nuclear DNA stained with DAPI. Plasma membrane stained using a rat CD41 primary antibody and donkey anti-rat Alexa Fluor 488 secondary antibody. Microtubules stained using rabbit a-tubulin primary antibody and donkey anti-rabbit Alexa Fluor 568. a-granules stained with goat CD62P primary antibody and chicken anti-goat Alexa Fluor 647. Scale bars = 20µm. Images captured using a Leica SP8 multi-laser confocal laser scanning microscope with the 63x HC PL APO oil lens equipped. Further details on microscopy specifications are found in the Materials and Methods section.

3.2 Assessing Productivity of Microfluidics Systems

In this dissertation, 3 microfluidics systems with different designs were tested. The designs aimed to alter different variables to unpick factors important for an *in vitro* platelet producing system. Fig. 7 shows schematics of these 3 systems.

3.21 Microfluidics system designs

Descriptions and rationale for these designs was as follows. The branched system was the first design and was designed to roughly mimic the shape of the capillary beds in the lungs(51, 52) (Fig. 7A). All channels had a rectangular shape. They were 10µm deep (top to bottom) with varying widths. The channels started with a width of 100µm. Each of these large channels halved in width at branching points until the smallest width of 12.5µm was reached. Cells flowed in through the large 100µm channels, travel through into the smaller channels and then progress back into larger channels before exiting the system. 6 sets of channels ran in parallel**.** The shear stress and pressure in this system was very high: much greater than physiological levels. Because of the small channel diameter, MKs passing through will undergo great amounts of compression. As mentioned previously, MK diameter can reach up to 100µm, which is much greater than 12.5µm(19). This branched system provided information on the importance of a) branching structure, b) compression of MKs through narrow channels and c) high shear stress on *in vitro* platelet production. The smooth branched microfluidics chip had all the same characteristics and structure as the branched chip with one exception. The branched microfluidics chip had sharp edged corners whilst the smooth branched chip had rounded edged corners (Fig. 7B). The rationale for this design was that sharp edges are not found *in vivo*. It was unknown whether sharp edges were damaging cells or facilitating capture of MKs on branch points. The third and final design was the sinusoidal design (Figs 7C, D and E). The rationale for this design was that the shear stress in the branched and smooth branched chips may be too high, risking damaging the cells or pre-activating platelets. Thus, the sinusoidal microfluidics chip was created to have much lower shear stress levels, closer to physiological. This system was also able to apply small amounts of compression to large MKs. To achieve this, minimal branching was present, and the width of the channels was greater. At its narrowest, the channels were 50µm (which was wider than many, but not all megakaryocytes. This design imparted much less pressure and compression to MKs. Therefore, the sinusoidal microfluidics design could elucidate if compression and branching are key factors for *in vitro* platelet production. Previous pilot data has shown that shear stress is important but not the only factor important in platelet production. When the shear stress was increased in the branched chip by increasing flow rate of cells passing through, the number of platelets produced did not increase linearly (data not shown). This indicates other factors are involved and need to be unpicked. Simulation data showed all systems exhibited laminar flow.

Figure 7

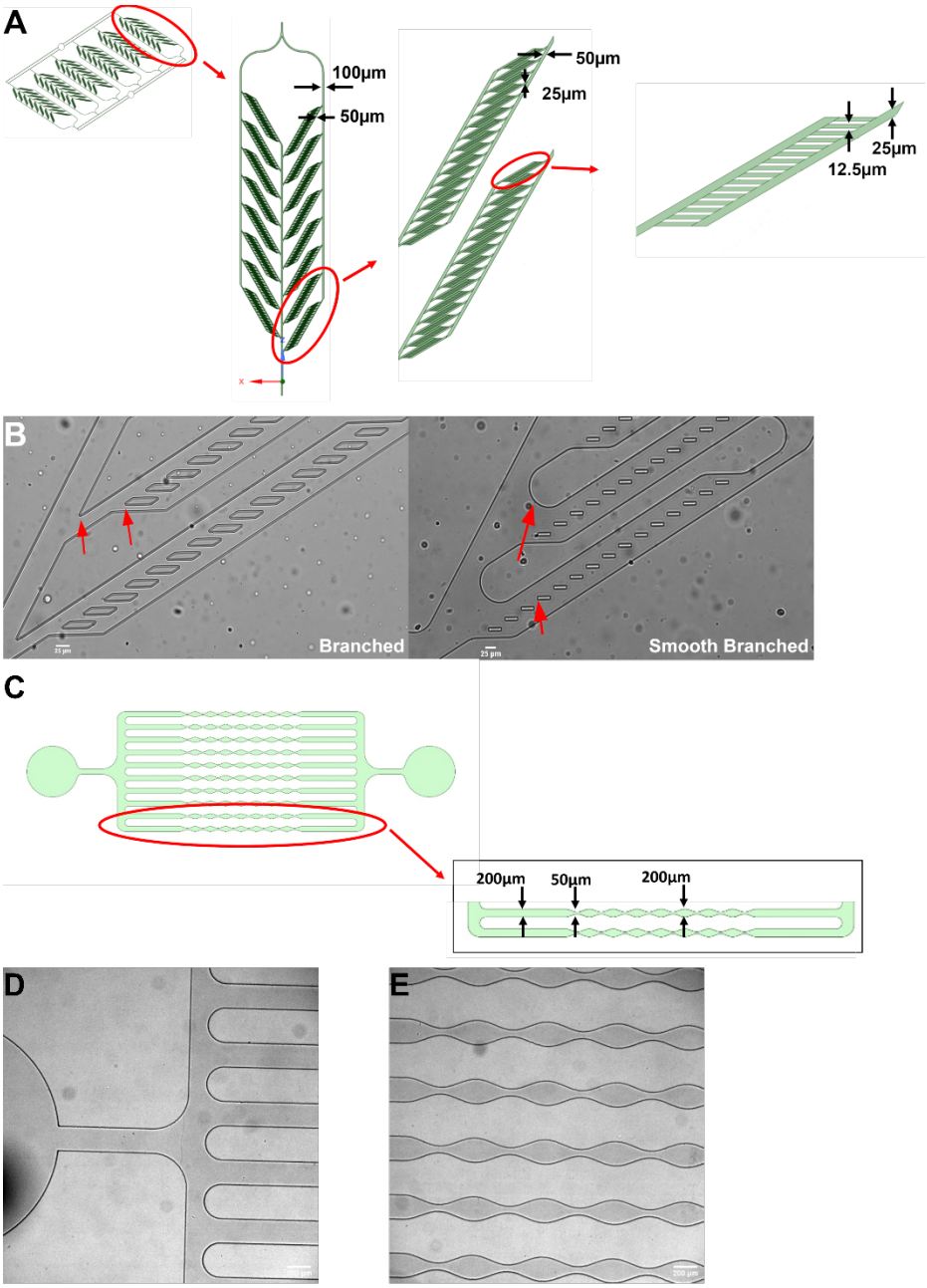

Figure 7 – The Structure of the 3 Microfluidics Systems.

(A) Schematic of the structure and measurements of the '**BRANCHED**' system. Red circles and arrows indicate zoomed in regions. Black arrows indicate measurements of the channels. The general structure and measurements were conserved in the '**SMOOTH BRANCHED'** system. The depth of the channels in the 'branched' and 'smooth branched' systems were 15µm. (B) Brightfield images showing the differences in structure of the 'branched' and 'smooth branched' systems. Red arrows highlight where the 'branched' system has sharp edges and 'smooth branched' system has rounded edges. Note – the magnification of the systems appeared different due to being imaged through different thickness of cover glass. This did not affect image interpretation. Images were captured on a Leica DMI6000 inverted microscope, using dry lenses. (C) Schematic of the structure and measurements of the

'**SINUSOIDAL**' system. Red circles and arrows indicated zoomed in regions. Black arrows indicate measurements of the channels. The depth of the channels in the 'sinusoidal' system was 50 µm. Brightfield images of the (D) inlet region and (E) 5 of the parallel channels from the 'sinusoidal' system.

3.22 Platelet producing efficiency

For the purposes of this work, anything that showed platelet characteristics was referred to as a platelet for ease of interpretation. The author believes that for a cell to truly be characterised as a platelet, functionality must be shown. Functional data for these assays was not feasible due to time constraints.

Platelet producing efficiency of the 3 chips was assessed using flow cytometry. (Note, all data from Fig. 8 was expressed as means with ± standard error of the mean (S.E.M)). Platelets were defined using the following gating strategy. Platelet sized, viable, lacking DNA and expressing surface CD41. Further details on designing this gating strategy can be found in the material and methods section and discussion of its validity is in the discussions section. By counting the number of total platelets produced per µl of sample, an estimate of how many platelets were produced per MK loaded into the system was calculated. Fig. 8A showed the results of this efficiency comparison. The main finding was that the branched system was more efficient in producing platelets (74.13 platelets/MK ±25.76) than the sinusoidal system (37.24 platelets/MK ±15.91) ($p = 0.0429$). There was no statistically significant difference in platelet production efficiency when comparing the branched and smooth branched (59.32 platelets/MK ±27.4) chips. However, a consistent trend for a decrease with the smooth branched chip was seen. Trends should be trusted with caution. In Fig. 8B, the percentage of platelet sized and DNA negative cells that were not viable (dead) was calculated. These cells were not gated on CD41, as presence of CD41 could have been altered by high shear and cell death. Interestingly, the sinusoidal chip was more damaging to platelets than the branched system. A higher percentage of cells were found to be dead following passage through the sinusoidal system (43.73% ±8.936), compared to the branched (31.68% ±9.511) ($p = 0.0429$). The smooth branched chip did not produce a statistically significant difference in percentage of dead cells from either the branched or sinusoidal system (35.7% ±9.548). However, a trend for higher percentage of dead cells compared to the branched and lower percentage compared to the sinusoidal was seen. Note, p values were the same between these experiments as the statistical tests performed were Friedman's tests with Dunn's post hoc multiple comparisons. The Friedman's test works on a ranking system, hence the pattern of p values.

Figure 8

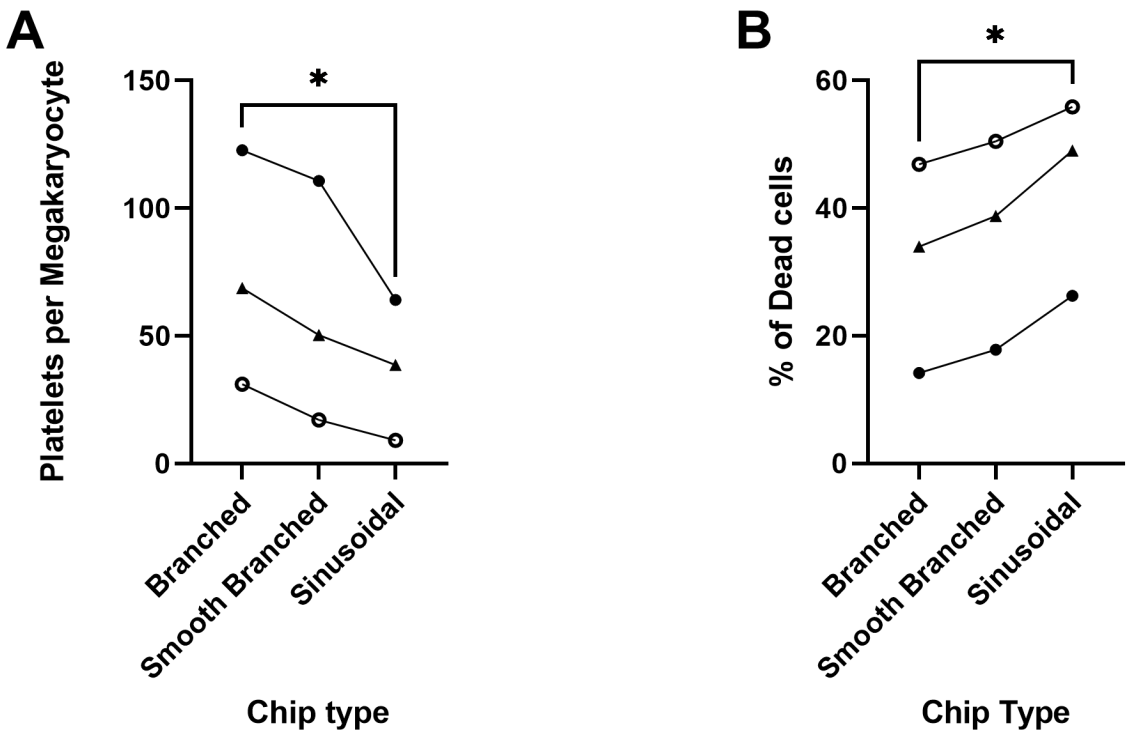

Figure 8 – 'Branched' system is the most efficient platelet producing system.

Mouse megakaryocytes were pre-stained with PE-CD41 for 3 hours prior to 6 repeated passages through one of three microfluidics systems (chips). The designs of these chips is found within the text (Fig. 7). Megakaryocytes were passaged at 300μl/min. The perfusate was quantified using flow cytometry. (A) Paired means comparing the number of platelets produced per megakaryocytes. Platelets were defined as being of platelet sized, intact membrane, lacking nuclear stain and expressing surface CD41. (B) Paired means of the percentage of dead 'platelets'. In this graph, platelets were characterised as dead if they were platelet sized, had no DNA and had a disrupted membrane. Both (A) and (B) are presented as before and after plots. Different symbols across A and B indicate which data came from the same culture and experimental run. The mean differences of the 3 independent experiments were statistically analysed using Friedman's test with Dunn's post hoc test. (* = $p \leq 0.05$).

The S.E.M of the branched and smooth branched chips appeared larger than the sinusoidal chip when comparing platelets produced per MK. This indicated more variability in performance in the branching design compared to the sinusoidal design. This was only a correlation, so should be trusted with caution. Using Fig. 8A, the following hypothesise were suggested. The channel designs seen in the branched and smooth branched system was better for producing platelets than the sinusoidal design. This could have been as a result of branching points, shear stress and/or compression. Interestingly, the sinusoidal chip was the most damaging of the 3 systems, even though it had the lowest shear stress. Having sharp edges in the branched system did not appear to be significantly damaging the platelets produced, as

there was no statistically significant difference in dead cells when comparing the branched and smooth branched chips.

In conclusion, the branched chip was the most efficient platelet producing system, indicating that the shape, shear stress and/or compression in this system were positively influencing platelet production.

3.3 Using Microscopy to Investigate In Vitro Platelet Production

3.31 Changes to megakaryocytes, following passage through microfluidics

With an optimised laser scanning confocal microscopy protocol, analysis of the perfusate of the 3 chips was conducted.

Figs 9, 10 and 11 showed MKs which had been able to pass through each of the chips. For the branched and smooth branched (Figs 9 and 10 respectively), this provided information on how MKs can alter their morphology greatly and survive high shear stress. In the perfusate, MKs many times larger than the smallest width in the branched and smooth branched chips (12.5µm at its narrowest) were seen. These cells remained viable (deduced by normal immunofluorescent staining of cells post passage, dead cells tend to be overly saturated with fluorophores). This also showed that, repeated passaging of the perfusate was justified, as the potential to produce more platelets remained after multiple passages.

Figure 9

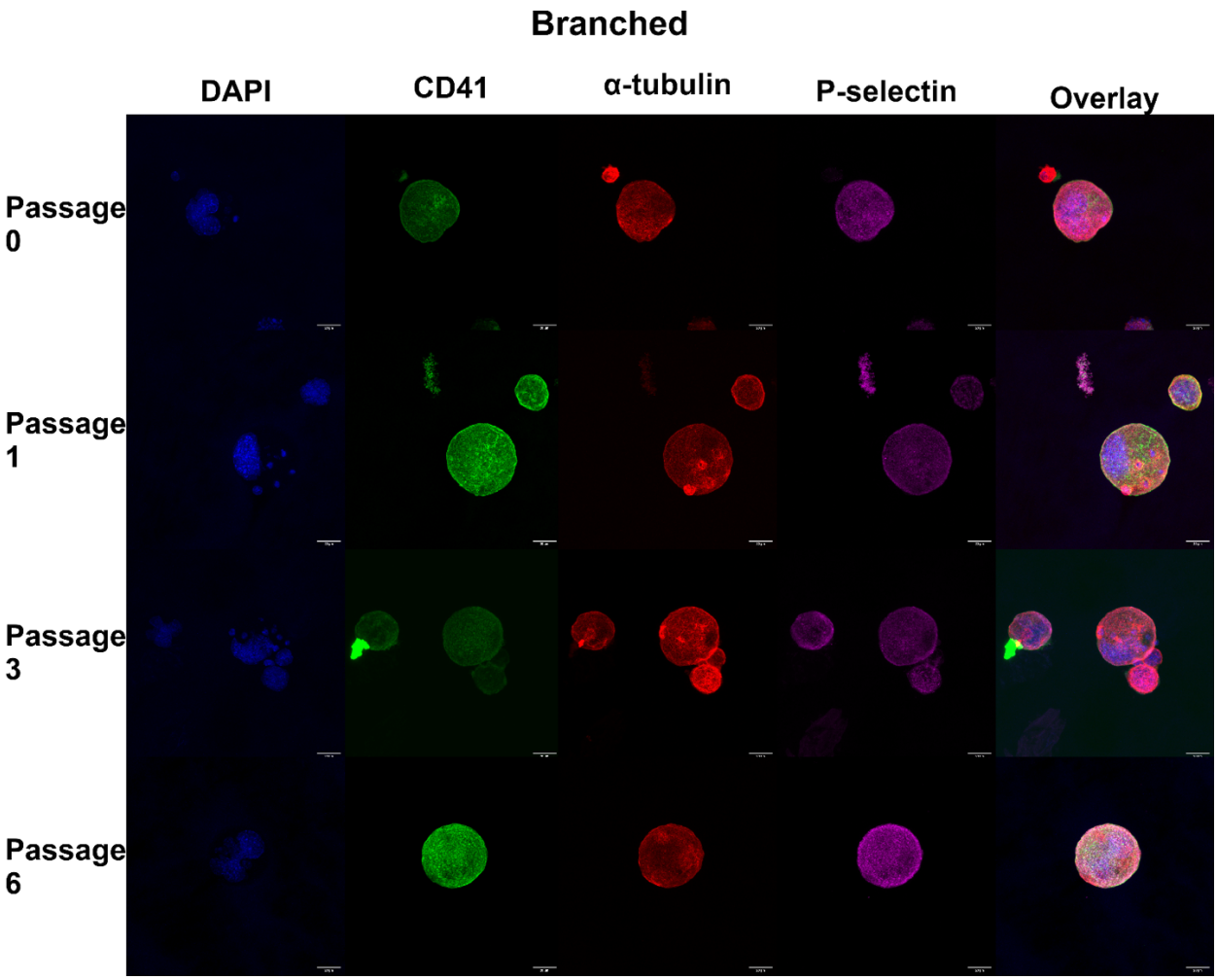

Figure 9 – Mouse Megakaryocytes Following 0, 1, 3 or 6 Passages Through the 'Branched' System. Mouse megakaryocytes were passed through the 'branched' microfluidics device 0, 1, 3 or 6 times at a flow rate of 300 ml/min. Following fixation, the perfusate was spun at 100g for 5 minutes, the pellet resuspended and the nucleus, CD41, a-tubulin and P-selectin stained. Representative laser scanning confocal micrographs of these cells are presented as maximum intensity projections of Z-stacks (n=3). Nuclear DNA stained with DAPI. Plasma membrane stained using an unconjugated rat CD41 primary antibody and donkey anti-rat Alexa Fluor 488 secondary antibody. Microtubules stained using rabbit a-tubulin primary antibody and donkey anti-rabbit Alexa Fluor 568. a-granules stained with goat CD62P primary antibody and donkey anti-goat Alexa Fluor 647. Scale bars = 20µm. Images captured using a Leica SP8 multi-laser confocal laser scanning microscope with the 63x HC PL APO oil lens equipped.

Figure 10

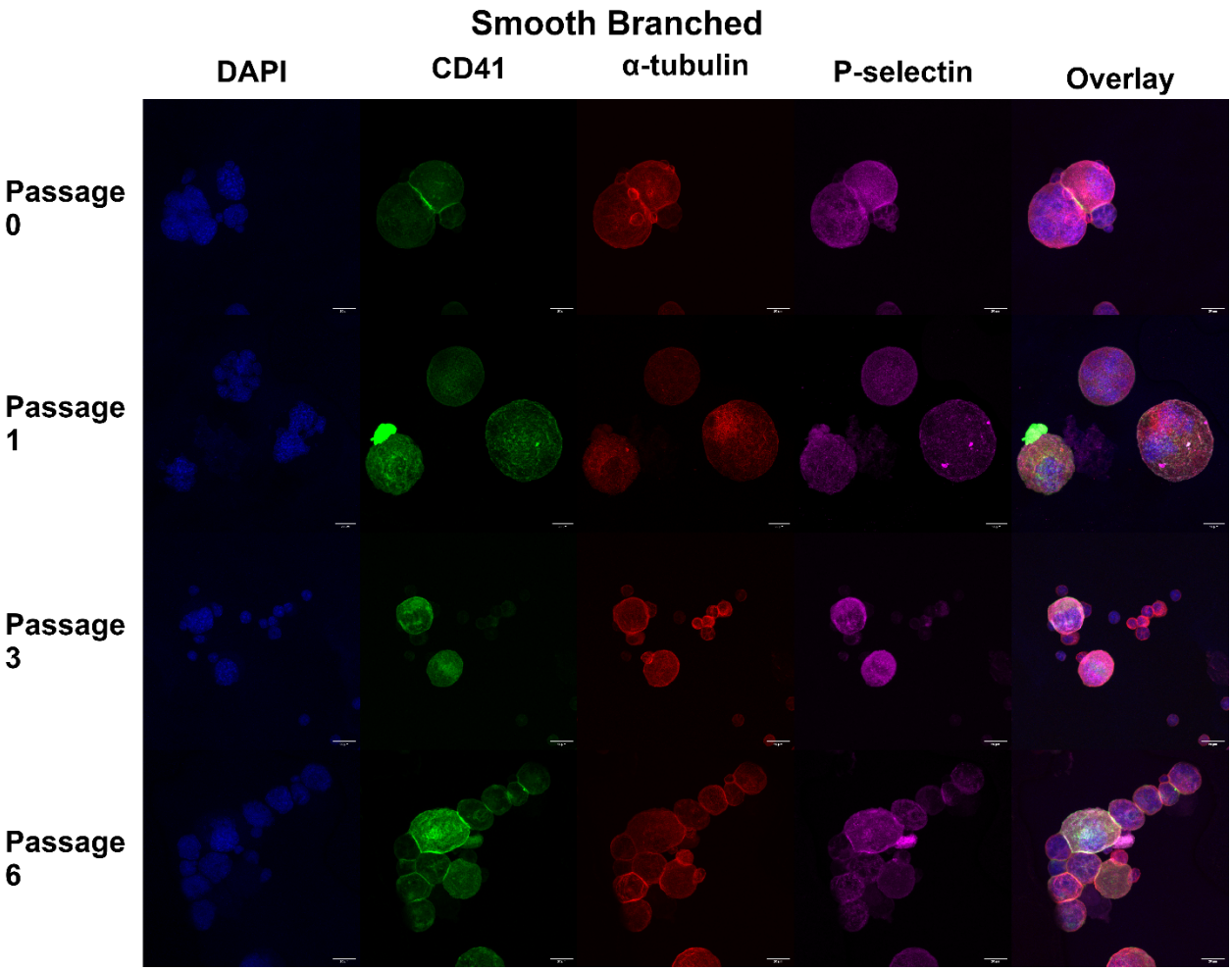

Figure 10 - Mouse Megakaryocytes Following 0, 1, 3 or 6 Passages Through the 'Smooth Branched' System.

Mouse megakaryocytes were passed through the 'smooth branched' microfluidics device 0, 1, 3 or 6 times at a flow rate of 300 μl/min. Following fixation, the perfusate was spun at 100g for 5 minutes, the pellet resuspended and the nucleus, CD41, α-tubulin and P-selectin stained. Representative laser scanning confocal micrographs of these cells are presented as maximum intensity projections of Z-stacks (n=3). Nuclear DNA stained with DAPI. Plasma membrane stained using an unconjugated rat CD41 primary antibody and donkey anti-rat Alexa Fluor 488 secondary antibody. Microtubules stained using rabbit a-tubulin primary antibody and donkey anti-rabbit Alexa Fluor 568. a-granules stained with goat CD62P primary antibody and donkey anti-goat Alexa Fluor 647. Scale bars = 20 μm. Images captured using a Leica SP8 multi-laser confocal laser scanning microscope with the 63x HC PL APO oil lens equipped.

Figure 11

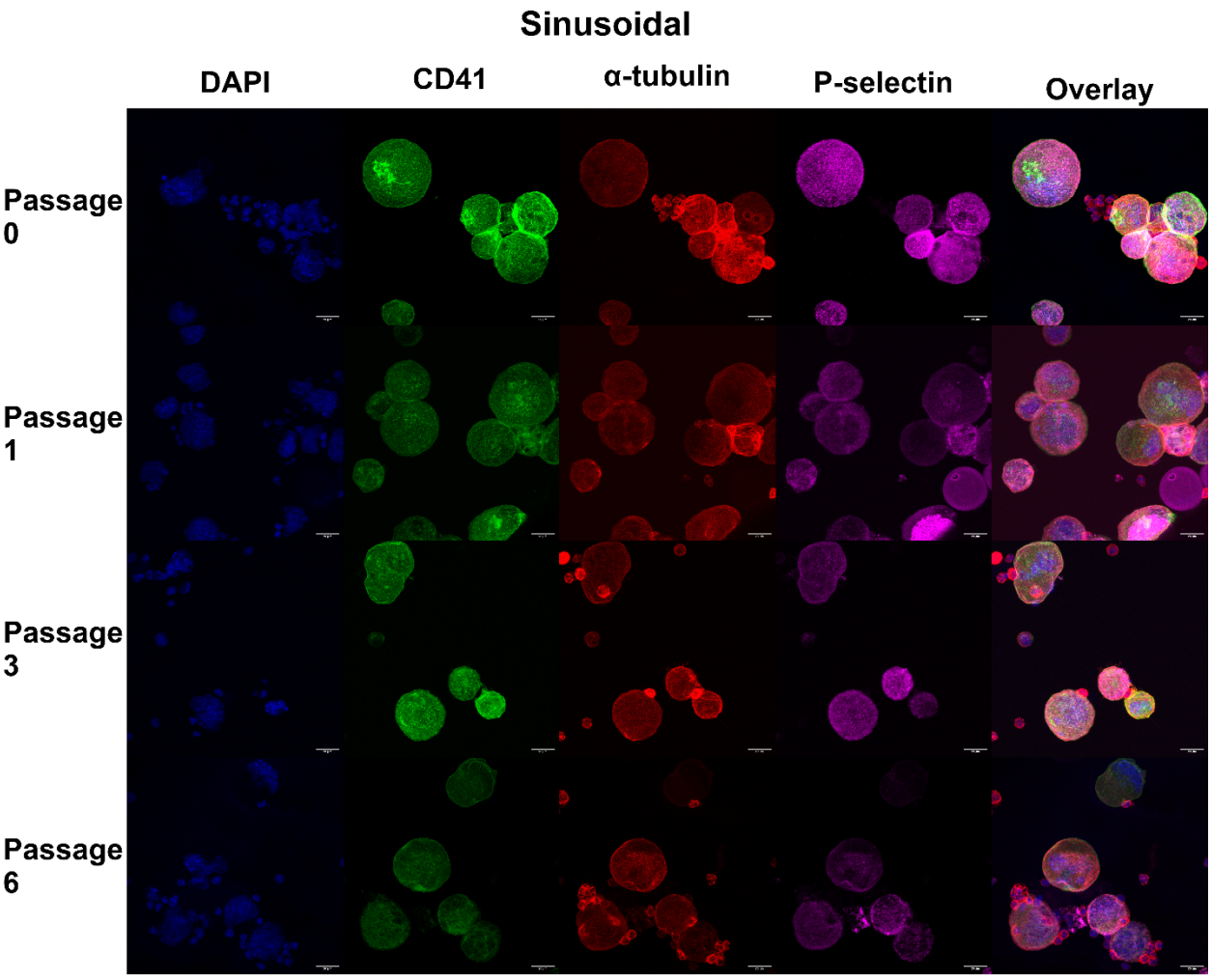

Figure 11 - Mouse Megakaryocytes Following 0, 1, 3 or 6 Passages Through the 'Sinusoidal' System.
Mouse megakaryocytes were passed through the 'sinusoidal' microfluidics device 0, 1, 3 or 6 times at a flow rate of 300 μl/min. Following fixation, the perfusate was spun at 100g for 5 minutes, the pellet resuspended and the nucleus, CD41, α-tubulin and P-selectin stained. Representative laser scanning confocal micrographs of these cells are presented as maximum intensity projections of Z-stacks (n=3). Nuclear DNA stained with DAPI. Plasma membrane stained using an unconjugated rat CD41 primary antibody and donkey anti-rat Alexa Fluor 488 secondary antibody. Microtubules stained using rabbit a-tubulin primary antibody and donkey anti-rabbit Alexa Fluor 568. a-granules stained with goat CD62P primary antibody and donkey anti-goat Alexa Fluor 647. Scale bars = 20μm. Images captured using a Leica SP8 multi-laser confocal laser scanning microscope with the 63x HC PL APO oil lens equipped.

3.31a Rationale for experiment

MKs following differing numbers of passages through the 3 chips were compared using the previously mentioned fluorescent panel. The rationale for this experiment was that, if producing platelets, the MKs may have changed to reflect this. The hypothesis was that if cells leaving the chip were producing platelets, they would exhibit the following changes. Decrease in cell size and amount of CD41 and microtubules as internal and external membrane, as well as microtubules would be sacrificed to form

platelets. The number of α-granules was also expected to decrease as produced platelets should be loaded with granules from parent MKs. An alternative hypothesis was that none of these markers would change as the MKs which were present in the perfusate of the chips were not producing platelets. The mechanism of platelet production may be occurring from MKs lodged within the system. Thus, the free flowing MKs passing through the chip were not producing platelets. How spherical the MKs were following passages was also analysed to deduce if compression in the small channels and/or shear stress was altering the shape of MKs.

3.31b Qualitative analysis

Figs 9, 10 and 11 showed representative laser scanning confocal microscopy images of MKs, following 0, 1, 3 or 6 passages, through the branched, smooth branched or sinusoidal chip respectively. Fig. 12 showed the quantification of these images. Qualitatively, MKs following any number of passages up to 6 in the branched, smooth branched or sinusoidal chip, appeared normal. Their poly-lobulated nuclei remained, they expressed CD41 on their plasma membrane and invaginated membranes, they had web-like structures of microtubules throughout the cell, and they contained α-granules, expressing P-selectin.

3.31c Quantitative analysis

All values, unless stated otherwise in the following analysis (Fig. 12) are expressed as medians as the data is presented in box and whisker plots, to improve transparency of data. The statistical tests performed were mixed-effects analysis with Dunnett's multiple comparisons. The rationale for using this test was that within each n, passages 1, 3 and 6 were matched from the same culture and run in parallel. The data for passage 0 was kept constant across the 3 chips. This was as a result of low n numbers, due to failures of the quantification system on these images. This analysis was chosen due to the absence of a non-parametric equivalent of a two-way ANVOA offered on GraphPad Prism 9. Further discussions on this analysis can be found in the discussions section.

Upon quantitative analysis, some changes were seen. All data on changes in cell diameter were shown in Fig. 12A. In the branched chip, following 6 passages, the MK cell diameter decreased from 40.55μm (passage 0) to 28.68μm ($p = 0.0217$). In the smooth branched chip, passage 3 and passage 6 MKs showed decreases in cell diameter (30.94μm and 29.66μm respectively) compared to passage 0 (40.55μm). The comparison of passage 0 and passage 3 gave a p value of 0.0061 and passage 0 and passage 6 comparison gave a p value of <0.0001. With regards to the sinusoidal chip, passages 1, 3 and 6 seemed to decrease cell diameter significantly compared to passage 0 (40.55μm) with the following medians and p values respectively: 33.03μm ($p =0.009$), 30.98μm ($p = <0.0001$) and 31.91μm ($p = <0.0001$). Data on cell sphericity was shown in Fig. 12B. In the branched chip, after 1 passage, cells became less spherical with a decrease in sphericity from 0.58 (arbitrary units) after 0 passages to 0.52 ($p = 0.0292$). The median values for passage 1, 3 and 6 were all decreased with respect to passage 0, however, passage 3 and 6 did not show statistical significance ($p =0.683$ and 0.200 respectively). The smooth branched chip showed no changes in cell sphericity between passages. 1 and 3 passages through the sinusoidal chip resulted in an increase in cell sphericity compared to passage 0 (0.578). The median and p values were 0.73 ($p = <0.0001$) and 0.64 ($p = 0.0376$) respectively.

The mean fluorescent intensities of nuclear DNA, CD41, α-tubulin and P-selectin were quantified. Analysis of nuclear DNA was shown in Fig. 12C. Using the branched chip, the amount of nuclear content increased after passage 3 (22.77 arbitrary units) with respect to passage 0 (11.81) ($p = 0.023$). No

significant change was seen after passages 1 or 6. The interquartile ranges and total ranges were large. Using the smooth branched system caused the amount of nuclear DNA to decrease after 1 passage (9.91. p = <-0.0001) but there was no significant change or trend for passages 3 and 6. For the sinusoidal chip, the same was seen. Post-passage 1, nuclear DNA decreased (9.47. p = 0.0013) but following passages 3 or 6, no significance or trend was seen.

Analysis of CD41 expression was shown in Fig. 12D. Using the branched chip, no statistically significant changes in CD41 were seen for any passage number. For the smooth branched chip, after 6 passages, the CD41 expression decreased (13.17) compared to passage 0 (18.13) (p = 0.0053). This supported the hypothesis that MKs lose membrane as a result of platelet production in the system. In the sinusoidal chip, after 1 passage, CD41 expression decreased (14.67) compared to passage 0 (18.13) (p = 0.0246). No statistically significant change was seen after passage 3 or 6, suggesting no true trend was present.

Analysis of α-tubulin expression was shown in Fig. 12E. In the branched chip, after 1 passage expression decreased (67.05. p = 0.0327) whereas expression increased after 3 passages (109.76. p = 0.0029) compared to passage 0 (96.02). Passage 6 showed a trend to increase expression, with a median greater than that of passage 3 (126.44) but no statistical significance was seen. This data appeared random, with no trend. In the smooth branched chip, tubulin expression increased after only passage 6 (111.03. p = <0.0001). For the sinusoidal chip, the same trend was seen with passage 6 increasing tubulin expression (110.59. p = 0.0145).

Finally, the analysis of P-selectin expression was visualised in Fig. 12F. In the branched chip, P-selectin expression increased only after 3 passages (44.02. p = 0.0322). After 6 passages, however, this significant change was lost, and the median value decreased (13.66) below the median of passage 0 (29.11). In the smooth branched chip, no statistically significant changes in P-selectin expression was seen for any of the passages. In the sinusoidal chip, decreases in P-selectin expression were seen after passages 1 (16.25. p =0.0001) and 6 (14.91. p = <0.0001).

All the data shown in Fig. 12 could not be interpreted with any confidence. This was as a result of poor experimental design and will be explained further in the discussions section. What could be concluded was that MKs were able to pass through all 3 chips, multiple times and remain viable.

Figure 12

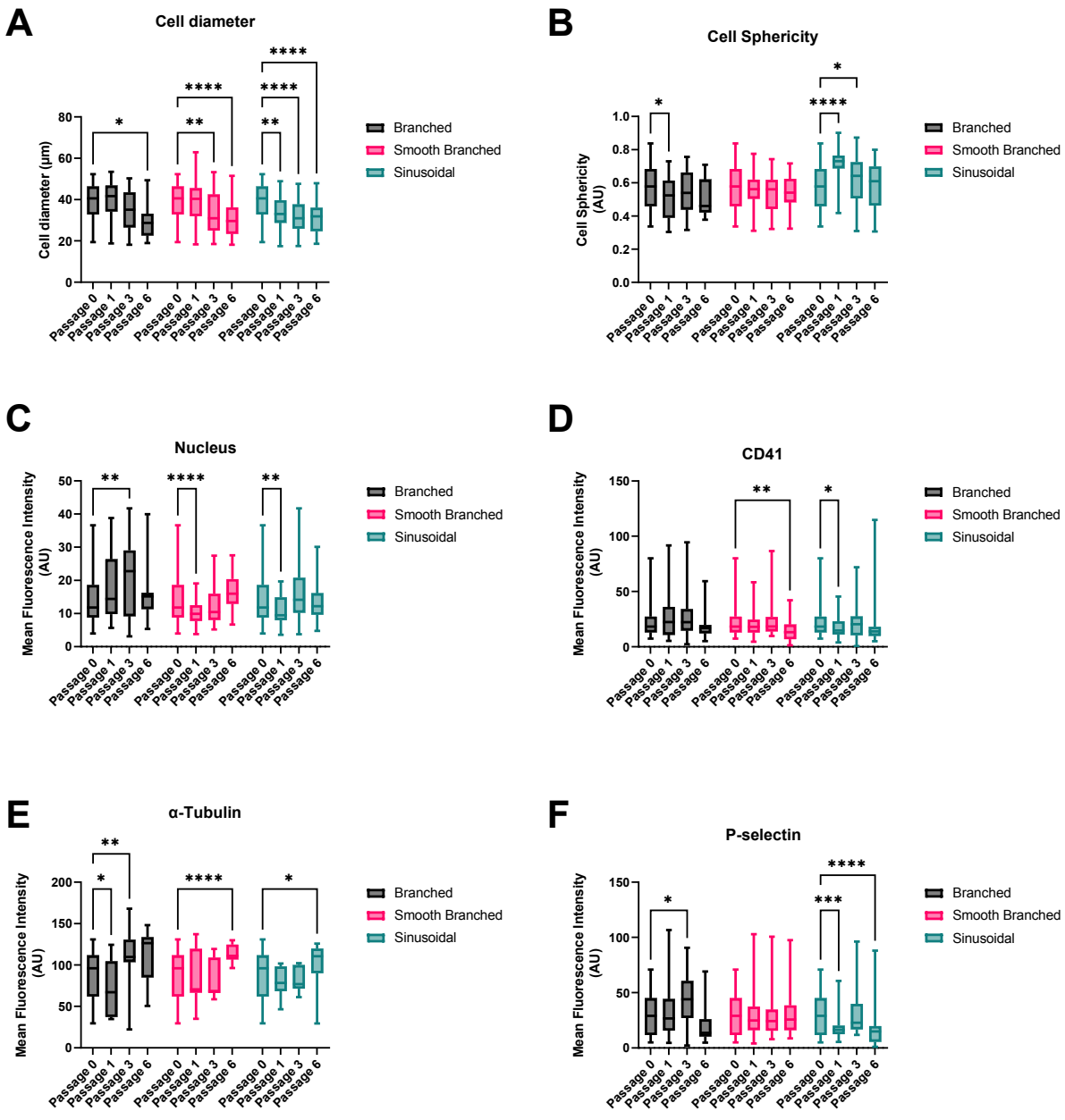

Figure 12 – Quantification of Laser Scanning Confocal Images of Megakaryocytes Passages Through the 3 Systems 0, 1, 3 or 6 Times.

Mouse megakaryocytes were passage through the 'branched', 'smooth branched' or 'sinusoidal' microfluidics systems (chips) described in the text (Fig. 7). The cells were passaged 0, 1, 3 or 6 times at a flow rate of 300 µl/min. Following fixation, the perfusate was spun at 100g for 5 minutes. The pellet was resuspended and the nucleus, CD41, α-tubulin and P-selectin stained. Laser scanning confocal microscopy was performed on the samples. 3-10 representative images were captured for each sample. 3 independent repeats for each condition were conducted (n=3). The images were quantified using a coded and trained macro, created by Dr Stephen Cross (Bristol, UK). All data is presented as separated box and whisker plots. Horizontal line within each box indicates median. Size of of

box indicates the interquartile range. Whiskers (bars extending from boxes) indicates the total range of data points. (A) Diameter of imaged megakaryocytes. (B) Sphericity of imaged megakaryocytes. Mean Fluorescent intensity of (C) Nuclear DNA, (D) CD41, (E) α-tubulin and (F) P-selectin measured in arbitrary units. All graphs statistically analysed using mixed-effects analyses with Dunnett's multiple comparison post hoc tests. (* = $p \leq 0.05$) (** = $p \leq 0.01$) (*** = $p \leq 0.001$) (**** = $p \leq 0.0001$).

3.32 Characterisation of produced platelets, enucleated megakaryocytes and debris

Immunofluorescence can be of great use when attempting to characterise a platelet. Platelet specific markers can be stained for, thus excluding any non-platelet particles of a similar size. Following passages, perfusates had MKs isolated out of the sample via fractional centrifugation. The larger cells (mostly MKs) were imaged, and that data was shown in Figs 9, 10 and 11. The remaining smaller cells and particles were imaged, and the major findings presented in Figs 13, 14 and 15.

3.32a Laser Scanning confocal images of platelets

Fig. 13 showed representative platelets produced in the branched, smooth branched and sinusoidal chips. All images shown were confidently characterised as platelets. They were comparable in size when qualitatively compared to a mouse platelet control (data not shown). Spreading of cells on cover glass increased cell diameter, which made comparisons to the literature difficult. The platelets lacked any nucleus when stained for with DAPI. A hallmark of platelets is their absence of a nucleus. The cells expressed CD41, a megakaryocyte and platelet specific protein, proving they were of the correct lineage. The P-selectin staining proved the presence of α-granules. A key function of platelets is the release of granules, thus a cell lacking these would not function, making the generation process unsuccessful. Finally, the presence of a microtubule ring (marginal band) was a failsafe identifier of a platelet-like particle(72). Note that there was some over exposure of non-platelet regions for P-selectin in Fig. 13. This did not affect interpretation of these results. The conclusion drawn from Fig. 13, was that the platelets being produced were characteristic normal, resting mouse platelets.

Figure 13

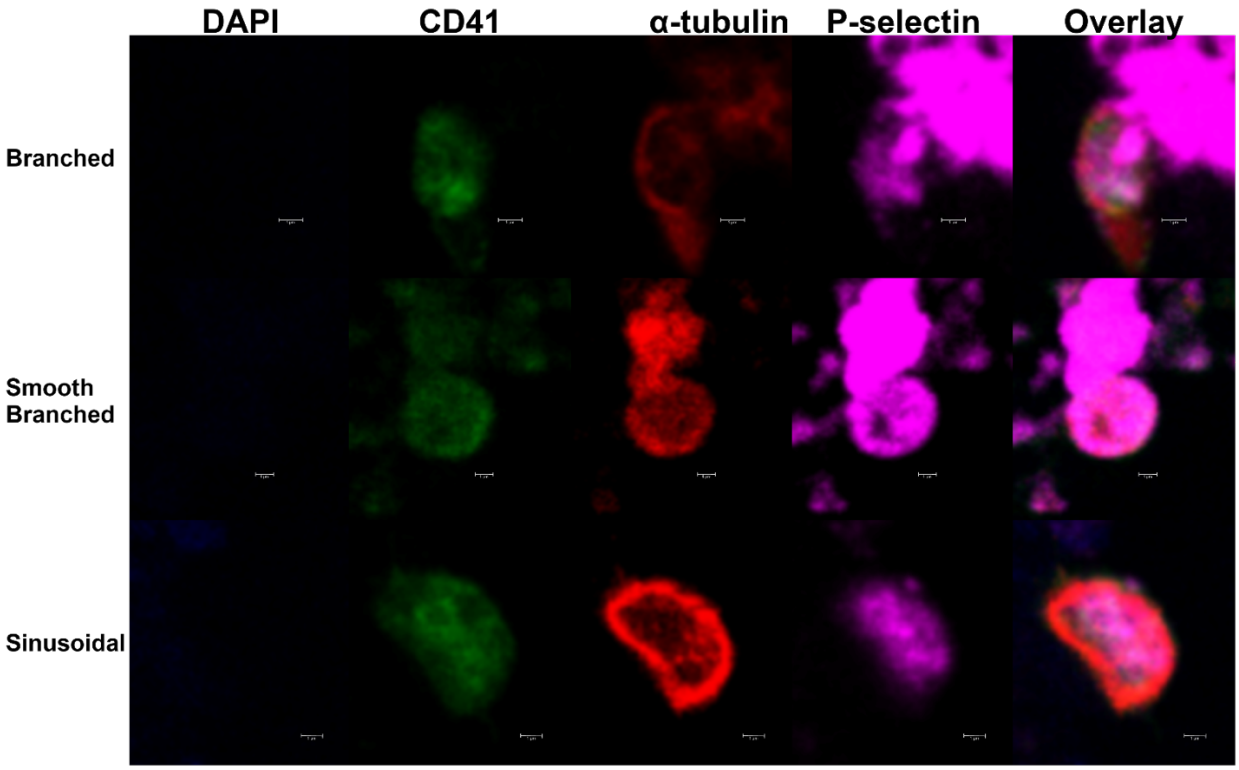

Figure 13 – Platelets Produced Using 3 Different Microfluidics Systems

Mouse megakaryocytes were passage through 'branched', 'smooth branched' or 'sinusoidal' microfluidics systems (chips). The structure of these chips is described in the text (Fig. 7). The cells were passaged 1, 3 or 6 times at a flow rate of 300μl/min. The perfusate was fixed and spun at 100g for 5 minutes. The supernatant was spun at 1000g for 10 minutes. The resultant pellet was resuspended and nucleus, CD41, α-tubulin and P-selectin were stained for. Representative laser scanning confocal images of **platelets** found in these preparations are shown (n=3 for each chip). Images are presented as single z-plane midsection of the cell. Nuclear DNA was stained with DAPI. Plasma membrane stained using an unconjugated rat CD41 primary antibody and donkey anti-rat Alexa Fluor 488 secondary antibody. Microtubules stained using rabbit a-tubulin primary antibody and donkey anti-rabbit Alexa Fluor 568. a-granules stained with goat CD62P primary antibody and donkey anti-goat Alexa Fluor 647. Scale bars = 1μm. Images captured using a Leica SP8 multi-laser confocal laser scanning microscope with the 63x HC PL APO oil lens equipped.

3.32b Enucleating megakaryocytes

The preceding *ex vivo* platelet producing system presented novel data of MKs enucleating during the platelet generation process(51, 52). The perfusate of all 3 of the chips showed MKs without nuclei (Fig. 14). There was a low number of these anucleate cells, compared to nucleated MKs, but their existence was consistent. These cells were of appropriately sized to be small MKs, considering average MK diameter is approximately 50μm. They expressed CD41 and P-selectin, proving they were of MK lineage. However, they lacked any sign of nuclear DNA when stained with DAPI. The repeat of this enucleating phenomenon in the microfluidics systems designed to mimic the *ex vivo* mouse heart-lung model, was encouraging. Presence of free nuclei and sub-nuclei, as described by Zhao et al, were also seen, in small numbers(51, 52) (data not shown). The absence of nuclei from MKs implied they had or were prepared to produce anucleate platelets. Figs 13 and 14 both provided strong evidence in supporting the

statement that the microfluidics systems were producing platelets via a true platelet producing mechanism, and not random fragmentation induced by shear stress. This mechanism may have been similar to the that responsible for producing platelets in the *ex vivo* heart-lung model.

Figure 14

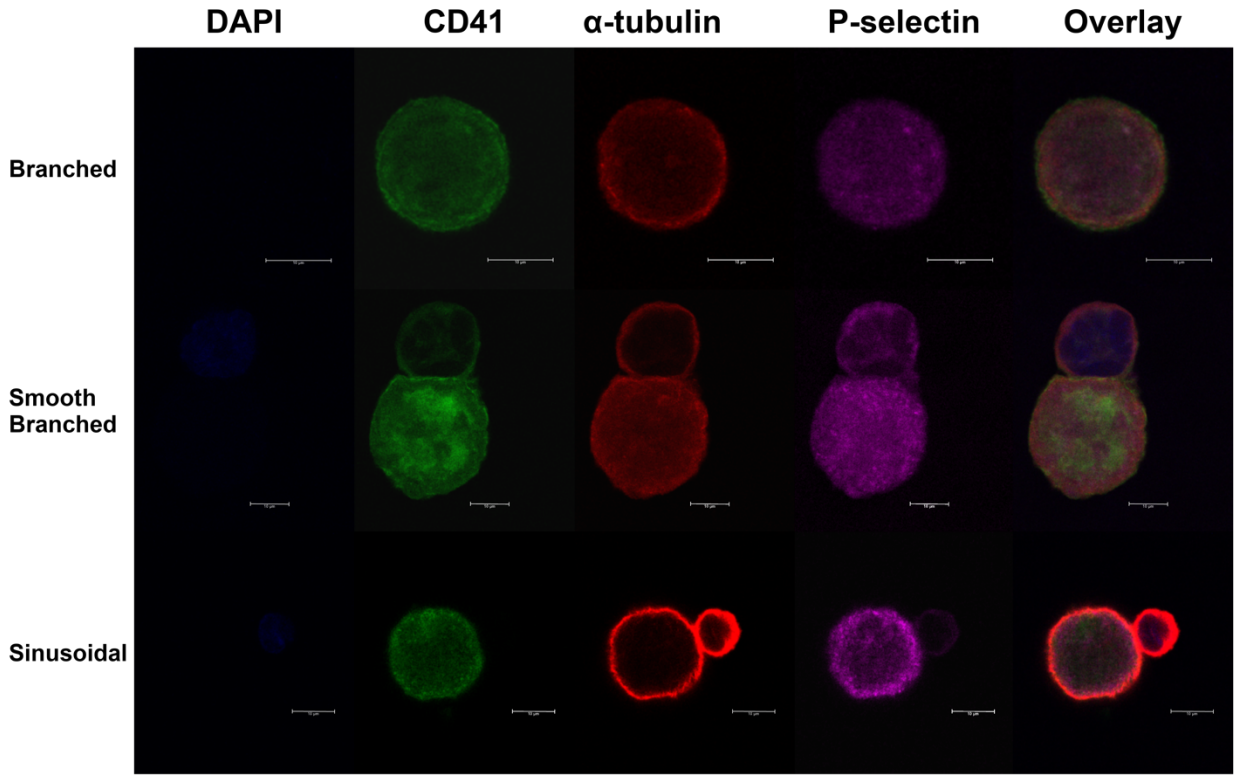

Figure 14 – Megakaryocytes Enucleate in All 3 Microfluidics Systems

Mouse megakaryocytes were passaged through the 'branched', 'smooth branched' or 'sinusoidal' microfluidics systems (chips). The structure of these chips is described in the text (Fig. 7). The cells were passaged 1, 3 or 6 times at a flow rate of 300μl/min. The perfusate was fixed and spun at 100g for 5 minutes. The supernatant was spun at 1000g for 10 minutes. The resultant pellet was resuspended and nucleus, CD41, α-tubulin and P-selectin were stained for. Representative laser scanning confocal images of **enucleated megakaryocytes** found in these preparations are shown (n=3 for each chip). Images are presented as single z-plane midsection of the cell. Nuclear DNA was stained with DAPI. Plasma membrane stained using an unconjugated rat CD41 primary antibody and donkey anti-rat Alexa Fluor 488 secondary antibody. Microtubules stained using rabbit a-tubulin primary antibody and donkey anti-rabbit Alexa Fluor 568. a-granules stained with goat CD62P primary antibody and donkey anti-goat Alexa Fluor 647. Scale bars = 10μm. Images captured using a Leica SP8 multi-laser confocal laser scanning microscope with the 63x HC PL APO oil lens equipped.

3.32c Damaged cell debris (laser scanning confocal)

Alongside the MKs, enucleated MKs, HSCs and platelets found in the perfusates of the chips, non-uniform cellular debris was extremely common. Due to the heterogeneous nature of these debris', it was difficult to representatively visualise them, however, Fig. 15 showed 3 commonly seen examples of

debris seen in the perfusate of all 3 chip systems (labelled A-C). Fig. 15A showed CD41 and P-selectin-stained debris which appeared to be attached to a cell body (arrow i). The stains were not oversaturated, indicating the debris may have been encapsulated or of a cell-like nature and not an artefact of fluorophores entrapped in folded proteins and membranes. Fig. 15B showed debris, which was positive for CD41, α-tubulin and P-selectin. Many of these areas were highly saturated with fluorophore. No apparent shape or structure to this debris was seen. Fig. 15C (arrow ii) showed debris, which was only positive for CD41, indicating it may have been membrane derived debris. Note that there was some staining seen on the α-tubulin channel at arrow ii, however this was likely due to the very bright, oversaturated CD41 in the 488-channel bleeding into the 568 channel of α-tubulin.

At this resolution, it was difficult to deduce what these debris were. Debris characterisation could potentially provide information on the flaws and/or mechanisms within the chips and, thus how they can be optimised. It was decided that scanning electron microscopy (SEM) would provide the greatest resolution for studying the debris.

Figure 15

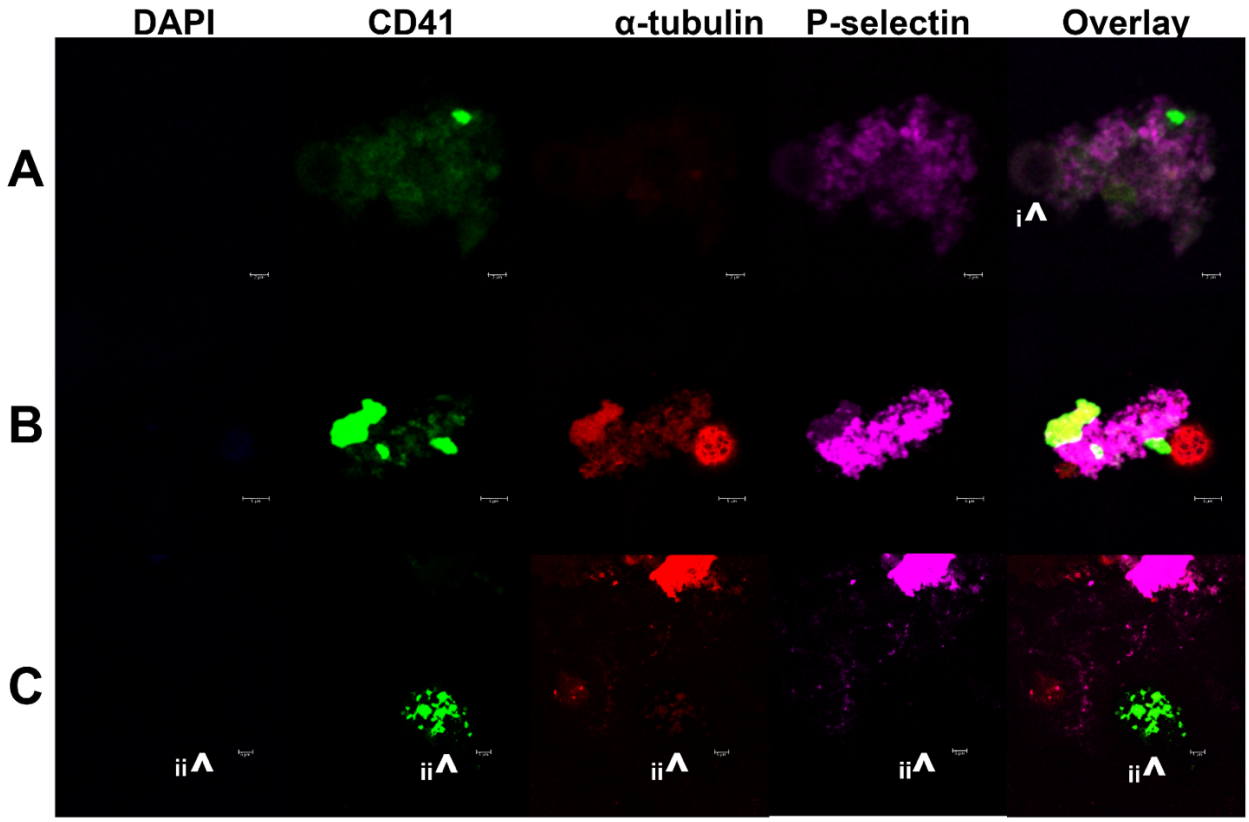

Figure 15 – All 3 Microfluidics Systems Exhibit Signs of Cell Damage.

Mouse megakaryocytes were passage through 'branched', 'smooth branched' or 'sinusoidal' microfluidics systems (chips). The structure of these chips is described in the text (Fig. 7). The cells were passaged 1, 3 or 6 times at a flow rate of 300µl/min. The perfusate was fixed and spun at 100g for 5 minutes. The supernatant was spun at 1000g for 10 minutes. The resultant pellet was resuspended and nucleus, CD41, α-tubulin and P-selectin were stained for. Representative laser scanning confocal images of **cellular damage** found in these preparations are shown (n=3 for each chip). Images are presented as single z-plane midsection of the cell. These, non-uniform areas of fluorescent debris were seen from all 3 microfluidics systems. Upon qualitative examination, debris was categorised into 3 groups. (A) debris which appeared (mostly) CD41 and P-selectin positive. This debris was co-localised with a CD41 and P-selectin positive cell body (labelled i). (B) Debris which was positive for CD41, tubulin and P-selectin. These stains did not perfectly co-localise, indicating presence of different markers within the debris and that stains were not due to non-specific binding to dead tissue. (C) Debris which appeared to be CD41 positive alone. This is labelled ii. Nuclear DNA was stained with DAPI. Plasma membrane stained using an unconjugated rat CD41 primary antibody and donkey anti-rat Alexa Fluor 488 secondary antibody. Microtubules stained using rabbit a-tubulin primary antibody and donkey anti-rabbit Alexa Fluor 568. a-granules stained with goat CD62P primary antibody and donkey anti-goat Alexa Fluor 647. Scale bars = 5µm. Images captured using a Leica SP8 multi-laser confocal laser scanning microscope with the 63x HC PL APO oil lens equipped. Arrows labelled i and ii are areas of interest and are referred to in the text.

3.32d Damaged cells (scanning electron microscopy)

Following optimisation, scanning electron micrographs were acquired. Unfortunately, correlative microscopy was beyond the scope of this study. Therefore, assumptions based on size and cellular

interactions was used as a guide to correlate SEM images to the immunofluorescent images seen in Fig. 15. Fig. 16A and *B* showed debris attached to a main cell body (indicated by arrow i), like that seen in Fig. 15A. The size of the cells, the presence of spread filipodia onto the coverslip, and the invaginated surface morphology suggested the cell bodies indicated may be platelets. Although the debris varied greatly in size, they appeared similar in characteristics between Fig. 16 A and *B*. These debris appeared very web-like in nature, and heavily interconnected. Fig. 16C and D showed debris that were free from a cell body, like that seen in Fig. 15C. There did seem to be a web-like nature to this debris also, however, upon qualitative review, the morphology differed. The arrow labelled ii in Fig. 16C was suggested to be an apoptotic body based on size and high shear stress these cells were exposed to. Fig. 17 showed representative images of cell exhibiting apoptotic-like blebbing produced from the microfluidics systems. This hypothesis of apoptotic bodies was based on comparisons to other SEM images in the literature of apoptotic cells (73). To prove apoptosis was occurring, apoptotic positive controls would be required. The cells seen in Fig. 17 were not common but were present in the perfusates of the 3 chips.

Using the confocal and scanning electron micrographs, hypotheses of what the debris seen were and their relevance to platelet generation were suggested. However, without further experimentation, these suggestions remain hypotheses. More detail on what these debris are thought to be, can be found in the discussions section.

Figure 16

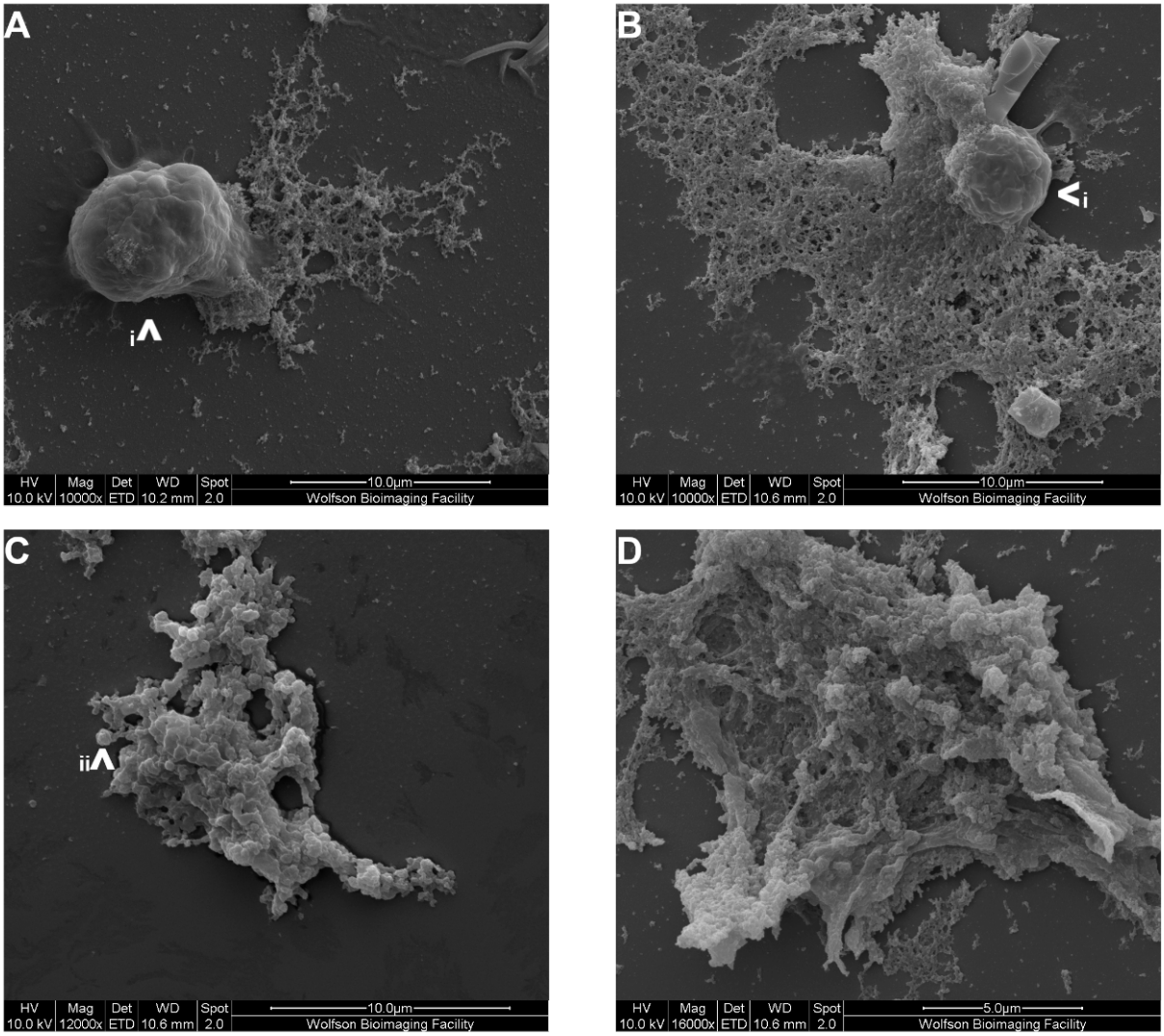

Figure 16 – Scanning Electron Micrographs of Cellular Damage Produced From All 3 Microfluidics Systems

Mouse megakaryocytes were passage through the 'branched', 'smooth branched' or 'sinusoidal' microfluidics systems (chips), 6 times at a flow rate of 300µl/min. The perfusate was fixed and allowed to settle onto a poly-l-lysine coated coverslip prior to post-fixation, dehydration, and heavy metal sputtering (Au/Pt). Representative scanning electron micrographs of cell damage are shown (n=3 for each chip). The cell damage was qualitatively categorised. (A) Small regions of debris attached to a cell body. The cell body was believed to be a platelet, based on size and morphology. (Note that produced platelets had a larger cell diameter than circulating mouse platelets. Cell bodies are labelled i. (B) Large regions of debris attached to a cell body. (C) Small regions of debris, not attached to a cell. ii is a small bleb, believed to be an apoptotic body. (D) Large regions of debris, not attached to a cell. Scale bars are shown on each individual micrograph. Note, the magnification, thus the scale bar, varies between the 4 images shown. Images captured using a Quanta 200 Scanning Electron Microscope, detecting secondary electron scatter.

Figure 17

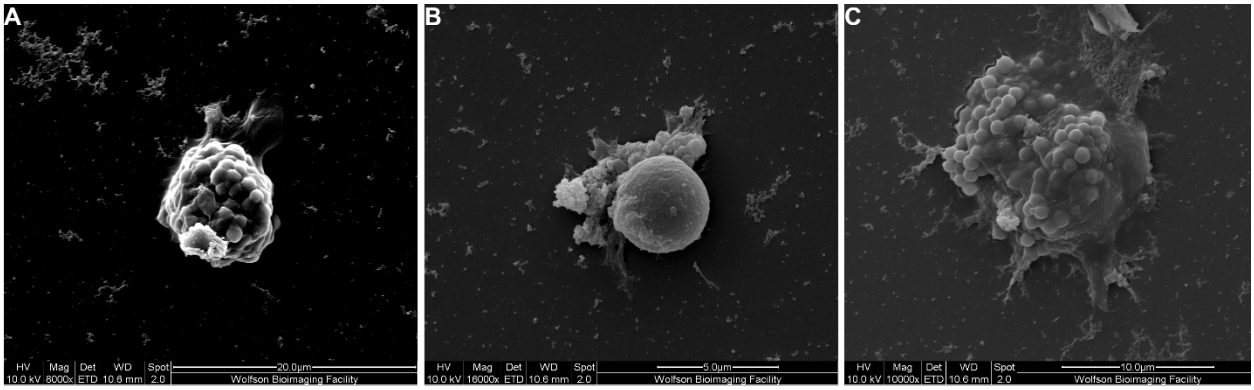

Figure 17 – Scanning Electron Micrographs of Intact, Damaged Cells Produced From the 3 Microfluidics Systems

Mouse megakaryocytes were passage through the 'branched', 'smooth branched' or 'sinusoidal' systems (chips), 6 times at a flow rate of 300µl/min. The perfusate was fixed and allowed to settle onto a poly-l-lysine coated coverslip prior to post-fixation, dehydration, and heavy metal sputtering (Au/Pt). Representative scanning electron micrographs of seldom observed cells with apoptotic-like blebs are shown (n=3 for each chip). A, B and C are not paired to the 'branched', 'smooth branched' and 'sinusoidal' chips. Scale bars are shown on each individual image. Scale bars vary in size due to different magnification of images. Images captured using a Quanta 200 Scanning Electron Microscope, detecting secondary electron scatter.

3.33 Characterising generated platelets using scanning electron microscopy

The confocal microscopy images of platelets in Fig. 13 provided good evidence to prove the generated platelets were true platelets. SEM allowed a higher resolution investigation into produced platelets characteristics.

3.33a Scanning electron micrographs of produced platelets

Fig. 18 showed platelets-like particles produced from the 3 chips and a mouse platelet control, isolated from mouse blood. This control allowed qualitative comparison of size and surface morphology, to confirm observed cells were platelets. The mouse platelets were seen to spread onto the cover glass, creating a larger cell diameter. Nascent platelets are larger than aged platelets(74). Thus, the larger diameter (5-6µm) of some generated platelets was explained by their young age and their contact spreading on the cover slip. The invaginated surface indicated they were platelets and lack of filipodia suggested they were in a resting state (Fig. 18). Fig. 19 showed representative images, of the frequently observed, preactivated platelet produced from all 3 systems. The filipodia of spreading platelets were indicated by white arrows. These platelets had not been chemically stimulated with a platelet agonist, thus preactivation occurred during the platelet production process.

Figure 18

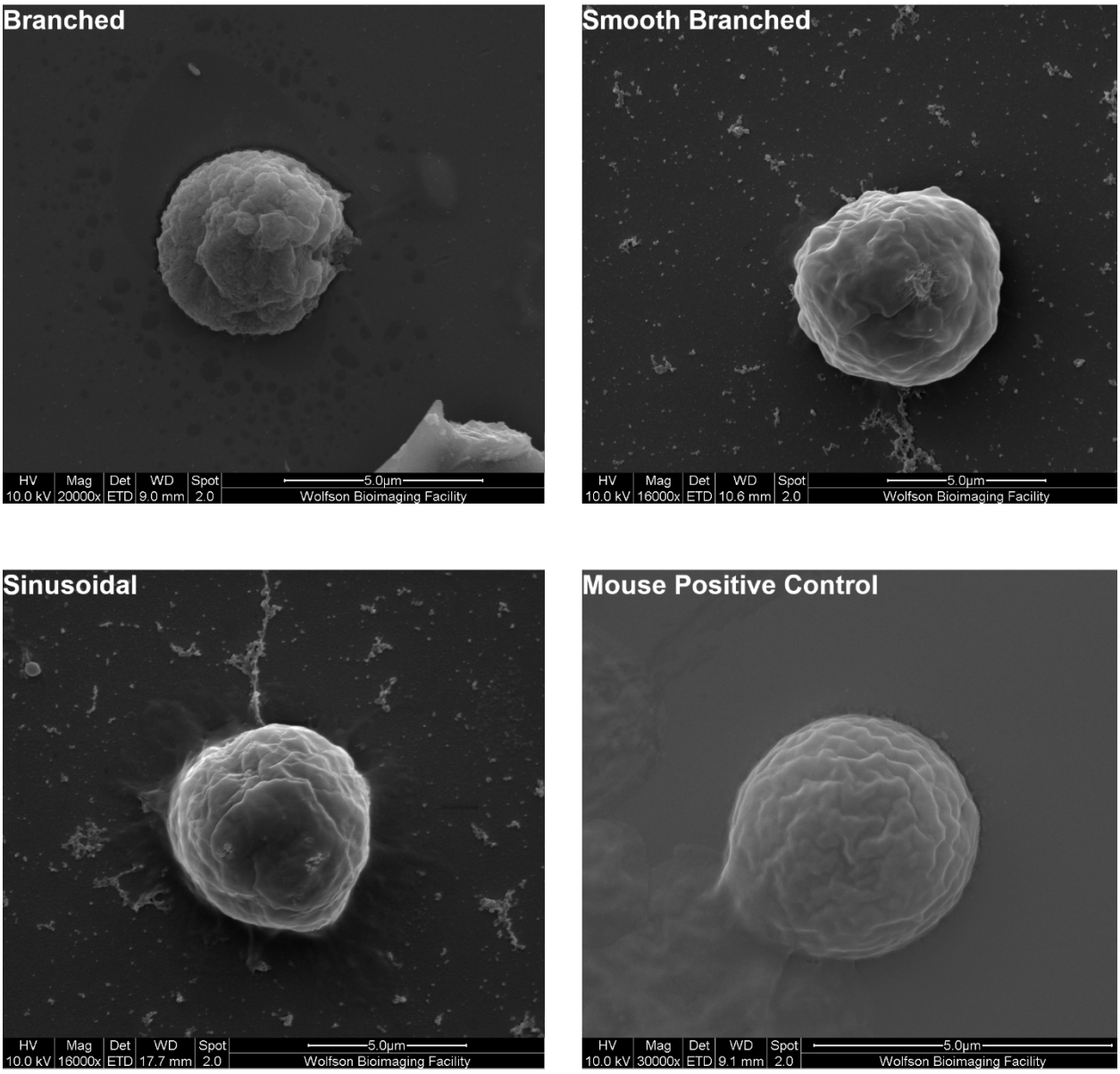

Figure 18 – Scanning Electron Micrographs of 'Platelet-like Particles'

Mouse megakaryocytes were passaged through the 'branched', 'smooth branched' or 'sinusoidal' microfluidics system (chip) 6 times at a flow rate of 300µl/min. The perfusate was fixed and allowed to settle onto a poly-l-lysine coated coverslip prior to post-fixation, dehydration, and heavy metal sputtering (Au/Pt). Representative scanning electron micrographs of platelet-like particles produced from each of the chips is shown as well as a platelet isolated from mouse blood (n=3 for each chip, n=1 for mouse platelet control). Platelets were characterised as resting due to the absence of filipodia. Scale bars are shown on each individual image. Due to different magnifications, across the 4 images, the scale bar size varies. Images captured using a Quanta 200 Scanning Electron Microscope, detecting secondary electron scatter.

Figure 19

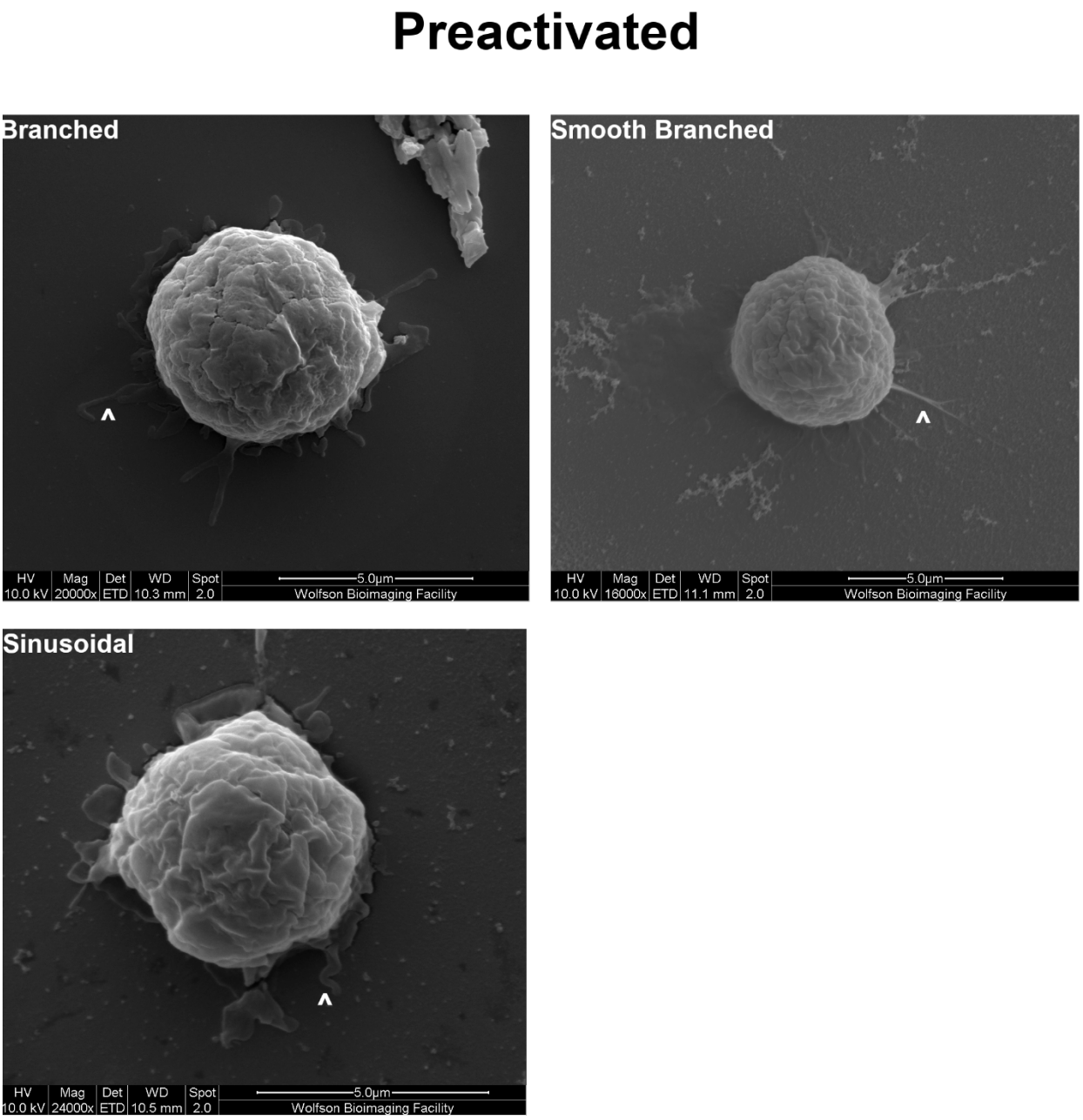

Figure 19 – Scanning Electron Micrograph of Preactivated Platelets Produced From the 3 Microfluidics Systems.

Mouse megakaryocytes were passaged through the 'branched', 'smooth branched' or 'sinusoidal' microfluidics system (chip) 6 times at a flow rate of 300µl/min. The perfusate was fixed and allowed to settle onto a poly-l-lysine coated coverslip prior to post-fixation, dehydration, and heavy metal sputtering (Au/Pt). Representative scanning electron micrographs of preactivated platelets produced from each of the chips is shown (n=3 for each chip). Platelets were characterised as preactivated due to the presence of filipodia, without the addition of platelet agonists. White arrows indicate filipodia. Scale bars are shown on each individual image. Due to different magnifications,

between the images, the scale bar size varies. Images captured using a Quanta 200 Scanning Electron Microscope, detecting secondary electron scatter.

3.33b Barbell platelets

A phenomenon not previously observed in the Poole group, during platelet production using microfluidics, was revealed when SEM was conducted on chip perfusates. Platelet barbells in various stages of separation were observed in the perfusate of all 3 chips (Fig. 20). These images were representative of what was seen across all the chips. Presence of characteristic barbells was indicative of a true, proplatelet-like, platelet producing mechanism being present and that platelets seen post perfusion were not as a result of spontaneous blebbing or fragmentation. These barbells being created in lung vasculature mimetic systems may help in marrying the lung vasculature and bone marrow sinusoid theories of platelet production. More detailed discussions of this are found in the discussions section. Fig. 21 showed what was labelled a 'tri-bell', produced from the sinusoidal chip. Morphologically, the tri-bell was very similar to the barbell but had three cell bodies, instead of two. These tri-bells were rare but were seen in the branched and smooth branched chips also.

Figure 20

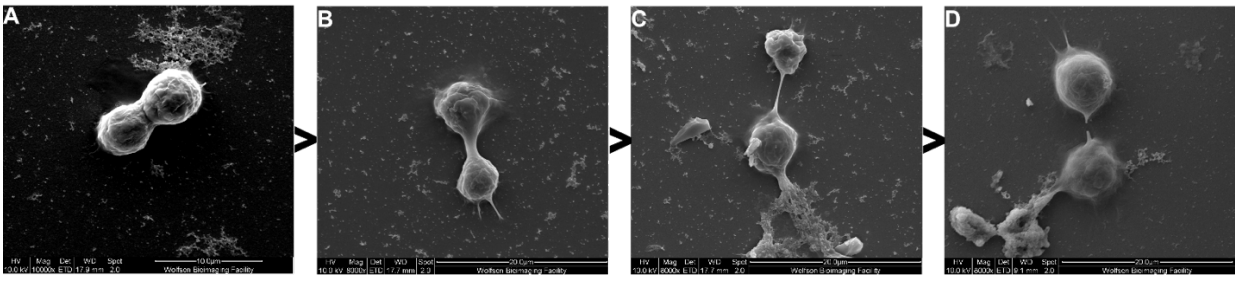

Figure 20 – Scanning Electron Micrographs of Platelet Barbells Produced From the 3 Microfluidics Systems.

Mouse megakaryocytes were passaged through the 'branched', 'smooth branched' or 'sinusoidal' microfluidics system (chip) 6 times at a flow rate of 300μl/min. The perfusate was fixed and allowed to settle onto a poly-l-lysine coated coverslip prior to post-fixation, dehydration, and heavy metal sputtering (Au/Pt). Representative scanning electron micrographs of barbell platelets produced from each of the chips is shown (n=3 for each chip). Images A-D shows the suggested progression of a platelet barbell until the separation of the barbell into two nasncent platelets in (D). The barbells showns are not a time-course and are different cells. The images are also a mixture from the 3 microfluidics systems, however they are representative of what was seen in each of the experiments. Scale bars are shown on each individual image. Due to different magnifications, between the images, the scale bar size varies. Images captured using a Quanta 200 Scanning Electron Microscope, detecting secondary electron scatter.

Figure 21

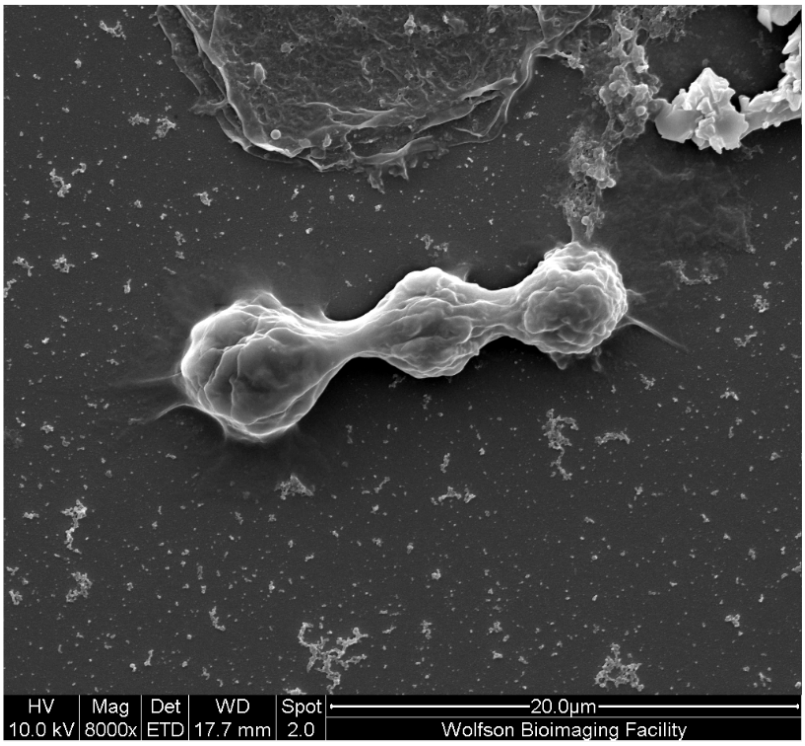

Figure 21 – Scanning Electron Micrograph of a 'Tri-bell' Produced From the 'Sinusoidal' Microfluidics System.

Mouse megakaryocytes were passaged through the 'branched', 'smooth branched' or 'sinusoidal' microfluidics system (chip) 6 times at a flow rate of 300µl/min. The perfusate was fixed and allowed to settle onto a poly-l-lysine coated coverslip prior to post-fixation, dehydration, and heavy metal sputtering (Au/Pt). Representative scanning electron micrograph of a platelet tribell platelets the 'sinusoidal' chip. This phenomenon was seldom seen but was observed in perfusates from the 'branched', 'smooth branched' and 'sinusoidal' microfluidics systems (n=3 for each chip). Scale bars is 20µm. Images captured using a Quanta 200 Scanning Electron Microscope, detecting secondary electron scatter.

3.33c Deformed cell-like objects

Among the clearly, characterizable platelets, cells marked as deformed cell-like objects were commonly seen after passage through all 3 chips (Fig. 22). These objects were angular, indicating they may be artefacts of preparation however they were extremely common. Qualitatively, they were much more common than regularly shaped platelets. Furthermore, these cell-like objects appeared to interact with other cells and each-other in a cell-like manner. Arrow i and iii on Fig. 22B and D, respectively, showed a cell-like object interacting or co-localising with debris similar to that previously discussed in Fig. 16. Arrow ii in Fig. 22C showed a cell-like object interacting with a spreading platelet. These cell-like objects were also approximately platelet sized, upon visual inspection. They lacked the characteristic invaginated surface morphology of a platelet. Without immunolabelling, it was difficult to characterise the cell-like objects. Ideally, the presence or number of these would decline in an optimised system and number of true platelets increase.

Figure 22

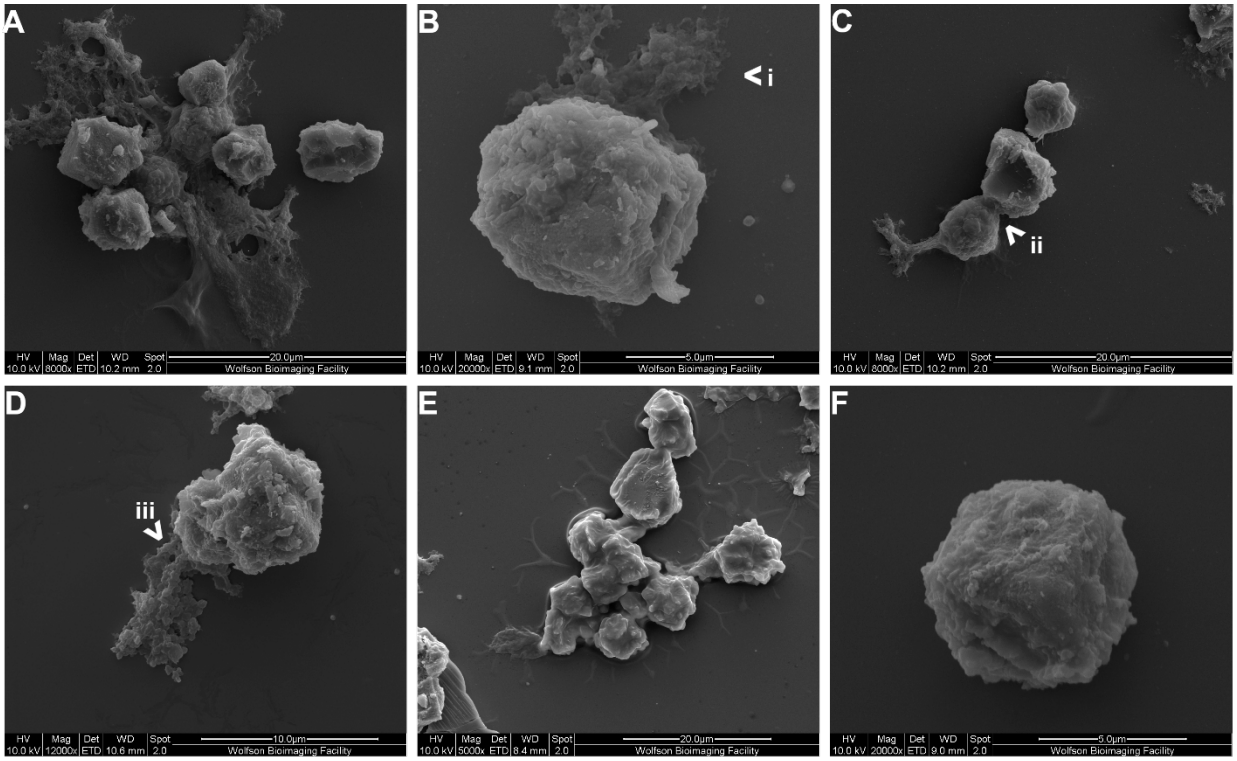

Figure 22 – Scanning Electron Micrographs of Deformed Cell-like Objects Produced From the 3 Microfluidics Systems

Mouse megakaryocytes were passaged through the 'branched', 'smooth branched' or 'sinusoidal' microfluidics system (chip) 6 times at a flow rate of 300μl/min. The perfusate was fixed and allowed to settle onto a poly-l-lysine coated coverslip prior to post-fixation, dehydration, and heavy metal sputtering (Au/Pt). Representative scanning electron micrograph of deformed cell-like objects is shown (n=3 for each chip). The objects appear more angular than a platelet. Arrows labelled i, ii and iii show interactions or behaviours of interest, which are discussed further in the text. Scale bars shown on each individual image. Scale bars vary in size due to different magnifications across images A-F. Images captured using a Quanta 200 Scanning Electron Microscope, detecting secondary electron scatter.

3.34 Platelet producing mechanisms and blockages within the microfluidics systems

To optimise a platelet producing system, knowledge of the mechanism by which platelets are being made is essential. Some insight into the mechanism was revealed using brightfield microscopy.

3.34a Catch and release proplatelets

All 3 chips showed a 'catch and release' mechanism (Fig. 23). The catch and release looked like an immobilised MK with long protrusions extending from the cell body. This is the hypothesised mechanism of platelet production in all 3 chips. Interestingly, although not designed to cause MK capture, the sinusoidal chip had branch points near the inlets which MKs appeared to be able to catch on to form extensions (Fig. 23G). Furthermore, the MKs were able to catch within blockages formed in the narrower regions of the sinusoidal chip (Fig. 23H). The fewer opportunities for MKs to catch on branch points was likely a major factor in why the sinusoidal chip was less efficient in producing platelets compared to the branched and smooth branched systems. Fig. 23A-C showed catch and release occurring at different branching points of the branched chip. The protrusions seen extended far away from the cell body before breaking off, suggesting structural integrity, even under high shear. The same catch and release mechanisms were seen in the smooth branched chip (Fig. 23D-F). Unfortunately, these images were not of the resolution to confidently identify individual platelets or barbell platelets detaching from these extensions. Thus, these catch and release mechanisms being the process of platelet production were merely a hypothesis and further testing would be required to confirm this theory.

Figure 23

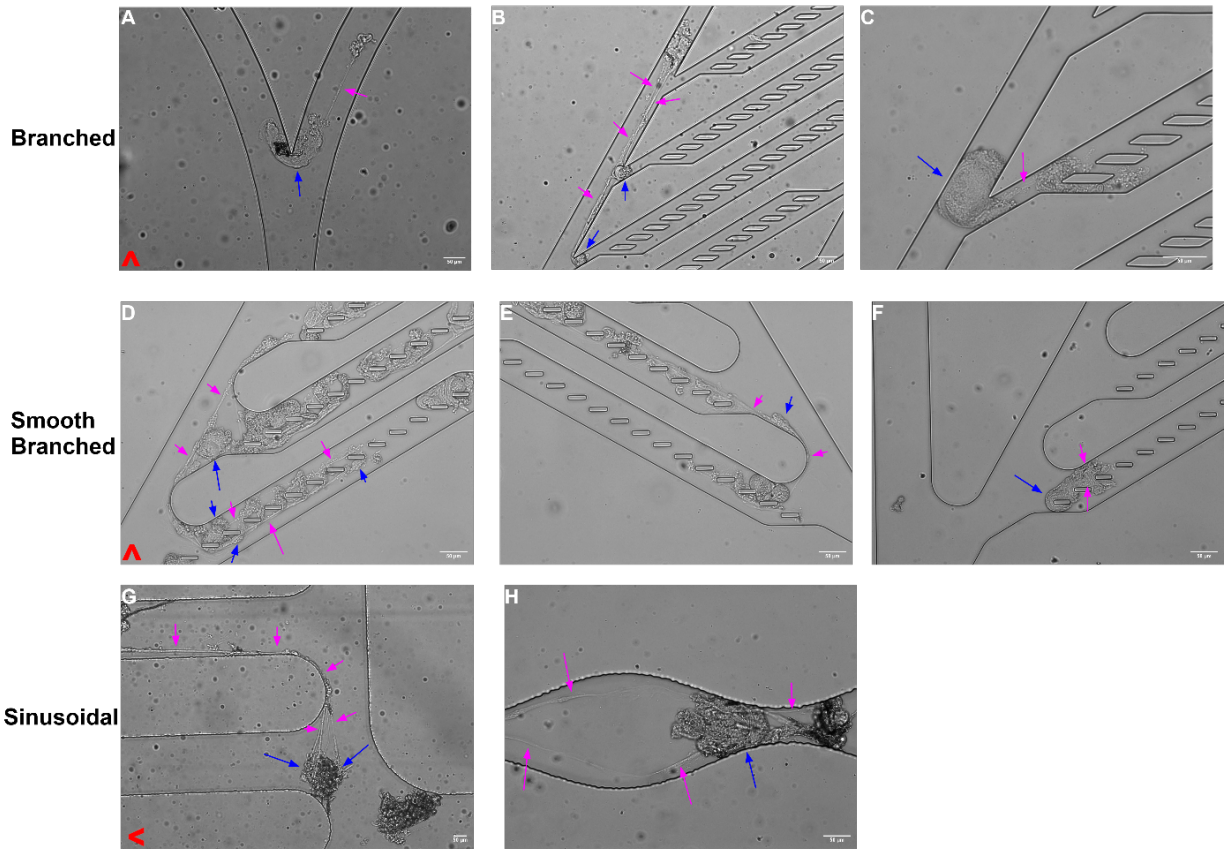

Figure 23 – Catch and Release is Hypothesised as the Mechanism of Platelet Production in all 3 Microfluidics Systems.

Mouse megakaryocytes were passaged through the 'branched', 'smooth branched' and 'sinusoidal' microfluidics systems (chips) 3 and 6 times at a flow rate of 300µl/min. After 3 and 6 passages, flowing of cells was halted and the channels within the microfluidics chips were imaged using brightfield microscopy. A-H shows representative images of megakaryocytes immobilising (catching) and extending long proplatelet-like protrusions (release) (n=3 for each chip). A-C shows the 'branched' chip. D-F shows the 'smooth branched' chip. G and H shows the 'sinusoidal' chip. Red arrow in bottom left corner indicates the direction of cell travel for all the images in that row. Blue arrows indicate cell bodies and magenta arrows indicate protrusions extending from megakaryocyte cell bodies. Scale bars = 50µm. Images were captured on Leica DMI6000 inverted microscope, using dry lenses.

3.34b Channel blockages

A commonly observed characteristic of the branched chip when obtaining pilot data was that some channels would become blocked with cellular debris. This was likely deleterious to the platelet production process platelets and MKs may have become caught in these blockages, decreasing the efficiency of platelet production. It was decided that these blockages should be quantified in an attempt to decipher their causes. Fig. 24 illustrated the chosen locations for imaging in the branched and smooth branched chips. Channels 1 and 3 were chosen as representative large channels. Due to the location of the inlet, cells were likely to flow through channel 3 first. Thus, imaging channel 1 and 3 gave a more representative variety of locations. Within each of these large channels, there was 2 x 8 sets of sections in parallel (also channels but for ease of communication, referred to as sections). Simulation data (not shown) previously conducted by the Poole lab has shown that in the branched chip the shear stress was much greater in sections 1 and 8 compared to section 4. The shear stress in sections 2-7 was lower than sections 1 and 8, thus section 4 was representative of the mid-section of these channels whilst section 1 represented the inlet of the channel whilst section 8 represented the outlet of that channel. Within each section, the first channel and last channel were ensured to be imaged (blue circles on Fig. 24). Due to the magnification required to observe the full channel, channels up or downstream of the desired channel were also imaged. This was beneficial in increasing the number of channels imaged however it was difficult to keep this consistent between experiments, resulting in slightly different number of channels imaged. This was compensated for by expressing blockages as a percentage of total channel blocked.

Figure 24

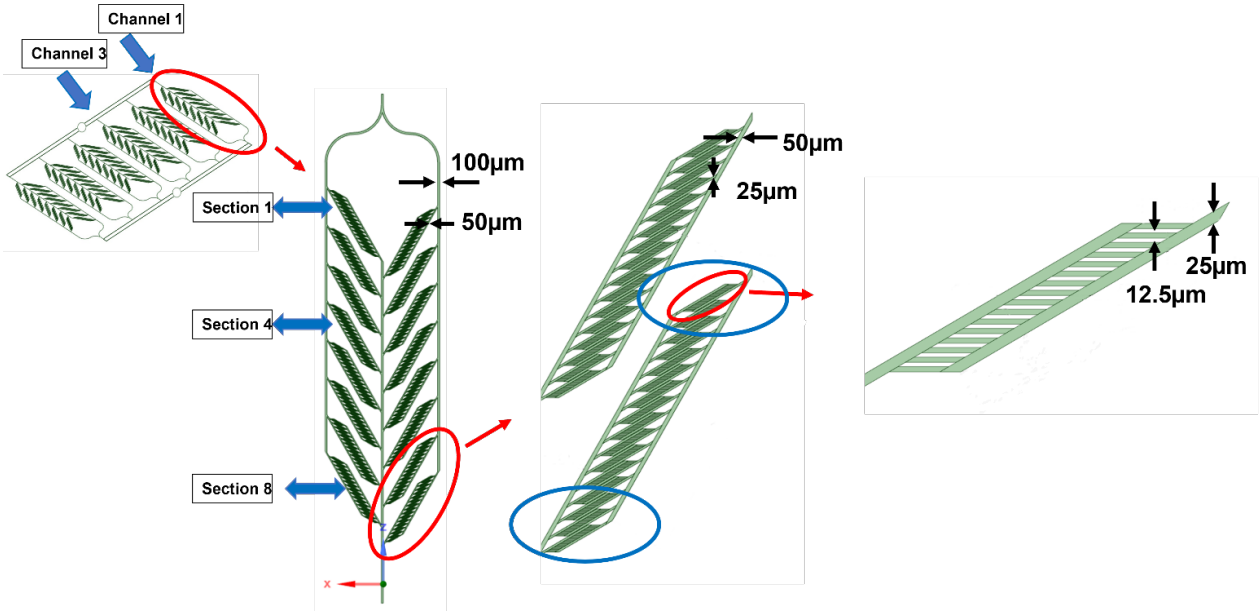

Figure 24 – Schematic of Locations Imaged for Quantification of Cellular Blockages within the 'Branched' and 'Smooth Branched' Microfluidics Systems.

Prior to brightfield imaging of the 'branched', 'smooth branched' microfluidics systems (chips), particular regions were chosen for to be imaged after 3 and 6 passages, in 3 repeated experiments. This could then be used for

unbiased quantification at a later date. Blue arrows and circles indicate locations for imaging. Red arrows and circles indicate areas being zoomed into for ease of interpretation. Channel 1 and channel 3 of the overall 6 channels were chosen for imaging (Single ended blue arrow). Within each of these channels, section 1, 4 and 8 were chosen as locations for imaging. For channel 1, the right-hand side channels were imaged and for channel 3 the left-hand side channels were imaged. This was decided by random coin toss. Note that the shear stress between sections 1, 4 and 8 vary significantly, allowing interpretations of the effect of shear stress on blockages to be made. Within section 1, 4 and 8 the first and last channel were imaged for quantification. Note, that due to the magnification required to image the entirety of that channel with one image, often other channels up and downstream were imaged also, however this only increases the sample size of channels imaged. These regions were imaged after 3 passages and then again after 6 passages. All imaged regions were then analysed using a computer programme to measure the percentage of the channel floor covered by cells in that region. Note that direction of travel is from top to bottom in this diagram.

3.34c Branched chip blockages

Representative images and quantification of blockages in the branched chip was shown in Fig. 25. Arrows in the figures drew attentions to blockages, for ease of viewing. The majority of blockages in sections 1 and 8 appeared immobilised and were not moved between passage 3 and 6. The blockages in section 4 appeared mobile as they were displaced between passage 3 and 6. The blockages showed no apparent cellular shape, indicating these blockages were not solely caused by MKs becoming lodged in small channels. It was hypothesised that the blockages consisted of a mixture of DNA, cellular membrane, BSA and cells. Fig. 25G showed the data generated from quantifying these blockages. This data was obtained by using a computer learned model which was able to measure the entire size of the channel and then how much of that was covered by debris and express that as a percentage of coverage of the channel floor. The major finding was that there were significantly more blockages in section 8, compared to section 1 and 4. This was true for the branched and smooth branched chip. The likely cause of this was due to flaws in the structural arrangement of channels, as well as high shear stress. All following data from Fig. 25G and 26G was expressed as mean percentage coverage with ± S.E.M. Analysis of the branched chip revealed the following. After 3 passages the mean percentage coverage of section 8 was 21.55% ± 4.51%. This was statistically significantly greater than section 1 (8.00% ±1.97%. $p = 0.0087$) and section 4 (1.48% ±0.85%. $p = 0.0003$). The same trend was seen after 6 passages. Section 8 had a mean percentage coverage of 28.20% ±5.83. This was statistically significantly greater than section 1 (9.33% ±1.84. $p = 0.0007$) and section 4 (1.61% ±0.85%. $p = <0.0001$). There was no statistically significant difference when comparing sections 1 and 4 after passage 3 or 6. However, a consistent trend, with no overlap of S.E.M bars did show, suggesting a potential difference. Trends should be trusted with caution. The number of channels imaged was inconsistent for some groups. This was as a result of poor experimental planning; however, the residuals were normally distributed and the Shapiro-Wilk test for normality was passed on this two-way ANOVA, making this analysis valid ($p = 0.158$). When comparing changes in blockages between passage 3 and 6 for each section in-turn, no statistical significance was seen for any section. This indicated that the blockage did not increase greatly between these passages.

Figure 25

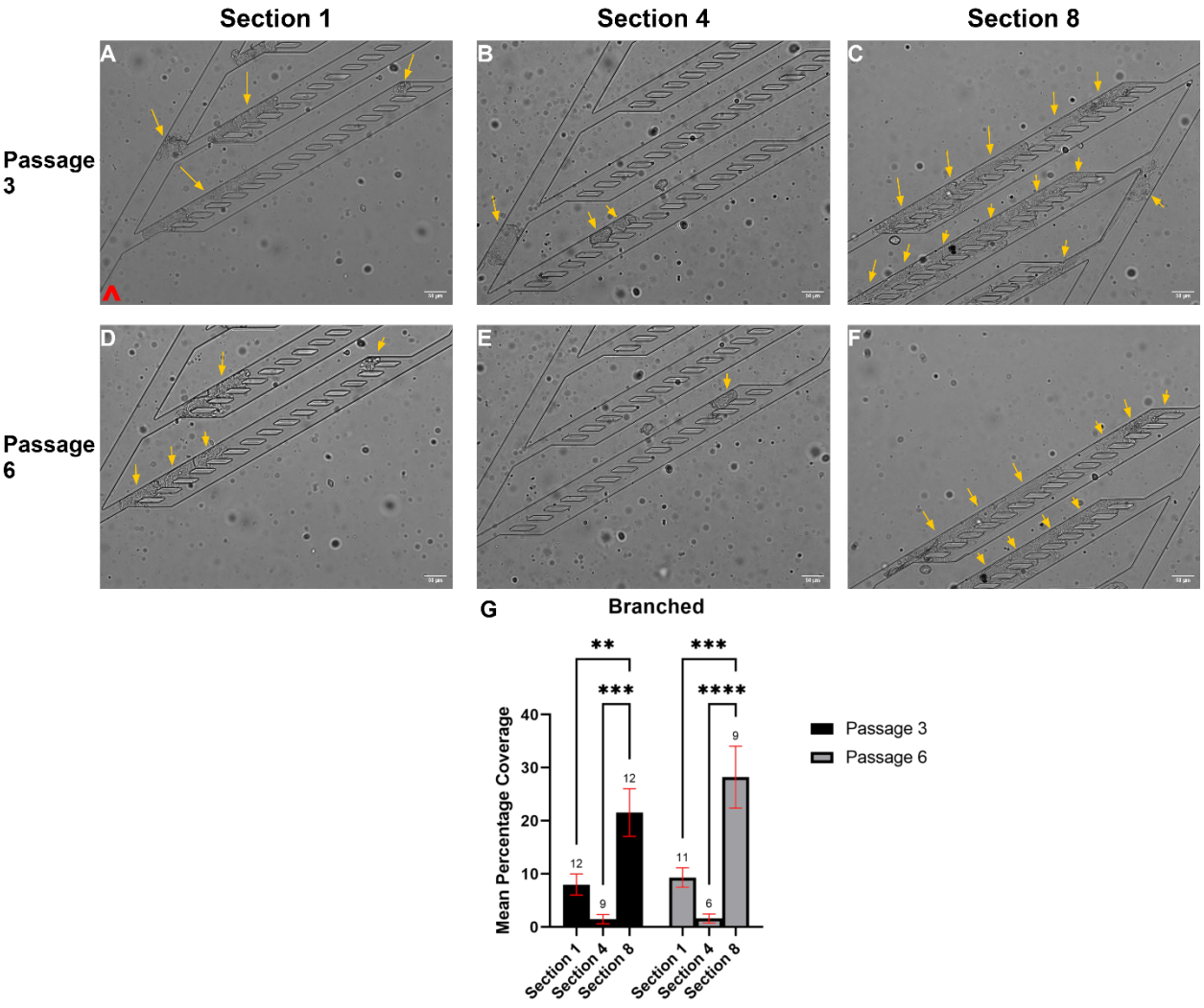

Figure 25 – The Outlet of the 'Branched' Microfluidics System Becomes the Most Blocked Due to Chip Architecture and Shear Stress.

Mouse megakaryocytes were passaged through the 'branched' microfluidics system (chip) at a flow rate of 300µl/min. Passaging was halted and channels imaged using brightfield microscopy after 3 and 6 passages. The locations specified in Fig. 24 were imaged for quantification and any region of interest also imaged for qualitative analysis. (A-F) shows representative brightfield images of the channels in sections 1, 4 and 8 after passages 3 and 6 (n=3). The images between passage 3 and 6 are paired. Orange arrows are to draw attention to blockages and/or content within channels. Red arrow on A indicates the direction of cell travel for images A-F. Scale bars = 50 µm.

Images were captured on Leica DMI6000 inverted microscope, using dry lenses. (G) shows a bar chart of the mean percentage coverage of the channel floor covered by cells or debris in sections 1,4 and 8 after passages 3 and 6. Standard error of the means (S.E.M) bars are shown. Numbers above each bar indicates the number of images across the 3 repeated experiments that were analysed. The percentage coverage was statistically analysed using a two-way ANOVA with Tukey's post-hoc test for multiple comparisons. (** = $p \leq 0.01$) (*** = $p \leq 0.001$) (**** = $p \leq 0.0001$).

3.34d Smooth branched chip blockages

Similar results to Fig. 25 were seen when analysing the smooth branched chip in Fig. 26. Very few blockages were seen in section 4. When quantified (Fig. 26G*)*, after 3 passages the mean percentage coverage of section 8 (22.25% ±3.45) was greater than the coverage of section 1 (4.79% ±1.38. p = <0.0001) and section 4 (0.00% ±0.00. p = <0.0001). Similarly, after 6 passages, section 8 (25.71% ±3.03) had greater coverage compared to section 1 (7.75% ±2.08. p = <0.0001) and section 4 (0.24% ±0.15%. p = <0.0001). A difference for the smooth branched, compared to the branched, was that the mean coverage of section 1 was greater than section 4 after 6 passages (p = 0.0355). This difference was not seen for passage 3. This data suggested that the branched and smooth branched chip behaved similarly, in terms of blockages. The quantification of the smooth branched chip should be trusted with some caution as the computer model was not specifically trained to detect the outlines of the smooth branched chip. The model was designed for the branched chip, however due to the similarity in structures the macro could be reused. The two-way ANOVA for Fig. 26G narrowly failed the Shapiro-Wilk test of normality (p = 0.0418. p = >0.05 passes the test). However, the Q-Q plot followed the linear relationship well (when observed visually). With this taken into consideration, the author believed that due to the extremely high significance values, these differences could be trusted as true.

Figure 26

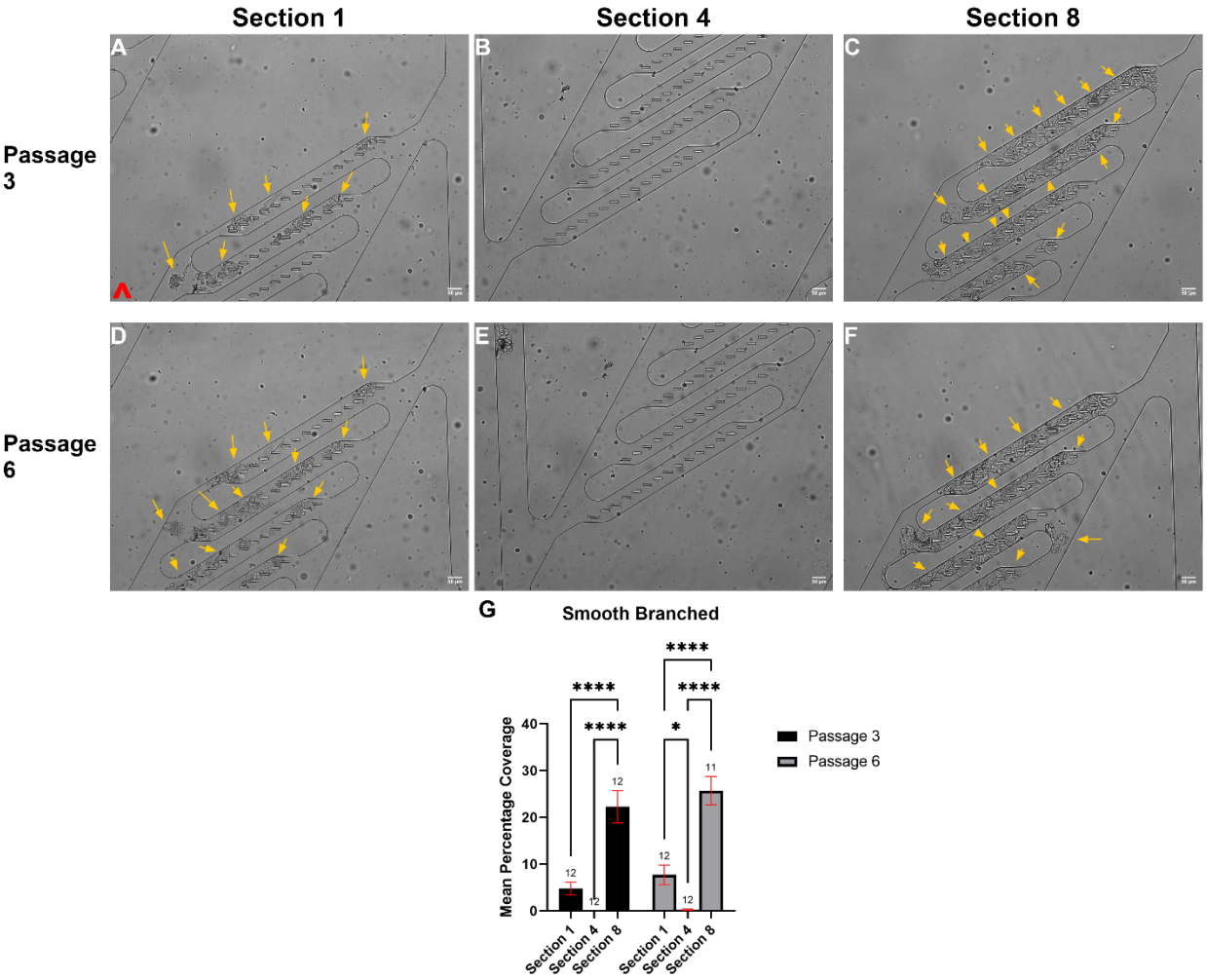

Figure 26 - The Outlet of the 'Smooth Branched' Microfluidics System Becomes the Most Blocked Due to Chip Architecture and Shear Stress

Mouse megakaryocytes were passaged through the 'smooth branched' microfluidics system (chip) at a flow rate of 300µl/min. Passaging was halted and channels imaged using brightfield microscopy after 3 and 6 passages. The locations specified in Fig. 24 were imaged for quantification and any region of interest also imaged for qualitative

analysis. (A-F) shows representative brightfield images of the channels in sections 1, 4 and 8 after passages 3 and 6 (n=3). The images between passage 3 and 6 are paired. Orange arrows are to draw attention to blockages and/or content within channels. Red arrow on A indicates the direction of cell travel for images A-F. Scale bars = 50 µm. Images were captured on Leica DMI6000 inverted microscope, using dry lenses. (G) shows a bar chart of the mean percentage coverage of the channel floor covered by cells or debris in sections 1,4 and 8 after passages 3 and 6. Standard error of the means (S.E.M) bars are shown. Numbers above each bar indicates the number of images across the 3 repeated experiments that were analysed. The percentage coverage was statistically analysed using a two-way ANOVA with Tukey's post-hoc test for multiple comparisons. (* = p≤ 0.05) (**** = p≤0.0001).). Note, the Shapiro-Wilk test for normally distributed residuals was failed with a p value of 0.0418 (>0.05 indicates normal distribution). However, the Q-Q plot and residuals plot were that of a sample that was normally distributed, given the small n number. Thus, these results are trusted with caution when the use of a Kruskal-Wallis non-parametric test was not available.

3.34e Sinusoidal chip blockages

Fig. 27 showed a characteristic blockage seen in the narrow portion of the sinusoidal chip. Visually, the blockage appeared darker and more concentrated in parts, compared to that seen in the branched and sinusoidal chip. Quantification of the sinusoidal chip was not available due to time constraints.

Figure 27

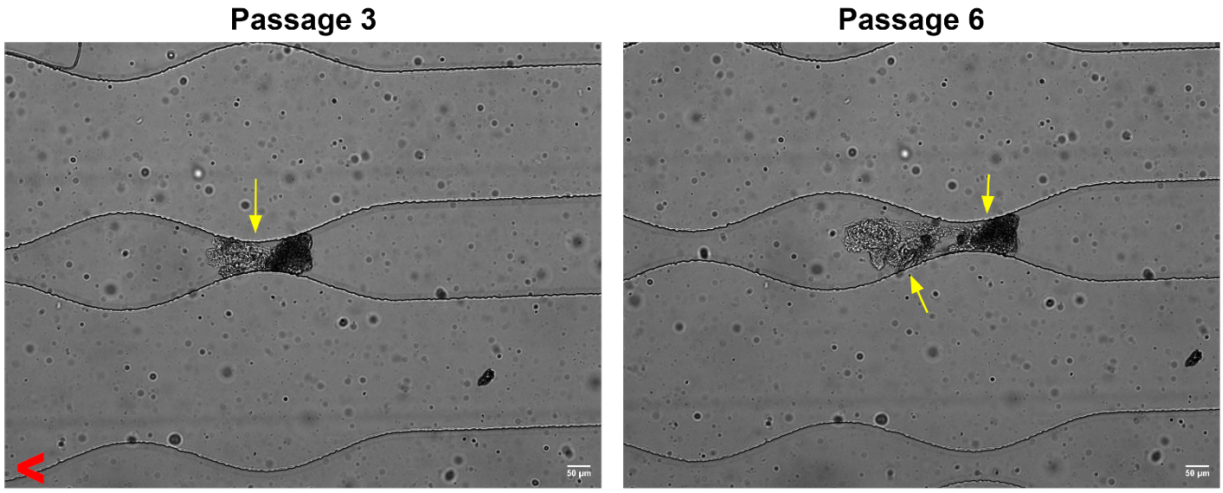

Figure 27 – Brightfield Images of Blockages Within the 'Sinusoidal' Microfluidics System

Mouse megakaryocytes were passaged through the 'sinusoidal' microfluidics system (chip) at a flow rate of 300µl/min. Passaging was halted, and channels imaged using brightfield microscopy after 3 and 6 passages. Representative brightfield images of a single channel of the 'sinusoidal' chip after 3 and 6 passages is shown (n=3). The two images are paired. Yellow arrows draw attention to blockages within the channel. The red arrow in the bottom left indicates that direction of cell travel for both images. Scale bars = 50µm. Images were captured on Leica DMI6000 inverted microscope, using dry lenses.

3.34f Conclusion about blockages

In conclusion, all 3 of the chips exhibited blockages. In the branched and smooth branched chip, the final section became most blocked, indicating that the structural design of the chip was creating too much resistance in some regions and not others, hindering platelet production. Having an improved understanding of the inner workings of the microfluidics chips has provided vital information in aiding future optimisation of these systems.

4. Discussions

These discussions delve into different aspects of the results section in further detail. Interpretations, limitations, alterations, and justifications will be discussed with a final set of conclusions and thought on the future of this work.

4.1 Platelet Counting – Limitations and Justifications

4.11 Summary

In Fig. 8 the efficiency of the 3 chips was compared using flow cytometry. The main finding was that the branched chip produced more platelets per MK than the sinusoidal chip. There was no statistically significant difference between the smooth branched chip compared to the branched or sinusoidal chip but there was a trend for consistently lower efficiency than the branched chip.

4.12 Gating

The author believes the gating strategy used to identify a platelet was valid, but it had limitations. Deducing platelet size was done using washed mouse platelets isolated from whole blood via venepuncture of the inferior vena cava. This was the best option for comparison as the MKs used to generate the platelets were mouse derived, thus the generated platelets would mimic mouse platelets. It is known that newly generated platelets are larger than aged platelets(51, 52, 74). This meant that the size gate may not be a perfect fit. This was often the case; thus, the gate was adjusted slightly in an attempt to encapsulate the majority of the proposed platelet population. The risk of this was inclusion of smaller, HSCs contaminated from the MK isolation process. This was accounted for by the inclusion of a DNA dye (Draq5). HSCs are nucleated and platelets are not. The gate for Draq5 was drawn by mixing HSCs and washed mouse platelets, staining with Draq5 and observing where the two populations were distinct on a quadrant plot. For the purposes of platelet generation, a platelet must be viable. A dead platelet would serve no use in a clinical setting. This was accounted for by using the viability dye, Calcein AM. This gate was set by staining a mixture of untreated washed mouse platelets with boiled and freeze plunged mouse platelets. This produced two distinct populations on a quadrant plot, and the gate was drawn. Finally, CD41 was used as the marker to truly distinguish a platelet sized, viable, DNA negative event as a platelet. The gate set for this was conducted by mixing a population of PE-CD41 stained washed mouse platelets with and unstained set of washed mouse platelets. On a histogram, two distinct populations were shown. There were some limitations to this CD41 gating. Firstly, the PE fluorophore may cross talk with the FITC fluorophore from Calcein AM(75). This can be compensated for but was not in this study. Furthermore, non-specific binding of the CD41 antibody to Fc receptors on platelets was likely present and was not accounted for in this study. Ideally an IgG control would have been used to

control for non-specific binding. This was difficult for this study as the MKs were pre-stained with the PE-CD41 antibody for 3 hours prior to passaging. As the 3 chips were being passaged in parallel, introduction of 3 more controls would have been difficult. That is why the gating strategy used was chosen. The pre-staining for 3 hours was the protocol used across the Poole group. As a protocol it has flaws. The PE-CD41 antibody used contained azides, potentially damaging the MKs during the incubation period. Pilot data (not shown), has suggested that some of the MKs may have died during this incubation period, reducing platelet production efficiency. The justification for staining for 3 hours was to attempt to stain the IMS of the MKs, as well as the plasma membrane. The number of counted platelets has been shown to decrease if the platelets were stained for CD41 post-production (data not available). The cause of this difference is unknown. It is hypothesised that CD41 on plasma membranes of platelets is sheared off due to the high shear stress conditions in the chips. If pre-stained with CD41, the internal membrane would still be fluorescently labelled. This hypothesis has not been tested. Future studies should address this and should use azide free antibodies, to reduce harm to MKs. Having MKs incubating for 3 hours prior to passaging may be damaging to them, further reducing efficiency.

4.13 Platelet Functionality

A major limitation of this entire body of work is the lack of functional data for produced platelets. It can be argued that a platelet is not truly a platelet if it does not respond to platelet agonists. Functional assessment of platelets is often performed using flow cytometry. Platelets are stimulated using agonists such as collagen related peptide or thrombin. Then measurement of activation markers on platelet surfaces such as P-selectin or the activated form of the αIIbβ3 integrin, taken(51, 52). Previous members of the Poole group have had difficulty in showing fully functional produced platelets using the branched chip (data not shown). The generated platelets out of the branched chip are often preactivated. They express P-selectin on the surface, prior to agonist stimulation. Fig. 19 shows signs of preactivation, indicated by the presence of filipodia. Qualitatively, the presence of filipodia was more common than not for the produced platelets. Filipodia were seldom seen in the mouse platelet controls (Fig. 18). This is a major limitation of the chips. The hypothesised reasons for preactivation of platelets are as follows. Introduction of air bubbles into the microfluidics system. Bubbles are known to activate platelets(76). When operating a microfluidics system, it is extremely difficult to not introduce air bubbles when refilling the syringe between passages. A modification of the microfluidics system would be to have a recirculating system where the opportunity to introduce air bubbles is reduced to one (when the chip is being loaded). Furthermore, the use of degassed buffers and a ‘bubble trap’ could reduce bubbles(77). Another potential activator of platelets in the chip is the high shear stress. The shear stress in the branched and smooth branched chips is many times higher than physiological levels, so may activate the platelets. However, Roka-Moiia et al (2020) showed that platelets activated by shear stress do not increase surface expression of αIIbβ3 integrin and P-selectin (78). Rather, shear activated platelets increases phosphatidyl serine exposure on the platelet surface. These differing marker expression to different stressors could be used in the future to unpick the cause of platelet activation within the chips. Finally, another potential activator of platelets in the chip is DNA. The blockage data seen in Fig. 24 and 25 shows large blockages. What these blockages consist of is not characterised. It is believed that at least one component of the blockages is DNA from either damaged MKs and/or enucleated MKs. DNA is a known activator of platelets via toll-like receptors(79). Thus, the potentially, high amount of DNA within the chip could be activating platelets. A potential solution to this would be to include a DNase in the perfusing solution, to degrade any DNA present. Functional data for the smooth branched and

sinusoidal chip have not been produced. These systems may produce more functional platelets due to fewer sharp edges and lower shear stress (respectively). Future studies should include functional data for produced platelets from all systems.

4.14 Megakaryocyte Counting

The number of MKs isolated from culture were counted, prior to dilution to a known concentration. Diluting the passaging solution to a known number of MKs allowed the number of platelets per MK to be produced. This value was used to compare the efficiency of the 3 chips. A limitation to this method of calculating efficiency is that the MKs were counted using a haemocytometer. This can create some variation in actual number of MKs loaded into the system. The MKs counted on the haemocytometer were of varying size, and thus maturity. It was difficult to consistently decide if a cell was 'large enough' to be a mature MK. Using the equipment available, this source of bias was best compensated for by having a second lab member perform a count of the MKs and then an average taken. An improvement would be to have a flow cytometer that could count and sort MKs by size and a late stage maturity marker, such as high ploidy or P-selectin(17).

4.15 Cell death

In Fig. 8B it was shown that the sinusoidal chip caused the death of a higher percentage of, DNA negative, platelet sized cells compared to the branched chip. This was an unexpected result as the sinusoidal chip was designed to have lower shear stress and pressure than the branched chip. The sinusoidal chip was shown to have laminar flow in simulations (Reynold's number <2000). This was just a simulation so there is the possibility that the wide channels and blockages produced in the sinusoidal chip have disrupted flow and induced turbulent flow, which has damaged the cells. The branched and smooth branched chips do also have relatively high proportions of dead cells. This is not ideal of efficient platelet production. The hypothesised reasons for the cell death are as follows. High shear stress. Blockages in channels may be increasing the shear stress to levels greater than predicted by simulations. Damaged cells in the chip may release reactive oxygen species or other similar stressors, that could trigger a positive feedback loop, damaging more cells(80). This is only a hypothesis and should be tested by assessing the level of reactive oxygen species or other stress markers or signs of apoptosis. This includes markers such as activated caspases(81). Note that the data in Fig. 8B was presented as a percentage for ease of interpretation. The statistical significance remained if the data was presented as total number of dead cells.

4.16 Data Presentation

The data in *Fig. 8* was presented as 'before and after' plots where each set of experiments was paired. This format of data interpretation was chosen due to the high variability seen between the MK cultures. As seen in Fig. 8A the platelet producing efficiency varied greatly between the 3 repeats, however the trend across the chips was consistent. It is believed that this variation was caused by the heterogeneity of cell cultures. MK cultures developed differently, even when the same quantity of media and cytokines was added to the isolated HSCs. The cells reached maturity (deduced via visual inspection of size), at different ages and some cultures struggled to reach full maturity. If a suitable flow cytometer was available, MK maturity could be measured using ploidy or P-selectin expression as a marker and then

only cultures of certain maturity would be used. Visual inspection of the cultures that produced the two lower sets of data in Fig. 8A looked visually less mature; the cells were smaller. Ideally this would have been visually recorded and quantified. Presenting the data as in Fig. 8 improved data transparency. The high variability made performing an ANOVA unsuitable, hence the choice to perform the Friedman's non-parametric test, where normality was not assumed.

4.17 Conclusion

In conclusion, using the facilities available, the platelet efficiency count was as accurate possible. However, the lack of functional data made interpretation of the 3 chips' efficiencies limited. Future iterations of platelet producing microfluidics systems should not only focus on increasing platelet efficiency but should irradicate platelet preactivation. The production of resting platelets is attainable; The *ex vivo* mouse heart-lung model published by Zhao et al produces platelets which show near to no platelet preactivation(51, 52).

4.2 Fluorescent Intensity Analysis – Limitations and Alterations

4.21 Summary

The theory behind the comparative study shown in Figs 9, 10 and 11 was valid. Unfortunately, the planning and execution of this experiment was poor and had many limitations. This made interpretation of these results difficult. This set of experiments visualised and quantified the changes in fluorescently labelled MK markers after different passage numbers through the 3 chips.

4.22 Experimental Design

Many factors should be controlled if wanting to compare the fluorescent intensity of cells. This includes, but is not limited to, concentrations of antibodies, laser intensity and microscope gain. Due to poor experimental planning, and lack of foresight when experimentation began, these were not controlled. Once the mistake had been realised, there was insufficient time to repeat the study. Furthermore, bias was present throughout the experiment. Sample preparations were not blinded. In the future, a colleague should take the sample preparations as early as possible and label the samples with code and only reveal the code once quantification and conclusions on data have been drawn. Furthermore, when imaging samples, cells/regions were not randomly chosen. An attempt to reduce bias was present. An unseen area on the navigator tool of the Leica LASX software was selected and if a cell was seen in that region, then that cell was imaged. The field of view was moved to try image as many cells as possible, ensuring the original cell was still in field of view. A better way of reducing bias would be by tile scanning. Scanning the entirety of the coverslip (or at least a large region of fit) would remove all selection bias from the image acquisition step. This will be done in future fluorescence analyses and/or any repeats of this data. This would provide enormous data sets, of unbiased, reliable data. Future, similar experiments will implement these changes. A set of pilot data, including optimisation steps of fluorophore concentration, permeabilization and blocking steps will be conducted prior to acquisition of data for analysis. Due to lack of experience, this was not considered at the beginning of this experiment and project. Jonkman et al (2020) provide an enlightening set of guidelines on designing quantifiable

microscopy experiments (82). Lee and Kitaoka (2018) created a similar document but with additional details on proper microscopy controls(83). Many of these controls were conducted including running single stained controls and controls replacing primary antibodies with IgGs to prove labelling was specific. Ideally every experiment would have IgG controls, however due to the number of samples this was not possible and having conducted these controls during the optimisations steps was sufficient. Although the quantification of these images was heavily flawed, the quality of the images was good and allowed qualitative conclusions to be made on cell morphology and cellular components. The sample preparation protocol can be used in future studies and adapted for a variety of related experiments.

4.23 Image Presentation

Many of the immunofluorescent images in this work were presented as maximum intensity projections of Z-stacks. Generally, for imaging, this is not an ideal way of presenting data. However, in this instance, this was the best method of presenting MK images. The MKs being imaged were extremely large, so many Z-stacks were needed to image the entirety of the cell. Due to the enormous, poly-lobulated nucleus of the MKs many of the internal components were not found in all planes. α-granules and microtubules were often pushed outwards by the nucleus, meaning that many of the granules and clear microtubule structures were located towards the top and bottom of the cells. If only the apexes of the cells were presented, then the IMS and nucleus would not be shown. If only mid sections of the cell were presented, then many granules would not be shown. As a compromise, maximum intensity projections were used to show the presence of all markers. This gives the illusion of background staining in the cell. Analysis of individual Z-stacks showed clear, images with low to no levels of background staining (data not shown).

4.24 Quantifying Macro

The images in Figs 9, 10 and 11 were quantified using a trained macro. For small to moderate sized MKs, this programme segmented and quantified intensity very well. However, with larger MKs, the programme failed. The perimeter outlines drawn by the system were often incorrect. This resulted in some images from passage 0 needing to be excluded from analysis. This potentially skewed results found in Fig. 12. Furthermore, this reduced the number of images analysed for passage 0. To compensate for this, passage 0 images across all the chip experiments were collated to increase power. In theory, the main source of variation between these cells should have been due to culture variability, making the collation valid. In a repeat of this experiment, more training of the computer programme would be done to improve its ability to detect large cells. More images from passage 0 would also be taken and then data could be paired to each culture to reduce variability in cultures, which is large. Furthermore, future studies should include pilot data which is then used to calculate the number of images per sample required to achieve sufficient statistical power. This was not done in this piece of work.

4.25 Conclusions

In conclusion, the quantitative analysis in Fig. 12 should be disregarded and no conclusions drawn from it. The images obtained in Figs 9, 10 and 11 showed that MKs could passthrough each of the 3 chips and remain viable and visually unchanged. This is impressive as the MKs were often multiple times larger than the narrowest channel in the branched and smooth branched system. This plasticity can be utilised in future systems. Narrow channels could be used to induce high levels of compression, without causing MK damage.

4.3 Cellular Debris Produced – Theories

4.31 Summary

Heterogenous and non-uniform debris was a commonly observed component of the perfusate from all 3 microfluidics systems. These debris were imaged using immunofluorescence and SEM. Although it was difficult to characterise and draw conclusions on what the debris consisted of, suggestions were made. An important note is that the debris seen on the SEM were assumed to be the same as those seen under immunofluorescence. These assumptions were based on size and lack of other artefacts.

4.32 Suggestions of the identity of debris

The likelihood of all the debris seen being of a homogenous population was low. The immunofluorescent staining patterns seen on the debris varied (Fig. 15*)*. Some of the debris may have been apoptotic bodies, released as a result of dying cells induced by high stress conditions within the system. The evidence to support this was that some pieces of debris were stained with only CD41 and P-selectin. Apoptotic bodies are known to be small, vesicle structures which use a membrane to encapsulate cytoplasmic components of a dying cell(84). Fig. 8B showed that cells were dying within the chips and Fig. 17 showed SEM images of cells that have passed through the chip and seem to have apoptotic bodies on their surface. The blebs seen on the surface of the cells in Fig. 17 were too small to be platelets, but do fall in the range of being apoptotic bodies or apoptotic extracellular vesicles(85). The debris seen in Fig. 15A was not over saturated. Oversaturated stains could be explained by dead membrane or protein that has trapped fluorophores. This supports the theory that some of the debris was encapsulated apoptotic bodies. This hypothesis suggests the stress undergone by cells in the chips was far too great. The co-localisation of the debris to a cell body (Fig. 15A*)* supports the suggestion of apoptotic bodies, as apoptotic bodies must be originated from a cell. The overly saturated regions seen on Fig. 15B and C suggest major signs of stress. The hypothesis for these debris is that they are accumulations of damaged cell membrane and other proteins from cells that have been severely damaged within the chips. The debris seen in Fig. 16D appeared to have no organised structure. It has strands of varying length and thickness with no indications of organisation. Furthermore, structures like this appeared to have small blebs attached or trapped within them. These may be apoptotic bodies, based on size and sphericity (e.g. Fig. 16C). The web-like and stranded debris in Fig. 16A and B was more difficult to interpret. It may be the same or similar to what is seen in Fig. 15B – highly expressive of α-tubulin but also of P-selectin and CD41. Although the cell bodies in Fig. 16A and B could be considered of platelet size, the debris cannot be mistaken as preactivation. The large sections of web-like debris could be a result of microtubules and sections of membrane spilling out of a severed or ruptured cell. These observations are all speculation. The use of immune-SEM may help identify what the debris is, which may provide information on how the chips can best be modified to reduce cellular damage.

4.33 Suggestions of the identify of deformed cell-like objects

Fig. 22 showed cell-like objects produced from the microfluidics systems. The morphology suggested these were potential artefacts, however some of the behaviour they exhibited seemed cell like. There is the possibility that these are artefacts. If this is the case, it is a limitation of the chips as it would further indicate stress and damage. Qualitatively, these objects constituted a large proportion of all events observed during SEM. An alternative theory could be that the deformed cells were platelets that have been damaged or unable to fully develop. Development could be stunted by high shear, lack of endothelial interactions or insufficient time to roll along the surface walls. Platelets are known to alter their morphology and exhibit plasticity(86); thus, it would not be unreasonable to believe that rolling along a vessel wall could influence the characteristic discoid shape of platelets. If a cell was not able to roll, it may be more angular and result in the shape seen in Fig. 22. This hypothesis could be tested using simple, straight microfluidics channels and various time points of platelet production and blood platelet controls.

4.34 Conclusions

The main conclusion is that the presence of debris following passage through the chips suggests that the stress the cells are being put through is too great. The chips require modification and optimisation to reduce the amount of debris. The absence of debris would be a good marker for a less severe system.

4.4 Observed In Vitro Platelet Production Mechanisms

4.41 Preplatelets, proplatelets and barbells

The immunofluorescent images in Fig. 13 and SEM images in Figs 18 and 19 imbued confidence in characterising the produced platelets, as platelets. The microtubule ring is a defining marker of platelets and the invaginated surface morphology and filipodia seen on SEM are also hallmark of platelets(72, 87). The presence of barbell-like structures (Fig. 20), with cell bodies of platelet size, indicates true platelet production mechanisms occurring. Barbells are proposed intermediates in platelet production. The typical proplatelet theory of platelet production suggests that MKs form proplatelets. These proplatelets break off and form preplatelets. Preplatelets are similar to a platelet but larger (3-10µm in diameter). These preplatelets can then (reversibly) stretch into barbell shapes. In this barbell conformation, the cytoplasmic bridge can sever into two platelets, with diameters <3µm(20, 88). This may explain why some produced platelets imaged were larger than 5 µm. They may in fact be preplatelets. The population of platelets in the perfusate likely contains a mixture of large preplatelets, small platelets and large (mature) platelets. The MKs were passaged in a solution containing EDTA. EDTA has been suggested to hold preplatelets in these states and reverse barbells into preplatelets. This could be reducing platelet production efficiency in the system(88, 89). Barbell like structures were very seldom seen when performing confocal microscopy, thus the data was not presented as it did not seem representative. The absence of the barbells in confocal preparations was likely due to the many spinning steps included in the sample preparation. Repeated experiments would optimise a confocal protocol more similar to that of the SEM protocol where generated platelets are allowed to fall onto a poly-l-lysine coated cover slip. Using this method, much fewer spins would be required, reducing probability of

platelet or barbell loss. In summary, the presence of barbell platelets is strong evidence supporting true platelet production within all 3 of the chips. It may also help explain why many of the 'platelets' are larger than expected as they could be preplatelets. It is worth noting that labelling of structures as barbells in based solely off assumptions and comparison to the literature. These structured are just correlated to platelet producing mechanisms. It could be argued that these elongated bridges are cell-to-cell interactions. Flow cytometry imaging by Kemble et al (2022) showed barbell platelets of a similar morphology to those observed here(88). The absence of long proplatelets within the perfusate is interesting. It suggests that the largest fragment that breaks away from immobilised MKs is the tribells or barbells.

4.42 Proplatelets in the chips

The data presented in Fig. 23 was illuminating for understanding the mechanism by which platelets are produced in the chips. The images appear to marry bone marrow sinusoid proplatelet theories and lung vasculature models. The morphology of the cell body and protrusions seen in Fig. 23 are extremely similar to the proplatelets seen within the vasculature of a mouses lung(37). In the chips, the large cell body of a MK became lodged and then a long proplatelet-like protrusion was stretched along the channels. These can confidently be referred to as proplatelets. As already mentioned in the results section, platelet release was not imaged due to poor resolution of the microscope used. However, the shape appeared proplatelet like. A bone marrow sinusoid mimetic microfluidics system tested by Blin et al (2016), showed MKs with the same morphology when bound to von Willebrand factor (vWf) coated pillars and shear applied(46). The use of vWf is something that the 3 chips used in this piece of work may benefit from. vWf is a surface protein found on platelets and endothelial cells(90). By coating a microfluidics chip with vWf, it will in part mimic the presence of an endothelium, whilst bypassing the difficulties of inserting endothelial cells into a microfluidics chip. Lung endothelial cells express greater levels of vWf than other endothelial cell populations(91, 92). vWf, coupled with shear force application, is beneficial in proplatelet formation(93). Culturing MKs with human umbilical endothelial cells, induced proplatelets which could be inhibited by preventing vWf interacting with MK, using a GPIb inhibitor(53). The complimentary receptor to vWf on MKs is the GPIbα receptor. It is a mechanoreceptor that has been shown to cause a 'stop-and-go', alternatively called 'catch-and release', mechanism(53). The described mechanism appears to reflect what is seen in Fig. 23. Coating the 3 chips, or future iterations of the chips, may help to cause more catching, not just at branch points but also at other locations within the system, improving platelet producing efficiency. The conditions that are optimal for inducing proplatelets within a microfluidics are not fully characterised. Intravital imaging of mouse lungs by Lefrançais et al (2016) showed proplatelet formation at branch points and in narrow capillary beds(37). This may indicate that a system with branch points and narrow channels, imparting compression onto MKs is important in platelet production. The branched and smooth branched chips are reflective of this. The limitations to mimic the lung vasculature comes from flaws in the architecture of the chips. This will be discussed in further detail when discussion of causes of blockages is mentioned in the next section. Shear stress is known to be an important factor in inducing proplatelets and is a commonly held belief in the platelet biogenesis field(46, 53). This does indicate that microfluidics are a valid method for platelet production. The 3 chips tested here all exhibit laminar flow. Interestingly, the platelet generating bioreactor used by the Eto lab induces turbulent flow(49). The bioreactor yields efficient production of functional platelets, however the platelets appeared to be cleared rapidly when injected into a

patient(94). The use of turbulent flow is a potential consideration for future iterations of our microfluidics systems. *In vitro* and *in vivo* evidence exists, showing the importance of turbulent flow in platelet shedding(49). The 3 chips have focused on laminar flow, but this may have been a mistake. Potentially a combination of laminar and turbulence is required for efficient platelet production. The data of proplatelets within the chips is promising. Any future designs should attempt to increase the number of these proplatelets. Quantification of proplatelets and improved imaging to visualise platelet or preplatelet release from the ends of proplatelets should also be striven for.

4.43 Durations of cell passaging

A limitation of 3 chips may be that the duration of perfusion may not be sufficient. Lefrançais et al showed that proplatelet formation and platelet release occurred after ~20 minutes and could continue for an hour(37). Similarly, in other microfluidics systems, showing proplatelet formation and platelet release, the first platelet release event occurred after 27 minutes and continued, post 60 minutes(46). In the branched, smooth branched and sinusoidal chips, each passage took no longer than 6.7 minutes. With 6 passages the maximum amount of time the cells were under shear was 40 minutes, but this was not continuous. The duration of passages frequently decreased as liquid was lost or stuck within the systems, thus the duration of passaging was likely less than 40 minutes. Future iterations of the chips should consider having recirculating or closed system that has continual flow for a duration greater than an hour. The duration of flow could be extended even further, to multiple days, if the MKs were passaged in a stable media and platelets were continually separated from the system.

4.44 Cellular compression

The author hypothesises that compression of MKs may also be an important variable in platelet generation. One of the justifications of this hypothesis is that other microfluidics systems without compression have had low production efficiency(46). Furthermore, the lung capillary beds found *in vivo* are smaller than the diameter of MKs, thus in physiological conditions MKs are compressed heavily at a proposed sites of platelet production(95). Townsley's review on all pulmonary vasculature includes the diverse and complicated architecture of the capillary beds. It may provide inspiration for future chip designs(96). The role of compression in platelet biogenesis can be studied using microfluidics and drugs. For examples, microfluidics devices that are completely straight channels which have intermittent regions of compression (same design as the sinusoidal chip (Fig. 7) but with narrower, narrow points). It is worth noting that the depth (y-axis) of the branched and smooth branched channels was 15μm, whilst the depth of the sinusoidal chip had a depth of 50μm. Thus, the branched and smooth branched channels would be constantly applying a compression to MKs in the y-axis. Chemical inhibition or activation of mechanoreceptors on MKs could elucidate the importance of compression. PIEZO1 is an ion channel mechanoreceptor found on erythrocytes. As erythrocytes and MKs originate from the same hematopoietic lineage, there is the possibility of MKs expressing PIEZO1 also(97, 98). Agonists and antagonists of PIEZO1 are available, making this experiment viable(99). GPIbα is a mechanotransducing receptor. It is known to detect and respond to shear stress(100). Its role in detecting compression should be further investigated.

4.45 Conclusions

The hypothesised mechanism of platelet production within the chip is as follows. MKs become immobilised within the chips. This is often at branching points. Shear forces will initiate long proplatelet extensions to extend from the MKs. Small sections of the proplatelet break off. Sections form large

preplatelets and barbells (or tribells). These barbells or tribells will sever to form individual platelets. This is similar to other hypothesised mechanism of platelet production in the field(20, 35, 37). Fig. 8A showed that the branched chip was more efficient in producing platelets than the sinusoidal chip. Proplatelets were seen within each of the 3 chips. Most proplatelets were located at branching points. The presence of more branching points is likely one of the main reasons for the branched chips higher productivity. Barbell platelets were seen using SEM. This supports a proplatelet theory of platelet release within the chips. Several modifications could be implemented to microfluidics designs and operation to facilitate more proplatelets.

4.5 Microfluidic Channel Blockages – Theories and Future Designs

4.51 Blockage composition and fixes

As shown in Fig. 25 and 26, the blockages within the branched and smooth branched chips are extreme. Without immunofluorescent staining, it was impossible to deduce the exact contents of the blockages. Even with immunofluorescence, the blockages may be too complex and heterogeneous for clear staining. It is hypothesised that the blockages may contain any number of the following components. DNA. It is known that cells are dying within the chip (Fig. 8B) and that MKs can enucleate when being passaged (Fig. 14), thus the presence of DNA is likely. The 'sticky' ability of DNA is exemplified by neutrophil NETosis(101). If large amounts of DNA are within the channels of the chip, they may be capturing MKs, platelets, HSCs and any other produced debris or cell membrane. This leads to the next proposed components of blockages: cell debris and membrane. The cell debris discussed previously and shown in Figs 15 and 16 may be becoming caught in narrow channels and/or DNA. This cell debris may contain membrane, cytoskeletal proteins and/or any other cytosolic contents. Although interesting, identifying the exact components of the blockages is not of highest importance; reducing or eradicating the blockages from the chips is key.

Including a DNase in the solution being perfused through the chips, could help break down any free nuclear material in the channels. A simple and interesting experiment would be to compare DNase containing and DNase free samples and quantify the blockages as done in this study. When this is done, the viability of cells in the perfusate and productivity of the chips should be re-assessed.

4.52 Chip structure causes blockages

Interpreting the quantification of blockages in the branched and smooth branched chips (Figs 25 and 26), it appears that the architecture of the chips, as well as shear stress may be responsible for the blockages. The arrangement of the chip channels is likely more deleterious than the shear stress. This is shown by the fact that section 8 was significantly more blocked compared to section 1, even though the shear stress is similar (if not higher in section 1). The way the branched and smooth branched chips were designed, means that the cells passing through the chips do not have equal decisions at each branching point. At each branching point, there is a wider channel in the direction of travel, with a channel half its width branching off (e.g. 100µm channel will have a 50µm branch, but the 100µm channel continues). Cells will flow through the path of least resistance. Thus, most cells will follow the wide, 100µm channel all the way past sections 1-7 before being forced to enter section 8. The much higher number of cells in one section could be increasing the probability of blockages. Future designs

should have all branching points be equal in resistance – e.g. a 100µm channel branching into two 50µm channels. A spiderweb-like design has been suggested as a potential method of implementing equal decision branching points. It would provide branching points for MKs to catch and form proplatelets whilst having an unbiased path for cells, reducing risk of cell blockages.

Collaboration with microfluidic and/or fluid dynamics specialists should be considered. A great understanding of fluid dynamics is required when designing a device to ensure that shear stress, resistance and pressure are in levels which will not damage MKs and/or preactivate produced platelets. The trend for section 1 to have increased blockages from section 4 (Fig. 25 and 26) suggests that higher shear stress regions is, in part, contributing the increased blockages. The causes for this could include increased cell damage (thus 'sticky' debris) and/or increased enucleation in the higher shear stress regions (section 1 and 8). Although data presented here shows MKs can pass through the narrow channels of the chips, the narrow channels may be contributing to blockages. The chips are fabricated from PDMS, and then bonded to a glass coverslip. PDMS is a flexible substance, but glass is not. This lack of flexibility may be preventing large MKs from getting through some of the channels. Blood vessels are flexible structures and future systems should consider having more flexible channels(102). This may reduce blockages but also replicate more physiological conditions, potentially increasing productivity.

The sinusoidal chip showed blockages also, however they appeared visually different from the branched and smooth branched chips (Fig. 27). The regions of blockages appeared darker and denser. The author suggests that this may be caused by higher number of damaged cells, thus presence of more free membrane. As the sinusoidal chip is of less interest in future iterations, exact characterisation of these blockages is not high priority.

4.53 Increasing throughput

Another design consideration should be the number of MKs that can be loaded into the system. For a system to be feasible for clinical use, it must be efficient and be able to be scaled up to an industrial scale. The standard protocol for the Poole lab was to passage the chips with a solution at a concentration of 8 MK/µl. This was done for Fig. 8. To produce as much sample as possible for imaging studies, greater concentrations were loaded. This may have contributed to differences in blockages across the chips. The concentration of cells loaded for the blockage analysis was not always controlled. This was a major limitation of this study; however, the trend seen was strong. In a repeat, or future similar studies, pilot studies should be conducted to find the optimal concentration of cells and then maintain that as a controlled parameter. The concentration of solution loaded into the chip for the blockage analysis (Fig. 25 and 26) was noted prior to loading so the results could be normalised to the number of MKs loaded. The S.E.M for each data set in these figures do not overlap, evoking confidence, even in the face of poor experimental design. Previous work in the Poole lab (unpublished) showed that increasing the concentration of MKs loaded into the system does increase platelet production. This suggests that the higher concentrations of MKs loaded into the chip for imaging analysis was not a major limitation. Modifications for increasing throughput of the chips could be achieved increase the number of channels and/or creating multiple inlets and outlets. Increasing throughput and increasing the scale of a system should be considered during design processes. Thon, Dykstra and Beaulieu's review lays some useful guidelines when designing platelet producing microfluidics(43). Although aimed towards bone marrow mimicking designs, the principals may be useful for future iterations of our designs.

Microfluidics has been the approach for platelet biogenesis in this piece of work. Other groups have used alternative methods, including the Eto group who utilise a large scale bioreactor where turbulence is induced through a large volume of liquid (49). This is a very interesting concept and yielded positive results. Future collaboration with this system would be interesting.

4.54 Conclusions

All 3 chips showed high levels of blockages. The cause of the blockages within the branched and smooth branch chip was likely a combination of unequal decision trees for passaging cells and high shear stress damaging MKs, which then produce debris that captures other cells. The sinusoidal chip also showed blockages. Future designs should have equally weighted decisions at each branch point, to prevent a bias for flow direction that may cause blockages. Use of a DNase may help remove or prevent blockages.

4.6 Conclusions about the physical parameters within the different systems

4.61 Introduction

The 3 chips imparted different levels of compression, pressure and shear stress on cells passing through them. The results of this dissertation can be used to hypothesises how these parameters are involved during *in vitro* platelet production and how these should be utilised in future systems.

4.62 Compression

The compression and pressure imparted on the MKs was much greater in the branched and smooth branched chips relative to the sinusoidal chip. This was caused by much narrower channels. This compression appears beneficial to producing platelets. The MKs were able to squeeze through the narrowest channels (12.5μm x 15μm) and remain viable (Figs 9 and 10). Using this information, future designs should include narrow channels that impart compression. Intravital images of mouse lungs appear to show compression on platelet producing MKs, supporting the design choice of compression(37).

4.63 Shear stress

The sinusoidal chip was designed as a system with lower shear stress relative to the branched and smooth branched chips. The data in Fig. 8 suggests that lower shear may produce fewer platelets, however this conclusion is muddled by other variables such as the number of branch points. The sinusoidal chip has a low number of branch points where the inlet splits into 10 individual channels. The presence of these channels means that we cannot deduce if the platelet produced are caused by MKs immobilising on the branches and forming proplatelets (as seen in Fig. 23) or by shear stress on flowing MKs. The author hypothesises that the majority of platelets produced in the sinusoidal system are coming from the immobilised MKs. This is based off the fact that there are far more branch points for MKs in the branched and smooth branched systems and they form more proplatelets and platelets. It is likely that there is an optimal range of shear stress. Too low and platelet production will may be lower, but too high and the risk of damaging or preactivating platelets becomes greater.

4.64 Branch points

This leads to the next design variable: branch points. It seems branch points are important in the platelet producing mechanism within the branched and smooth branched systems. They are likely not the only location where platelets were produced, as proplatelets were seen forming from MKs immobilised to the side of a channel wall, and not at branch points. This indicates that branch points are not essential for platelet production but facilitate the immobilisation of MKs which is essential for platelet production. Therefore, future designs should keep branching but could also utilise narrower channels and/or adhesive proteins such as vWf to create more immobilisation points within the system. The only potential issue with narrow channels is the risk of blockages. This could be compensated for by having many channels, equal decision trees at each branching point and include a DNase to irradicate any sticky DNA. The design should also try to impart lower shear stress, to reduce the risk of damaging MKs and preactivating platelets.

4.65 Laminar flow vs turbulent flow

The bioreactor used by the Eto group produces platelets using turbulent flow(49). Here, platelets were produced using laminar flow. This proves that turbulent flow is not the only way that platelets can be produced. Future systems should consider this and can utilise either or both. Historically, it was believed that disturbances in laminar flow were pathological(103). This is now disputed, with findings showing that physiological blood flow exhibits turbulence(104). These pieces of information may help explain why platelet production can be induced by laminar and turbulent flow; both laminar flow and turbulent flow conditions are physiological.

4.66 Future experiments

If physical parameters such as shear stress, compression, pressure, flow dynamics and flow rate want to be studied more accurately, different microfluidics which isolate each parameter in turn would need to be designed. The 3 chips used in this piece of work can indicate the role of some of these parameters but cannot make confident conclusions owing to the presence of these parameters not being controlled in each of the systems. Fig. 28 summaries the hypothesised mechanisms by which platelets are formed within the more productive, branched and smooth branched chip. It also shows the believed reason and contents of blockages. This is an overly simplified schematic.

4.67 Comparison to *ex vivo* model

The conditions within the microfluidics systems are far from physiological conditions. A good comparison point is the *ex vivo* heart-lung system previously used in the Poole lab(51, 52). A major difference is that the chips lack endothelial cell linings. Coating the inside of a microfluidics chip with endothelial cells is difficult, given the size restrictions and sub-optimal culturing conditions. Coating the chip with key MK interacting proteins may be a suitable alternative. This could include vWf, other adhesion proteins or activators of MKs. The author hypothesises that endothelial cells likely induce intracellular signalling in MKs which potentiates platelet production. This hypothesis is based on the large difference in platelet producing productivity of the chips and the *ex vivo* heart-lung system.

Figure 28

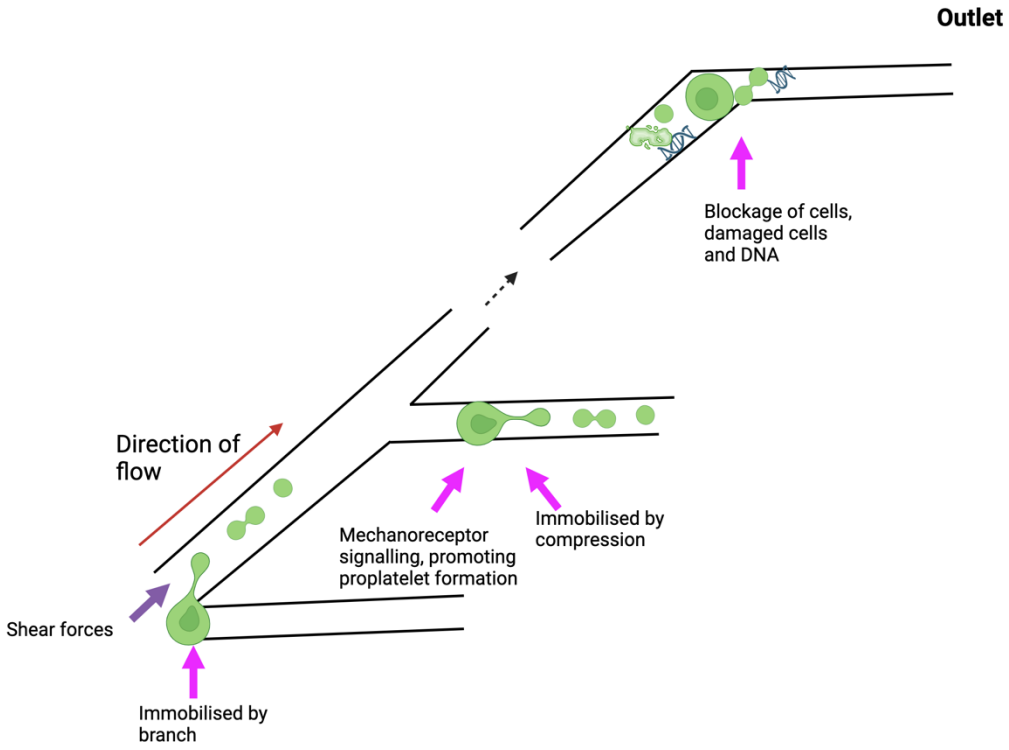

Figure 28 – Simplified Schematic of Hypothesised Mechanisms Within the 'Branched' and 'Smooth Branched' Microfluidics Systems

This schematic shows an overly simplified version of the hypothesised mechanisms of platelet production and blockages within the 'branched' and 'smooth branched' systems. The green nucleated cells are megakaryocytes. They immobilise at branch points, and occasionally, in narrow channels. When immobilised, the shear stress of fluid passing by them can induce proplatelet formation, releasing pre platelets and barbell platelets, and finally producing platelets. It is hypothesised that mechanoreceptors on megakaryocytes are stimulated upon compression through

narrow channels which may facilitate proplatelet formation. Towards the end of the channels, viable cells, damaged cells and DNA form large aggregates and block the outlet of the channel. These blockages become wedged and will continue to capture more and more contents. Created using Biorender.com.

4.7 Summary of the 3 Microfluidics Systems

All 3 microfluidics systems produce platelets. Light and electron microscopy data, suggests the platelets are being made via the same mechanism. This mechanism is a catch and release mechanism, where proplatelets are formed from immobilised MKs. The MKs appear, mostly, to catch on branch points. This is likely why the branched and smooth branched system were more efficient than the sinusoidal chip. The sinusoidal chip imparted less compression onto the MKs and this is potentially another cause for its poorer yield.

The platelets produced from all 3 chips appear morphologically normal under SEM, however they show signs of preactivation.

The architecture of the branched and smooth branched chip resulted in major blockages. This should be modified to improve yield. The contents of the blockages is unknown. DNA is a suggested component, thus use of a DNase in the perfusion solution may be beneficial.

Introduction of bubbles into the microfluidics is likely a major cause of platelet preactivation. Future systems should be closed systems to minimise opportunities to add bubbles. The conditions within all the chips are damaging, resulting in large amounts of debris. Reducing this debris should be considered with future designs.

Improved designs would have equal decision trees, many branch points, narrow channels for compression and a vWf coating. A DNase within the perfusing solution should also be included.

4.8 Final words and future directions

This body of work has explored 3 different microfluidics chips through the lens of different microscopes. It has evoked confidence in characterising the platelets produced as morphological platelets. Furthermore, it has revealed much about the platelet producing mechanism occurring within the chips. With this, it has been possible to explore the factors important in platelet generation and the limitations of microfluidics. Collaboration and further experimentation is required to design new microfluidics designs that will utilise the catch and release, proplatelet mechanism, whilst applying compression and preventing major blockages and cell damage. Notes of caution, as well as interpretation of data, have been provided at the appropriate places and limitations of each experiment have been disclosed. This body of work hopes to contribute to the platelet biogenesis field, in the collaborative effort in producing a feasible platelet producing tool for therapeutic development.

5. Bibliography

1. Frelinger A, Michelson A, Gremmel T. Platelet Physiology. Seminars in Thrombosis and Hemostasis. 2016;42(03):191-204.
2. Gaetano GD, Cerletti C. Platelet adhesion and aggregation and fibrin formation in flowing blood: a historical contribution by Giulio Bizzozero. Platelets. 2002;13(2):85-9.
3. Wang S, Li Z, Xu R. Human Cancer and Platelet Interaction, a Potential Therapeutic Target. International Journal of Molecular Sciences. 2018;19(4):1246.
4. Cho MS, Bottsford-Miller J, Vasquez HG, Stone R, Zand B, Kroll MH, et al. Platelets increase the proliferation of ovarian cancer cells. Blood. 2012;120(24):4869-72.
5. Zizzo N, Patruno R, Zito FA, Summa AD, Tinelli A, Troilo S, et al. Vascular endothelial growth factor concentrations from platelets correlate with tumor angiogenesis and grading in a spontaneous canine non-Hodgkin lymphoma model. Leukemia & Lymphoma. 2010;51(2):291-6.
6. Heldin CH, Lennartsson J, Westermark B. Involvement of platelet-derived growth factor ligands and receptors in tumorigenesis. Journal of Internal Medicine. 2018;283(1):16-44.
7. Repsold L, Pool R, Karodia M, Tintinger G, Joubert AM. An overview of the role of platelets in angiogenesis, apoptosis and autophagy in chronic myeloid leukaemia. Cancer Cell International. 2017;17(1).
8. Twelves C, Cortes J, Kaufman PA, Yelle L, Awada A, Binder TA, et al. “New” metastases are associated with a poorer prognosis than growth of pre-existing metastases in patients with metastatic breast cancer treated with chemotherapy. Breast Cancer Research. 2015;17(1).
9. Seyfried TN, Huysentruyt LC. On the Origin of Cancer Metastasis. Critical Reviews™ in Oncogenesis. 2013;18(1 - 2):43-73.
10. Sylman JL, Mitrugno A, Tormoen GW, Wagner TH, Mallick P, McCarty OJT. Platelet count as a predictor of metastasis and venous thromboembolism in patients with cancer. Convergent Science Physical Oncology. 2017;3(2):023001.
11. Takemoto A, Okitaka M, Takagi S, Takami M, Sato S, Nishio M, et al. A critical role of platelet TGF-β release in podoplanin-mediated tumour invasion and metastasis. Scientific Reports. 2017;7(1):42186.
12. Yeung KT, Yang J. Epithelial-mesenchymal transition in tumor metastasis. Molecular Oncology. 2017;11(1):28-39.
13. Hayes BD, Brady L, Pollak M, Finn SP. Exercise and Prostate Cancer: Evidence and Proposed Mechanisms for Disease Modification. Cancer Epidemiology, Biomarkers & Prevention. 2016;25(9):1281-8.
14. Nieswandt B, Hafner M, Echtenacher B, Männel DN. Lysis of tumor cells by natural killer cells in mice is impeded by platelets. Cancer Res. 1999;59(6):1295-300.
15. Chaffer CL, Weinberg RA. A Perspective on Cancer Cell Metastasis. Science. 2011;331(6024):1559-64.

16. Ali RA, Wuescher LM, Worth RG. Platelets: essential components of the immune system. Curr Trends Immunol. 2015;16:65-78.
17. Deutsch VR, Tomer A. Megakaryocyte development and platelet production. British Journal of Haematology. 2006;134(5):453-66.
18. Kaushansky K. Thrombopoietin. New England Journal of Medicine. 1998;339(11):746-54.
19. Noetzli LJ, French SL, Machlus KR. New Insights Into the Differentiation of Megakaryocytes From Hematopoietic Progenitors. Arteriosclerosis, Thrombosis, and Vascular Biology. 2019;39(7):1288-300.
20. Machlus KR, Italiano JE. The incredible journey: From megakaryocyte development to platelet formation. Journal of Cell Biology. 2013;201(6):785-96.
21. Corash L, Levin J. The relationship between megakaryocyte ploidy and platelet volume in normal and thrombocytopenic C3H mice. Exp Hematol. 1990;18(9):985-9.
22. Mazzi S, Lordier L, Debili N, Raslova H, Vainchenker W. Megakaryocyte and polyploidization. Experimental Hematology. 2018;57:1-13.
23. Noh J-Y. Megakaryopoiesis and Platelet Biology: Roles of Transcription Factors and Emerging Clinical Implications. International Journal of Molecular Sciences. 2021;22(17):9615.
24. Ebaugh FG, Bird RM. The Normal Megakaryocyte Concentration in Aspirated Human Bone Marrow. Blood. 1951;6(1):75-80.
25. Ribatti D, Crivellato E. Giulio Bizzozero and the discovery of platelets. Leukemia Research. 2007;31(10):1339-41.
26. Martin JF, Paolo D'Avino P. A theory of rapid evolutionary change explaining the de novo appearance of megakaryocytes and platelets in mammals. Journal of Cell Science. 2022;135(24).
27. Becker RP, De Bruyn PPH. The transmural passage of blood cells into myeloid sinusoids and the entry of platelets into the sinusoidal circulation; a scanning electron microscopic investigation. American Journal of Anatomy. 1976;145(2):183-205.
28. Cramer EM, Norol Fo, Guichard J, Breton-Gorius J, Vainchenker W, Massé J-M, et al. Ultrastructure of Platelet Formation by Human Megakaryocytes Cultured With the Mpl Ligand. Blood. 1997;89(7):2336-46.
29. Italiano JE, Patel-Hett S, Hartwig JH. Mechanics of proplatelet elaboration. Journal of Thrombosis and Haemostasis. 2007;5:18-23.
30. Junt T, Schulze H, Chen Z, Massberg S, Goerge T, Krueger A, et al. Dynamic Visualization of Thrombopoiesis Within Bone Marrow. Science. 2007;317(5845):1767-70.
31. Schwertz H, Köster S, Kahr WHA, Michetti N, Kraemer BF, Weitz DA, et al. Anucleate platelets generate progeny. Blood. 2010;115(18):3801-9.
32. Brown E, Carlin LM, Nerlov C, Lo Celso C, Poole AW. Multiple membrane extrusion sites drive megakaryocyte migration into bone marrow blood vessels. Life Science Alliance. 2018;1(2):e201800061.
33. Pedersen NT. Circulating Megakaryocytes in Blood from the Inferior Vena Cava in Adult Rats. Scandinavian Journal of Haematology. 1971;8(3):223-30.
34. Trowbridge EA, Martin JF, Slater DN, Kishk YT, Warren CW. Platelet production: A computer based biological interpretation. Thrombosis Research. 1983;31(2):329-50.
35. Lefrançais E, Looney MR. Platelet Biogenesis in the Lung Circulation. Physiology. 2019;34(6):392-401.
36. Kallinikos-Maniatis A. Megakaryocytes and Platelets in Central Venous and Arterial Blood. Acta Haematologica. 2009;42(6):330-5.
37. Lefrançais E, Ortiz-Muñoz G, Caudrillier A, Mallavia B, Liu F, Sayah DM, et al. The lung is a site of platelet biogenesis and a reservoir for haematopoietic progenitors. Nature. 2017;544(7648):105-9.
38. Woods MJ, Greaves M, Lawford PV, Trowbridge EA. Isolation of Megakaryocytes from Human Placentae. Platelets. 1994;5(2):109-12.

39. Davis RE, Stenberg PE, Levin J, Beckstead JH. Localization of megakaryocytes in normal mice and following administration of platelet antiserum, 5-fluorouracil, or radiostrontium: evidence for the site of platelet production. Exp Hematol. 1997;25(7):638-48.
40. Stegner D, Vaneeuwijk JMM, Angay O, Gorelashvili MG, Semeniak D, Pinnecker J, et al. Thrombopoiesis is spatially regulated by the bone marrow vasculature. Nature Communications. 2017;8(1).
41. Xiao DW, Yang M, Yang J, Hon KL, Fok FT. Lung damage may induce thrombocytopenia. Platelets. 2006;17(5):347-9.
42. Kosaki G. In Vivo Platelet Production from Mature Megakaryocytes: Does Platelet Release Occur via Proplatelets? International Journal of Hematology. 2005;81(3):208-19.
43. Thon JN, Dykstra BJ, Beaulieu LM. Platelet bioreactor: accelerated evolution of design and manufacture. Platelets. 2017;28(5):472-7.
44. Balduini A, Buduo CAD, Kaplan DL. Translational approaches to functional platelet production ex vivo. Thromb Haemost. 2016;115(02):250-6.
45. Lasky LC, Sullenbarger B. Manipulation of oxygenation and flow-induced shear stress can increase the in vitro yield of platelets from cord blood. Tissue Eng Part C Methods. 2011;17(11):1081-8.
46. Blin A, Le Goff A, Magniez A, Poirault-Chassac S, Teste B, Sicot G, et al. Microfluidic model of the platelet-generating organ: beyond bone marrow biomimetics. Scientific Reports. 2016;6(1):21700.
47. Thon JN, Mazutis L, Wu S, Sylman JL, Ehrlicher A, Machlus KR, et al. Platelet bioreactor-on-a-chip. Blood. 2014;124(12):1857-67.
48. Tozzi L, Laurent P-A, Di Buduo CA, Mu X, Massaro A, Bretherton R, et al. Multi-channel silk sponge mimicking bone marrow vascular niche for platelet production. Biomaterials. 2018;178:122-33.
49. Ito Y, Nakamura S, Sugimoto N, Shigemori T, Kato Y, Ohno M, et al. Turbulence Activates Platelet Biogenesis to Enable Clinical Scale Ex Vivo Production. Cell. 2018;174(3):636-48.e18.
50. Pongérard A, Mallo L, Do Sacramento V, Boiron O, Eckly A, Gachet C, et al. Development of an efficient, ready to use, blood platelet-release device based on two new flow regime parameters: The periodic hydrodynamic loading and the shear stress accumulation. New Biotechnology. 2023;77:68-79.
51. Zhao X, Alibhai D, Walsh TG, Tarassova N, Birol SZ, Williams CM, et al. Platelet generation from circulating megakaryocytes is triggered in the lung vasculature. 2021.
52. Zhao X, Alibhai D, Walsh TG, Tarassova N, Englert M, Birol SZ, et al. Highly efficient platelet generation in lung vasculature reproduced by microfluidics. Nature Communications. 2023;14(1):4026.
53. Ouzegdouh Y, Capron C, Bauer T, Puymirat E, Diehl J-L, Martin JF, et al. The physical and cellular conditions of the human pulmonary circulation enable thrombopoiesis. Experimental Hematology. 2018;63:22-7.e3.
54. Chen Z, Hu M, Shivdasani RA. Expression analysis of primary mouse megakaryocyte differentiation and its application in identifying stage-specific molecular markers and a novel transcriptional target of NF-E2. Blood. 2007;109(4):1451-9.
55. Mookerjee S, Foster HR, Waller AK, Ghevaert CJ. In vitro-derived platelets: the challenges we will have to face to assess quality and safety. Platelets. 2020;31(6):724-30.
56. Mott K, Schulze H. Isolation, In Vitro Differentiation, and Culture of Murine Megakaryocytes From Fetal Liver and Adult Bone Marrow. Current Protocols. 2023;3(5):e783.
57. Shivdasani RA, Schulze H. Culture, Expansion, and Differentiation of Murine Megakaryocytes. Current Protocols in Immunology. 2005;67(1):22F.6.1-F.6.13.
58. Vijey P, Posorske B, Machlus KR. In vitro culture of murine megakaryocytes from fetal liver-derived hematopoietic stem cells. Platelets. 2018;29(6):583-8.

59. Nakamura S, Takayama N, Hirata S, Seo H, Endo H, Ochi K, et al. Expandable Megakaryocyte Cell Lines Enable Clinically Applicable Generation of Platelets from Human Induced Pluripotent Stem Cells. Cell Stem Cell. 2014;14(4):535-48.
60. Evans AL, Dalby A, Foster HR, Howard D, Waller AK, Taimoor M, et al. Transfer to the clinic: refining forward programming of hPSCs to megakaryocytes for platelet production in bioreactors. Blood Adv. 2021;5(7):1977-90.
61. Schlesinger M. Role of platelets and platelet receptors in cancer metastasis. Journal of Hematology & Oncology. 2018;11(1).
62. Lu Q, Ye H, Wang K, Zhao J, Wang H, Song J, et al. Bioengineered Platelets Combining Chemotherapy and Immunotherapy for Postsurgical Melanoma Treatment: Internal Core-Loaded Doxorubicin and External Surface-Anchored Anti-PD-L1 Antibody Backpacks. Nano Letters. 2022;22(7):3141-50.
63. Cohn CS. Platelet transfusion refractoriness: how do I diagnose and manage? Hematology Am Soc Hematol Educ Program. 2020;2020(1):527-32.
64. Estcourt LJ, Birchall J, Allard S, Bassey SJ, Hersey P, Kerr JP, et al. Guidelines for the use of platelet transfusions. British Journal of Haematology. 2017;176(3):365-94.
65. Organisation WH. Global Status Report on Blood Safety and Availability 2016. 2017.
66. Rajashekaraiah V, Rajanand MC. Platelet storage: Progress so far. Journal of Thrombosis and Thrombolysis. 2022;55(1):9-17.
67. Cortin V, Pineault N, Garnier A. Ex Vivo Megakaryocyte Expansion and Platelet Production from Human Cord Blood Stem Cells. Humana Press; 2009. p. 109-26.
68. Heald R, Nogales E. Microtubule dynamics. Journal of Cell Science. 2002;115(1):3-4.
69. Kimmerlin Q, Strassel C, Eckly A, Lanza F. The tubulin code in platelet biogenesis. Seminars in Cell & Developmental Biology. 2023;137:63-73.
70. Polek A, Sobiczewski W, Matowicka-Karna J. [P-selectin and its role in some diseases]. Postepy Hig Med Dosw (Online). 2009;63:465-70.
71. Blair P, Flaumenhaft R. Platelet α-granules: Basic biology and clinical correlates. Blood Reviews. 2009;23(4):177-89.
72. Pluthero FG, Kahr WHA. Imaging Platelets and Megakaryocytes by High-Resolution Laser Fluorescence Microscopy. Springer New York; 2018. p. 13-31.
73. Belizário J, Vieira-Cordeiro L, Enns S. Necroptotic Cell Death Signaling and Execution Pathway: Lessons from Knockout Mice. Mediators of Inflammation. 2015;2015:1-15.
74. Thompson CB, Jakubowski JA, Quinn PG, Deykin D, Valeri CR. Platelet Size and Age Determine Platelet Function Independently. Blood. 1984;63(6):1372-5.
75. Spurgeon BEJ, Naseem KM. Platelet Flow Cytometry: Instrument Setup, Controls, and Panel Performance. Cytometry Part B: Clinical Cytometry. 2020;98(1):19-27.
76. Thorsen T, Klausen H, Lie RT, Holmsen H. Bubble-induced aggregation of platelets: effects of gas species, proteins, and decompression. Undersea Hyperb Med. 1993;20(2):101-19.
77. Gao Y, Wu M, Lin Y, Xu J. Trapping and control of bubbles in various microfluidic applications. Lab on a Chip. 2020;20(24):4512-27.
78. Roka-Moiia Y, Walk R, Palomares DE, Ammann KR, Dimasi A, Italiano JE, et al. Platelet Activation via Shear Stress Exposure Induces a Differing Pattern of Biomarkers of Activation versus Biochemical Agonists. Thrombosis and Haemostasis. 2020;120(05):776-92.
79. Estevez B, Du X. New Concepts and Mechanisms of Platelet Activation Signaling. Physiology. 2017;32(2):162-77.
80. Circu ML, Aw TY. Reactive oxygen species, cellular redox systems, and apoptosis. Free Radical Biology and Medicine. 2010;48(6):749-62.

81. Sarkar FH, Li Y. Markers of apoptosis. Methods Mol Med. 2006;120:147-60.
82. Jonkman J, Brown CM, Wright GD, Anderson KI, North AJ. Tutorial: guidance for quantitative confocal microscopy. Nature Protocols. 2020;15(5):1585-611.
83. Lee J-Y, Kitaoka M. A beginner's guide to rigor and reproducibility in fluorescence imaging experiments. Molecular Biology of the Cell. 2018;29(13):1519-25.
84. Yu L, Zhu G, Zhang Z, Yu Y, Zeng L, Xu Z, et al. Apoptotic bodies: bioactive treasure left behind by the dying cells with robust diagnostic and therapeutic application potentials. Journal of Nanobiotechnology. 2023;21(1).
85. Santavanond JP, Rutter SF, Atkin-Smith GK, Poon IKH. Apoptotic Bodies: Mechanism of Formation, Isolation and Functional Relevance. Springer International Publishing; 2021. p. 61-88.
86. Yun SH, Sim EH, Goh RY, Park JI, Han JY. Platelet Activation: The Mechanisms and Potential Biomarkers. Biomed Res Int. 2016;2016:9060143.
87. Swanepoel AC, Pretorius E. Ultrastructural analysis of platelets during three phases of pregnancy: A qualitative and quantitative investigation. Hematology. 2015;20(1):39-47.
88. Kemble S, Dalby A, Lowe GC, Nicolson PLR, Watson SP, Senis Y, et al. Analysis of preplatelets and their barbell platelet derivatives by imaging flow cytometry. Blood Advances. 2022;6(9):2932-46.
89. Thon JN, Macleod H, Begonja AJ, Zhu J, Lee K-C, Mogilner A, et al. Microtubule and cortical forces determine platelet size during vascular platelet production. Nature Communications. 2012;3(1):852.
90. Mojzisch A, Brehm MA. The Manifold Cellular Functions of von Willebrand Factor. Cells. 2021;10(9).
91. Mojiri A, Alavi P, Lorenzana Carrillo MA, Nakhaei-Nejad M, Sergi CM, Thebaud B, et al. Endothelial cells of different organs exhibit heterogeneity in von Willebrand factor expression in response to hypoxia. Atherosclerosis. 2019;282:1-10.
92. Pan J, Dinh TT, Rajaraman A, Lee M, Scholz A, Czupalla CJ, et al. Patterns of expression of factor VIII and von Willebrand factor by endothelial cell subsets in vivo. Blood. 2016;128(1):104-9.
93. Poirault-Chassac S, Nguyen KA, Pietrzyk A, Casari C, Veyradier A, Denis CV, et al. Terminal Platelet Production is Regulated by Von Willebrand Factor. PLoS One. 2013;8(5):e63810.
94. Sugimoto N, Kanda J, Nakamura S, Kitano T, Hishizawa M, Kondo T, et al. iPLAT1: the first-in-human clinical trial of iPSC-derived platelets as a phase 1 autologous transfusion study. Blood. 2022;140(22):2398-402.
95. Tufto I, Rofstad EK. Interstitial fluid pressure and capillary diameter distribution in human melanoma xenografts. Microvasc Res. 1999;58(3):205-14.
96. Townsley MI. Structure and Composition of Pulmonary Arteries, Capillaries, and Veins. Comprehensive Physiology. 2012.
97. Coste B, Mathur J, Schmidt M, Earley TJ, Ranade S, Petrus MJ, et al. Piezo1 and Piezo2 Are Essential Components of Distinct Mechanically Activated Cation Channels. Science. 2010;330(6000):55-60.
98. Zarychanski R, Schulz VP, Houston BL, Maksimova Y, Houston DS, Smith B, et al. Mutations in the mechanotransduction protein PIEZO1 are associated with hereditary xerocytosis. Blood. 2012;120(9):1908-15.
99. Deivasikamani V, Dhayalan S, Abudushalamu Y, Mughal R, Visnagri A, Cuthbertson K, et al. Piezo1 channel activation mimics high glucose as a stimulator of insulin release. Scientific Reports. 2019;9(1).
100. Hansen CE, Qiu Y, McCarty OJT, Lam WA. Platelet Mechanotransduction. Annual Review of Biomedical Engineering. 2018;20(1):253-75.

101. Papayannopoulos V. Neutrophil extracellular traps in immunity and disease. Nature Reviews Immunology. 2018;18(2):134-47.
102. Boutouyrie P, Chowienczyk P, Humphrey JD, Mitchell GF. Arterial Stiffness and Cardiovascular Risk in Hypertension. Circulation Research. 2021;128(7):864-86.
103. Chiu J-J, Chien S. Effects of Disturbed Flow on Vascular Endothelium: Pathophysiological Basis and Clinical Perspectives. Physiological Reviews. 2011;91(1):327-87.
104. Saqr KM, Tupin S, Rashad S, Endo T, Niizuma K, Tominaga T, et al. Physiologic blood flow is turbulent. Scientific Reports. 2020;10(1):15492.